To the Graduate Council:

I am submitting herewith a thesis written by Walter Scott Pope entitled "Investigation of a Bending Vibration Absorber and, or Damper for an Internal Combustion Engine Crankshaft". I have examined the final copy for form and content and recommend that it be accepted for partial fulfillment of the requirement for the degree of Masters of Science, with a major in Mechanical Engineering.

Frank H. Speckhart

Dr. Frank Speckhart, Major Professor

We have read this thesis and recommend its acceptance:

J. W. Hodgson

Stanley E. Becker

Accepted for the Council:

Cw Minkel

Associate Vice Chancellor and Dean of The Graduate School

Investigation of a Bending Vibration Absorber and, or Damper for an Internal Combustion Engine Crankshaft

A Thesis
Presented for the
Master of Science
Degree
The University of Tennessee at Knoxville

Walter Scott Pope
May 1997

Dedication

This thesis is dedicated to my parents

who have encouraged me throughout my entire education

Abstract

The objective of this study was to invent, mathematically model, and evaluate bending vibration absorbers for use as flywheels on crankshafts of spark ignition internal combustion engines. In this study, a two dimensional discrete mass model of an inline four cylinder spark ignition engine's crankshaft was developed to predict the bending vibration response during firing. Variations of five different absorber flywheel designs were added to the model in an attempt to reduce the bending vibration. Two of these designs were invented in the course of the study. The viscous roller damper dissipated vibrational energy using viscous friction. An elastomer dissipated vibrational energy in a second design. Mathematical models of these absorber and, or damper designs were evaluated using the crankshaft model. The displacement information was analyzed using a fast Fourier transform. A theoretical damper was the only design that reduced the free end vibration through the entire speed range. Results obtained in this study show that the vibration can be reduced by the addition of a damper in place of a flywheel. Tuning the crankshaft and absorber /damper system within a smaller speed range is a more feasible solution.

Table of Contents

List of Tables

List of Figures

Chapter One

Introduction

Overview

Lower fuel consumption, higher output, environmental safety, and passenger comfort drive the design of today's passenger cars. Automobile designers have tried to achieve the first two of these goals by using smaller engines operating at higher speeds and reducing powertrain and body weight. Reduction of the number of cylinders and of the engine component weight has led to the increase of powertrain vibration. Automotive customers, however, want a quiet, comfortable, and luxurious ride. There have been many attempts to resolve this vibration by attacking its transmission routes. Improved engine mounts and passenger compartment insulation have not been successfully eliminated the sound quality problems.

Crankshaft vibrational behavior strongly influences the passenger compartment sound pressure level and total engine vibration amplitude. The crankshaft vibration has three components, torsional, bending, and axial. The gas and inertial forces from the firing of the individual cylinders excite each of these vibration components.

The pulsing output torque from each piston's firing causes torsional vibration. Crankshaft fatigue and failure are the primary products of the pulsing torsional vibration. Attempts to solve torsional vibration involve increasing flywheel inertia. The added inertia acts to smooth the output torque.

Crankshaft bending during firing causes the crankshaft to whirl about the crankshaft's rotational axis. The whirling causes increased bearing forces and deformations. These deformations are suspected to cause "bearing noise." The bending vibration propagates through the bearings to the engine block and the rest of the vehicle. Traditionally, the crankshaft stiffness has to be increased to lessen the bending vibration. The increased stiffness also increases the weight. There has been limited success in the reduction of the bending vibration using improved flywheel designs.

The axial vibration is caused by the bending vibration. As the piston force bends the crankshaft, the crankshaft's length is increased. When it returns to its unstrained position, it returns to its original length. Thus, the axial vibration is caused by the bending vibration.

Elimination or large reduction of this bending vibration would be an important breakthrough. This could lead to improved crankshaft designs and lower power plant weights. Many studies and designs have contributed to improvements in this important area.

Literature Review

In a study by Kamiya, Atsumi, and Tasaka [1] for the Toyota Motor Corporation, intermittent rumble audible in the passenger compartment during acceleration was investigated. The study was performed on an in-line six cylinder spark ignition engine Toyota passenger car. The passenger compartment's sound pressure levels were measured. From these measurements, they determined that the problem was dominate in the 150 Hz to 500 Hz range. Another method to confirm these measurements was a hammering test. In a hammering test, a structure is physically hammered, and its vibrational response is monitored using an accelerometer. By conducting hammering tests on the crankshaft, they concluded that one of the crankshaft's natural bending frequencies existed in the problem frequency band. They further concluded that a 315 Hz vibration is generated by bending vibration and was caused by the first cylinder's combustion. To reduce this bending vibration a new crankshaft pulley was developed. Effectiveness, cost of manufacturing, and effects on engine performance were the design factors of the new pulley. This pulley utilized an inner ring separated from the pulley hub by an elastomer washer in addition to the torsional vibration damper. The inner ring and elastomer washer damp the bending vibration. The addition of the new pulley was reported to reduce the passenger compartment sound pressure level in the 200 Hz to 500 Hz in the 2000 RPM to 5000 RPM engine speed range. This new pulley was also qualitatively compared to increasing the crankshaft stiffness for reducing the bending vibration. The pulley performed better than increasing the crank stiffness in terms of effectiveness, cost, and effect on engine performance.

Another experimental study of a torsional/bending damper pulley for an engine crankshaft explored the use of elastomer damping. The 1990 study by Kinoshita, Sakamoto, and Oakamura [2] proposed and tested an elastomer damper pulley for the front end of the crankshaft. The engine used in the experiment was a 1.6 liter water cooled in-line four cylinder gasoline engine. A crankshaft hammering test provided a natural bending frequency peak at 330 Hz with two nodes in plane with the crankshaft throws. To check this result under firing conditions, a device was designed to measure the longitudinal, radial, and torsional vibration at the front end of the crankshaft. From the firing test, the natural frequency of the first torsional mode occurred at 360 Hz. This peak came from the dominant resonance of the fourth, sixth, and eighth modes of crankshaft speed. A second peak at 330 Hz from the one half and third order components signified the natural frequency of the radial vibration mode. The damper model combined an inlaid-type torsional damper with a disk type bending damper. The two dampers were tuned to combat the respective crankshaft natural frequencies. Vibrations are damped when the damper's natural frequency was tuned to the crankshaft's problem natural frequency. The natural frequency of the torsional damper can be expressed by

$$f_{torsional} = \frac{1}{2\pi}\sqrt{\frac{k_t}{I}}$$

where k_t = torsional dynamic spring constant of the elastomer,
I = inertial mass of the vibration ring.

The bending damper's natural frequency is chosen by

$$f_{Bending} = \frac{1}{2\pi}\sqrt{\frac{k_r}{m}}$$

where k_r = radial dynamic spring constant of the elastomer,
m = mass of the vibration ring.

The torsional damper and the torsional/bending damper produced the same torsional damping effects under running conditions. However, the 330 Hz resonant peak was not present while the new pulley was in use proving that the new damper was effective at damping the bending vibration. The torsional/bending damper reduced the vibration level in the 200 Hz to 400 Hz range by one third to one half when compared to the torsional damper alone.

In a similar study by Ide, Uchhida, Ozawa, and Izawa [3] for the Nissan Motor Company, attention focused on the bending vibration of the crankshaft at the flywheel. This study was conducted to clarify the mechanism producing the 200 Hz to 500 Hz "rumble." The study used an in-line four cylinder spark ignition engine test vehicle. Sound pressure measurements were made in the passenger compartment during acceleration. The study reported that the sound quality problems in the 200 Hz to 500 Hz band were caused by solid propagation of vibration from the engine through the motor mounts. They also concluded that the vibrations were composed of harmonic components of crankshaft revolution. Bending vibration resonance was investigated by measuring the bending stress in the fourth cylinder's rear crank arm during engine operation. The third order bending stress component of engine speed peaked at an engine speed of 5400 RPM, which indicated the bending vibration resonance occurred around 270 Hz. The second order bending stress component was estimated to peak at 8100 RPM. They improved the sound quality during engine acceleration by using a "flexible flywheel." This flywheel design flexibly mounted the flywheel mass to the crankshaft with a flexible plate. The circular flexible plate was mounted perpendicular to the crankshaft's rotational axis. Inertial mass is mounted along the outside of the flexible plate. The flexible flywheel was designed to tune the third order bending vibration component outside the 200 Hz to 500 Hz sound pressure problem range. The authors concluded that the flexible flywheel reduced the rumbling noise, but they provided no quantitative data to support their conclusion.

The frequencies and mode shapes of the coupled whirling, torsional, and axial vibration were studied by Hodgetts [4]. A theoretical three-dimensional model was developed. Forces that excite the crankshaft are due to gas pressure and inertia. The frequencies of the harmonic components of these periodic forces are integer and half multiples of the engine speed. To find these frequencies, experiments were carried out on a water cooled four stroke four cylinder spark ignition engine of 1100 cc displacement. The experimental study indicated two resonant peaks at 255 Hz and 425 Hz. The 255 Hz peak was shown in the study both experimentally and theoretically to be a reverse whirl. This is a consequence of the phase between cranks being 180 degrees apart. This peak occurs at a critical engine speed of 5100 RPM. The study explored the modeling of the crankshaft's five journal bearings. The bearing oil film causes a nonlinear deflection and adds damping. The study assumed that the bearings were "pinned" with respect to ground. A pinned bearing allows no movement from its initial point. The pinned journal's calculated and measured frequencies of vibration at 5100 RPM agreed and were within 9% at two slower speeds. However, the modeling of the bearings in this manner is unsatisfactory for predicting vibrational amplitudes. This is due to the substantial damping effects of the oil film for finite displacements of the journal, cavitation in the oil film, and bearing erosion.

In a 1988 study, Okamura, Sogabe, and Shinno [5] developed a dynamic stiffness matrix method for three-dimensional analysis of crankshaft vibration. The purpose of this study was to develop a precise description of the vibrational behavior of the crankshaft in the early design stages. This description provided designers with information to improve their crankshaft designs. The model idealized the crankshaft as a set of joined structures consisting of round rods and beams. The front pulley and the flywheel were idealized as masses having moments of inertia about their center of gravity. The journal bearings were modeled as a set of linear springs. The spring constants were sized based upon Sommerfield's number and Reynold's equation graphical data for their operating conditions. The equation for Sommerfield's number is,

$$S = \frac{\mu NLD}{W} \left(\frac{R}{Cp}\right)^2$$

where μ = viscosity of the lubricant,
N = rotational speed,
L = bearing width,
D = bearing diameter,
W = bearing load,
R = bearing radius,
Cp = machined clearance.

The calculations of the natural frequencies were compared to firing tests performed on a 1.6 liter inline four cylinder spark ignition engine. The bending stress' third order harmonic component peaked at 210 Hz at 4200 RPM. The experimental data agreed with the 233 Hz third order peak of the model. A torsional peak of 400 Hz occurred at 4000 RPM in the experimental study.

An SAE technical paper by Shwibinger, Hendrick, Wu, and Imanishi [6] described the theoretical approach to solving vibration and noise problems in the powertrain with elastomer vibration control products. The crankshaft vibrations can be reduced to 25-30% of their original levels by adding an elastomer damper to the front end of the crankshaft. The elastomer damper consisted of an inertial ring attached to a hub by an elastomer. The vulcanized elastomers as opposed to the pressed elastomer provided a wider range of material selection. This selection was based on the expected engine operating conditions. With the use of the elastomer damper the bending and torsional vibration amplitudes can be significantly reduced. This reduction reduces stress in the crankshaft and noise in the car.

Objective

A careful review of the relevant literature has shown that crankshaft bending vibration has been extensively studied due to its effects on the passenger compartment's sound pressure level during acceleration. There is an audible rumble in the 200 Hz to 500 Hz range during acceleration. Several damper designs either dampen or tune this vibration. Therefore, the objective of this study was to invent, mathematically model, and evaluate bending vibration absorbers and/or dampers for use as flywheels on crankshafts of spark ignition internal combustion engines.

Chapter Two

Solution Procedure

The crankshaft bending vibration problem was solved in two phases. Phase one involved building a computer code to model the vibrational response of a crankshaft. The purpose of this code was to provide a means of quantitatively comparing flywheel designs. The second phase consisted of modeling different flywheel designs, and evaluating these models using the crankshaft bending vibration response code. The objective of this phase was to evaluate the different damper designs in terms of their effectiveness in decreasing the bending vibration of the crankshaft model.

Bending Vibration Response Model

Crankshaft Model

To aid in the building of the model, an unknown make inline four cylinder crankshaft was borrowed from a local engine shop. A drawing of the crankshaft is provided as Figure 1. This steel crankshaft has five bearings, and a 0-180-180-0 cylinder index design. The crankshaft's machined diameters at the bearing positions are 2.25 inches. The crankshaft diameters at the connecting rod bearings are 2.25 inches also.

The crankshaft was modeled by first dividing it into discrete sections. The divisions

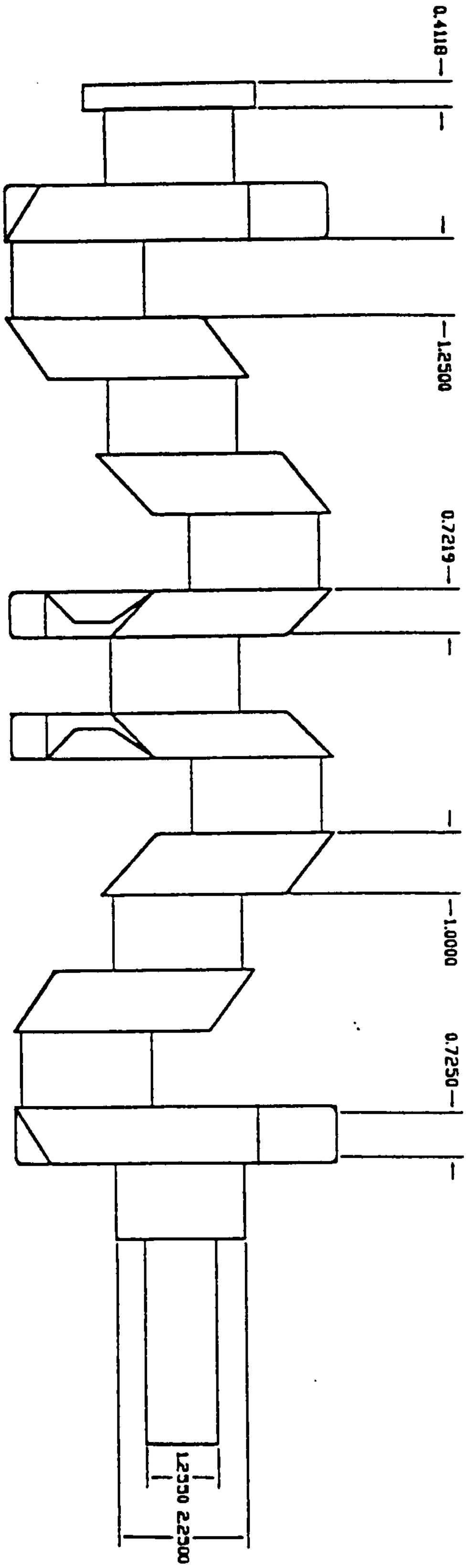

Figure 1 In line Four Cylinder Crankshaft

for the crankshaft model coincided with the crankshaft's feature changes. Each of the divisions defined a discrete mass joined by weightless beams. These discrete masses and weightless beams formed the crankshaft model. Each of the discrete masses was considered mathematically as a point mass. This division is illustrated in Figure 2. External forces and moments acting on the crankshaft are modeled as well. The forces and moments influence the motion of all the neighboring masses in the system. Each point's motion is described by its translational and rotational components. Second order linear differential equations govern these components of motion for each mass point. These equations apply to the center of mass of each mass point, and they are derived from the summation of forces and torques acting on the mass point. From the summation of forces the general equation of motion is

$$\Sigma F = m\frac{d^2 y_i}{dt^2} = V_i^L - V_{i+1}^L - c_i\frac{dy_i}{dt} - k_i y_i + F_i \tag{1}$$

where F = Force at the center of mass,
m = mass of the mass point,
y = vertical displacement of the center of mass,
V_i = shear forces in the model,
c = damping factor,
k = spring constant,
F_i= external forces.

After the summation of moments, the rotational equation of motion is

$$\Sigma T = J_i\frac{d^2\theta}{dt^2} = M_i^R - M_i^L \tag{2}$$

where T = Torque on the center of mass,
J_i = mass moment of inertia,
θ = Angular displacement of the center of mass,
M= moment.

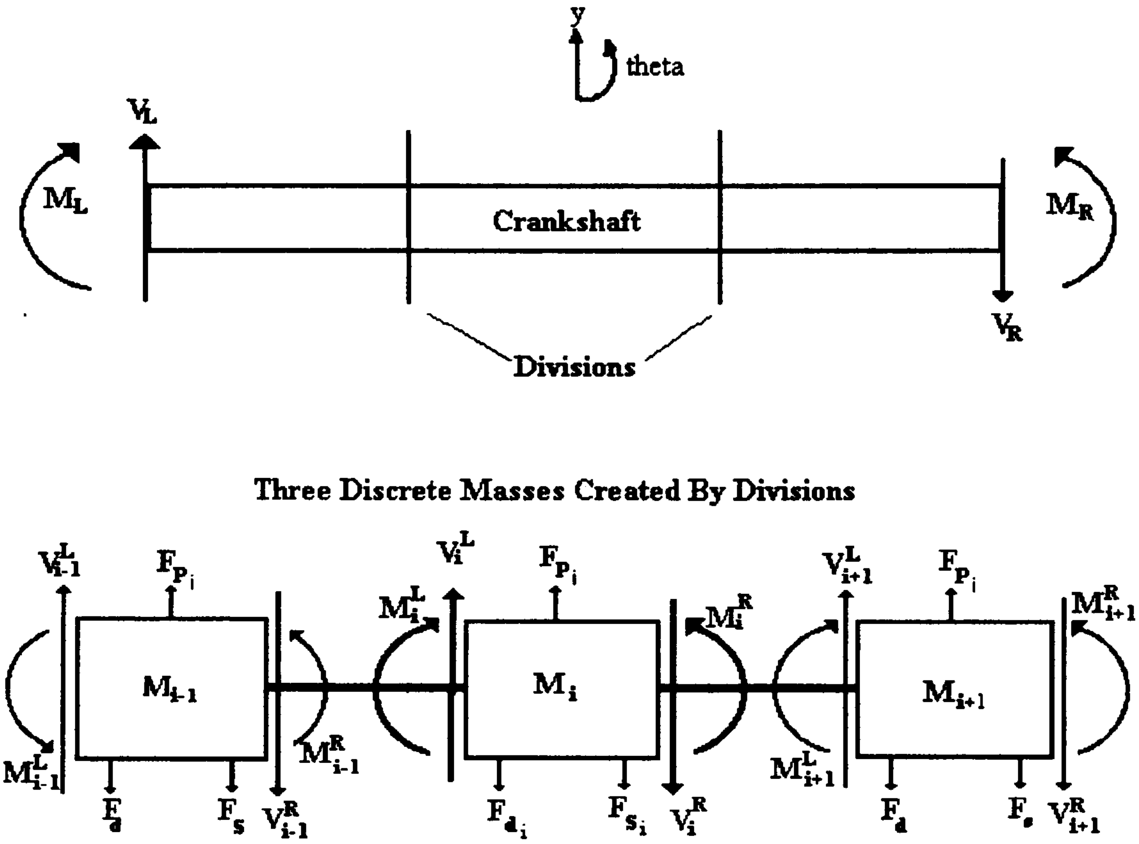

where V = shear force,
M = moment,
F_p = piston force,
Fd = damping force,
Fs = spring force

Figure 2. Discrete Mass Model

To aide in the solution of these equations the beam equations are employed. The solution of the translational equation of motion of a beam, y, is

$$y_i = y_{i-1} + L\theta_{i-1} + \frac{M_i^L L^2}{2EI} - \frac{V_i^L L^3}{3EI} \qquad (3)$$

where θ = angular displacement,
M = moment,
L = length between masses,
E = modulus of elasticity of the mass,
I = area moment of inertia of the mass,
V = shear force.

The solution to the rotational equation of motion of a beam, θ is

$$\theta_i = \theta_{i-1} + \frac{M_i^L L}{EI} - \frac{V_i^L L^2}{2EI} \qquad (4)$$

where θ = angular deflection,
L = length of weightless beam,
M = moment,
E = modulus of elasticity of the mass,
I = area moment of inertia of the mass,
V = shear force.

The shear forces and the moments acting on the mass points are related by

$$V_{i-1}^R = V_i^L \qquad (5)$$

and

$$M_{i-1}^R - M_i^L + V_i^L L = 0 \qquad (6)$$

$$i = 1 \text{ to } N$$

where V = shear force,
M = moment,
L = length between masses,
N = number of masses,
R and L superscripts denote the side of the mass point.

The beam equations reduce the summation equations, (1) and (2), into a useful form. This conversion starts by solving equations 3 and 4 in terms of M^L and V^L respectively,

$$M_i^L = \frac{2}{3}V_i^L + \frac{2EI}{L^2}(y_i - y_{i-1} - L_i\theta_{L-1}) \qquad (3)$$

and

$$V_i^L = \frac{2}{L}M_i^L + \frac{2EI}{L^2} \qquad (4).$$

From solving equations 3 and 4 through substitution into each other, the force and moment acting on the left hand side of the mass points are obtained,

$$V_i^L = \frac{6EI}{L^2}\left[\theta_i - \theta_{i-1} - \frac{2}{L}(y_i - y_{i-1} - L\theta_{i-1})\right] \qquad (7)$$

and

$$M_i^L = \frac{2EI}{L}\left[2(\theta_i - \theta_{i-1}) - \frac{3}{L}(y_i - y_{i-1} - L\theta_{i-1})\right] \qquad (8)$$

To find the right hand side equations, 5 and 6 are utilized. The substitution of equations 7 and 8 into equations 5 and 6 is done providing the remaining unknowns in the summation equations, 1 and 2. With the external forces, spring and damping constants, mass, torque, and moment of inertia known, the translational and rotational accelerations are calculated at each time step.

To numerically model the crankshaft, a numbering system was imposed on the mass points starting at the first mass point that corresponds to the pulley. Displacement for the first mass point is represented by Y(1), and the velocity of the first mass point is represented by Y(2). The numbering continues along the crankshaft model to the last point (N). Angular displacement for the first point is represented by Y(2N+1), and the angular velocity is represented by Y(2N+2). Numbering continues with the displacement at the second point being represented by Y(3), and its velocity being represented by Y(4). Its angular displacement is represented by Y(2N+3), and its angular velocity is represented by Y(2N+4). Table 1 describes this imposed numbering system.

Mass Point	Vertical Position	Vertical Velocity	Angular Position	Angular Velocity
1	Y(1)	Y(2)	Y(39)	Y(40)
2	Y(3)	Y(4)	Y(41)	Y(42)
3	Y(5)	Y(6)	Y(43)	Y(44)
4	Y(7)	Y(8)	Y(45)	Y(46)
5	Y(9)	Y(10)	Y(47)	Y(48)
6	Y(11)	Y(12)	Y(49)	Y(50)
7	Y(13)	Y(14)	Y(51)	Y(52)
8	Y(15)	Y(16)	Y(53)	Y(54)
9	Y(17)	Y(19)	Y(55)	Y(56)
10	Y(18)	Y(20)	Y(57)	Y(58)
11	Y(21)	Y(22)	Y(59)	Y(60)
12	Y(23)	Y(24)	Y(61)	Y(62)
13	Y(25)	Y(26)	Y(63)	Y(64)
14	Y(27)	Y(28)	Y(65)	Y(66)
15	Y(29)	Y(30)	Y(67)	Y(68)
16	Y(31)	Y(32)	Y(69)	Y(70)
17	Y(33)	Y(34)	Y(71)	Y(72)
18	Y(35)	Y(36)	Y(73)	Y(74)
19	Y(37)	Y(38)	Y(75)	Y(76)

Table 1. Imposed Mass Point Numbering System

To numerically solve the governing equations, each second order translational component equation was reduced to two coupled first order equations by substitution. To perform the substitution a separate variable array, YD(x), is created. The displacement and velocity are then produced using a Runge-Kutta solver.

The crankshaft was modeled by nineteen mass points, each having a different weight. The first mass point is at the accessory drive pulley location. It was represented by a 2.25 inch diameter by 1.025 inch solid shaft weighing 1.45 lbs. Each of the four connecting rod connections and five bearing positions was also represented by a mass point. The pistons were modeled by 2.25 inch diameter by 1.025 inch solid shafts with 0.92 lb weights added to account for the reciprocating weights of the connecting rods. The second, sixth, tenth, fourteenth, and eighteenth mass points correspond to the five bearings were modeled as 2.25 inch diameter by 1.025 inch solid shafts.

The crank web is the structure that displaces the crankshaft centerline and connects the connecting rod to the crankshaft. Different shapes and weights of crank webs balance the crankshaft on its rotational axis. Mass points were also placed at each of the crank webs. There are three different crank web types in the model's crankshaft each having a different mass. The largest of the crank webs are found between the first bearing and piston and the last piston and bearing. These correspond to the third and seventeenth mass points each weighing 3.69 lb. Mass points five, seven, thirteen, and fifteen model the next kind of crank webs that are the smallest weighing 1.14 lb. The last type crank web weighs 1.177 lb. These are modeled by the ninth and eleventh mass points. The final mass point is used to describe the flywheel which is the function of this tool.

Table 2 describes the type, mass, and weight of each of the mass points. The 1981-86 Chevrolet Chevette 2.0L engine's crankshaft weighs 38 lbs, and the 1991-94 Saturn 1.9L engine's crankshaft weighs 30 lbs. The 35.1 lbs calculated by the program is

Point Mass Number	Type	Mass (lb sec^2 in)	Non-Crankshaft Additions (lbm)	Weight (lb)
1	Free	0.003764		1.4529
2	Bearing	0.003764		1.4529
3	Crank	0.009566		3.69248
4	Piston	0.003764	0.00239	2.37544
5	Crank	0.002956		1.14102
6	Bearing	0.003764		1.4529
7	Crank	0.002956		1.14102
8	Piston	0.003764	0.00239	2.37544
9	Crank	0.004578		1.76711
10	Bearing	0.003764		1.4529
11	Crank	0.004578		1.76711
12	Piston	0.003764	0.00239	2.37544
13	Crank	0.002956		1.14102
14	Bearing	0.003764		1.4529
15	Crank	0.002956		1.14102
16	Piston	0.003764	0.00239	2.37544
17	Crank	0.009566		3.69248
18	Bearing	0.003764		1.4529
19	Free	0.003764		1.4529
			total	35.1553

Table 2. Mass Point Description

about the mean weight of the four cylinder engine crankshaft weight range. The pulley point, five bearing points, four piston points, eight crank web points, and the flywheel point account for the nineteen mass points used in the crankshaft model.

Program Testing

To start the programming, nine mass points were used. The mass point/solver program was tested statically after the system came to rest. The points modeled a 2.25 inch diameter by 19 inches long round steel beam Springs with spring constants of $1X10^9$ lb/in were used at both ends of the system. The springs simulated a pinned end, even though they oscillated a maximum of $3X10^{-4}$ inch during the test. A 1000-pound constant force was placed at the tenth, or center mass points. The crankshaft damping factor (ZETACS) was set at three, and the program was let run until it came to rest. The static deflection of a uniform beam with twin loads and simple supports provided a comparison for the system. The equation for the static deflection at any point on the beam is

$$y_{max} = \frac{Fl^3}{48EI}$$

where y = deflection,
l = length of the beam
F = load,
E = modulus of elasticity,
I = second moment of inertia.

The second moment of inertia for the model beam was 1.25806 in^4, and the modulus of elasticity of steel is $30x10^6$ Mpsi. The theoretical solution for the deflection at the tenth mass point is -0.003466 inch. The program calculated the deflection as -0.003466 inch. These deflection values differ by 0.00 %.

A dynamic test was also performed on a round steel beam model. With the nineteen mass points and pinned ends, the model was bent into a half sine wave. The maximum deflection of the initially bent model was 0.0001 inch at the midpoint. All the system's damping was removed, and the model was released by starting the program. The midpoint of the model, mass point number ten, oscillated between 0.0001 inch and-0.0001 inch at 533.47 Hz. The closed form solution for the natural frequency of a round beam is

$$f = \frac{\pi}{2L^2}\sqrt{\frac{EIL}{m}}$$

where f = frequency,
E= modulus of elasticity,
I = second moment of inertia,
L = beam length,
m = mass.

This method predicted the beams natural frequency to be 528.14 Hz. The difference in the solutions is 1.009%. This test proved that the solver worked correctly in a dynamic situation.

Support Model

Due to the hydrodynamic effect of the lubricant, bearings do not deform linearly. However, an exact model of the bearings is outside the scope of this study. The crankshaft model idealized the bearing as linear springs. Past studies indicate the magnitude of the spring constants to be on the order of $1X10^6$ pounds per inch [5,8,9]. The spring constants were set at $1X10^6$ pounds per inch after trying spring constants between $1X10^5$ pounds per inch and $1X10^7$ pounds per inch. The chosen value agreed with values obtained through the sum of hydrodynamic and structure elasticity stiffness bearing models [5, 8, 9]. The first model enabled modeling of the elastohydrodynamic effects in the oil film, accounting for the pressure interaction in the oil film and bore deformation effects. The second model used a hydrodynamic calculation for the oil film and stiffness and damping properties for the bearing parts. The chosen spring stiffness value allowed the model's flywheel to vibrate in the experimentally and theoretically reported frequency range [1-5]. A spring was added to the model to account for this effect. This spring is accounted for in equation 1 by the $k_i y_i$ term.

To account for the viscous damping effects of the bearing lubricant, dampers were added to the model to work with the springs. Their values were set at 0.05 lb*sec/inch. Since the damper value affects the amplitude of the vibration and not the frequency, this value was estimated. Damping in the crankshaft itself was also added. A crankshaft damping factor of 0.003 lb*sec/inch damps the relative motion of neighboring mass points. This value is also an estimate based on the crankshaft's material properties. The damping is modeled by the $c_i\, dy_i/dt$ term in equation 1.

Firing Model

To model the vibration of the crankshaft, the piston force needed to be added to the model. This force is caused by gas pressure created during the burning of fuel in the cylinder. Because the measurement requires the engine be modified, there is no way to accurately measure this pressure as a function of time for a real cycle. Torque, however, can be measured without changing the engine. The shape of the gas pressure torque was derived from [12],

$$M(t) = \sum W_n \sin(n\theta + \phi_n)$$

where $M(t)$ = Gas pressure torque,
W_n = Function of the ratio of instantaneous to mean torque,
n = Harmonic order,
θ = Crankshaft angle,
ϕ_φ = Angle between Fourier coefficients of torque ratio.

Figure 3 contains the coefficients, W_n and ϕ_n, which were used in the gas pressure torque calculations. The calculation's accuracy was increased with increasing the harmonic order in the calculations. The Figure 3 coefficients are for a compression ratio of 6.0. A normalized gas pressure torque curve for a single cylinder four cycle spark ignition engine is shown in Figure 4. This curve is an ideal model, and it does not include inertial effects. In the case of bending, the gas pressure exerts the only bending force. This curve is the basis for the firing model used in the crankshaft bending response code.

The ideal gas pressure torque curve was simplified to allow for easier computing. By assuming the firing force creates the dominant vibrational effect, the simplification diminishes only the high frequency vibrations outside the problem range. A sine wave with the maximum torque as its amplitude was used for the first 180 degrees. A constant value of negative one tenth the maximum torque represented the torque for the next 420 degrees. The final 120 degrees was represented by a sine wave with an amplitude of four tenths the maximum torque. The simplified torque curve is provided as Figure 5. To make an accurate model as possible, the firing characteristics for the model were adapted from a University of Tennessee owned Saturn engine. The maximum torque of a Saturn in line four cylinder engine operating at 2400 RPM is 107 foot pounds or 321 inch pounds

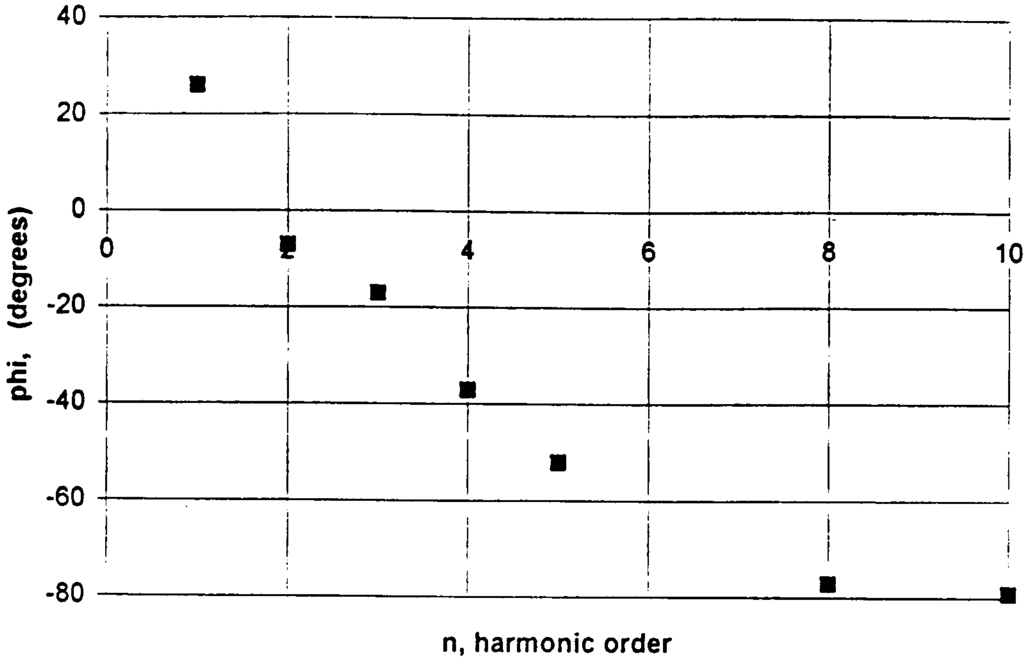

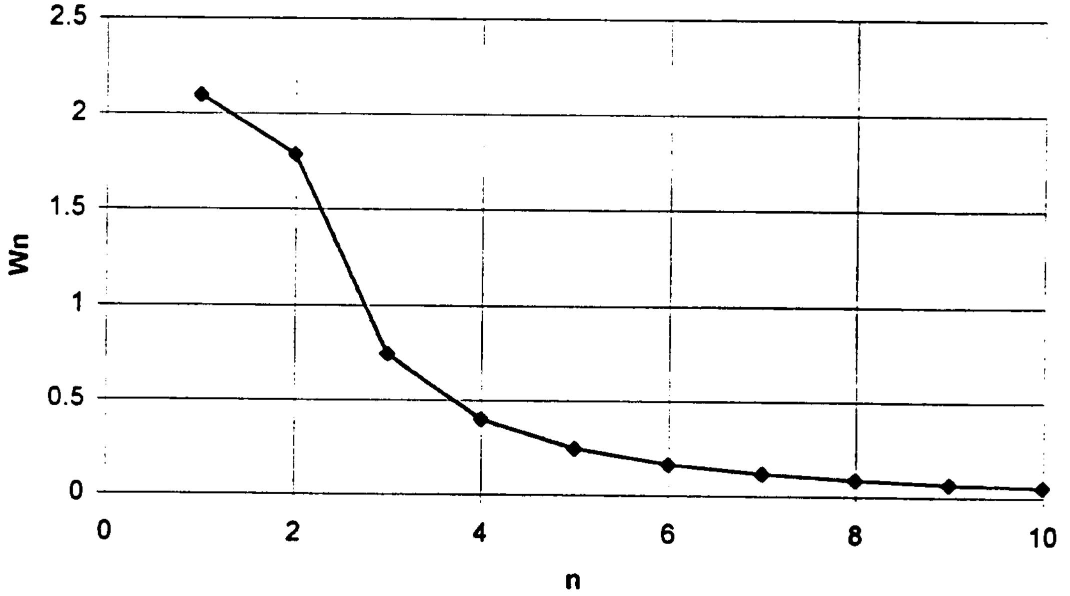

Figure 3. W_n and Φ Coefficients for Use in Gas Pressure Torque Calculation

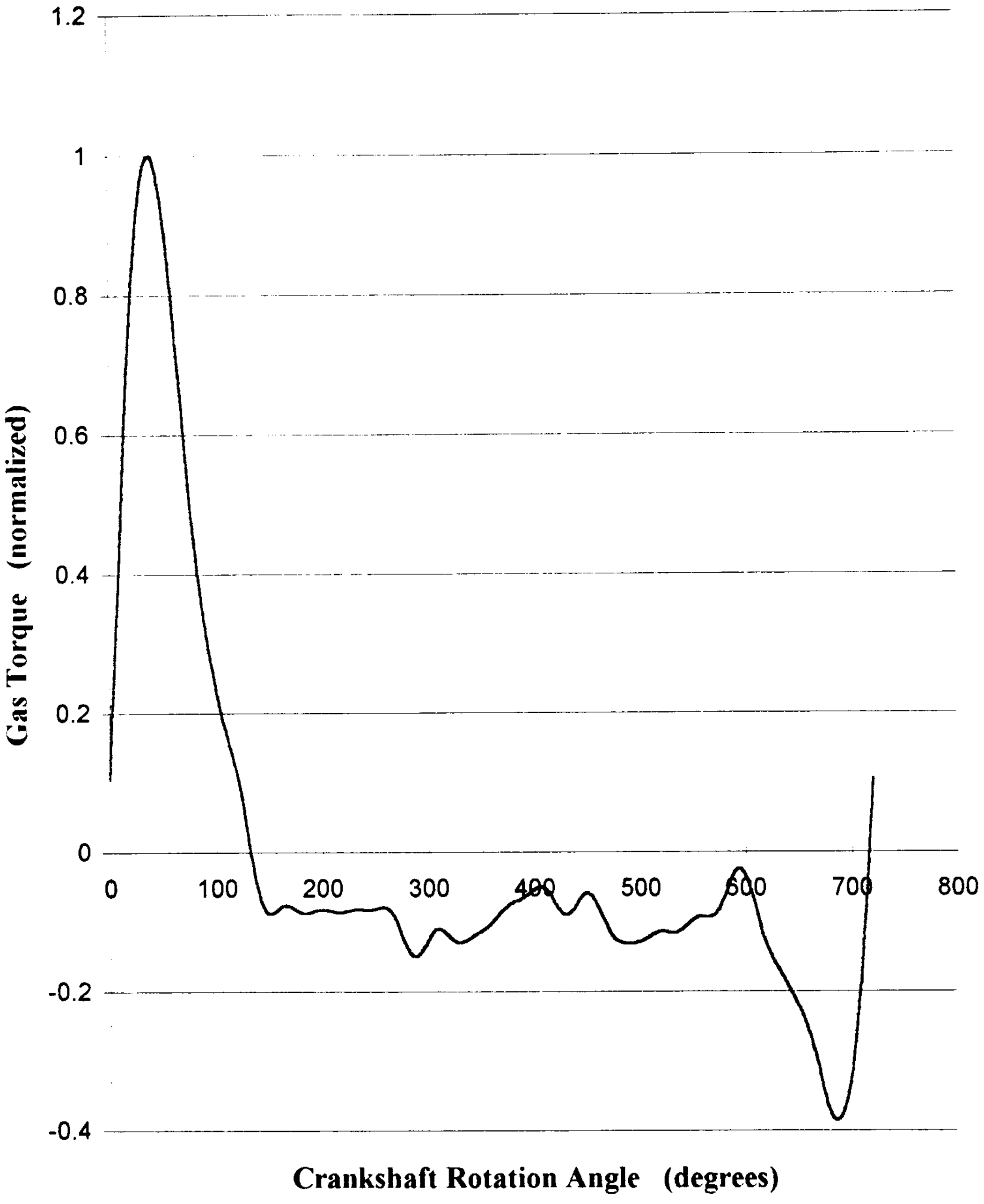

Figure 4. Normalized Gas Pressure Torque Curve for a Single Cylinder Spark Ignition Engine

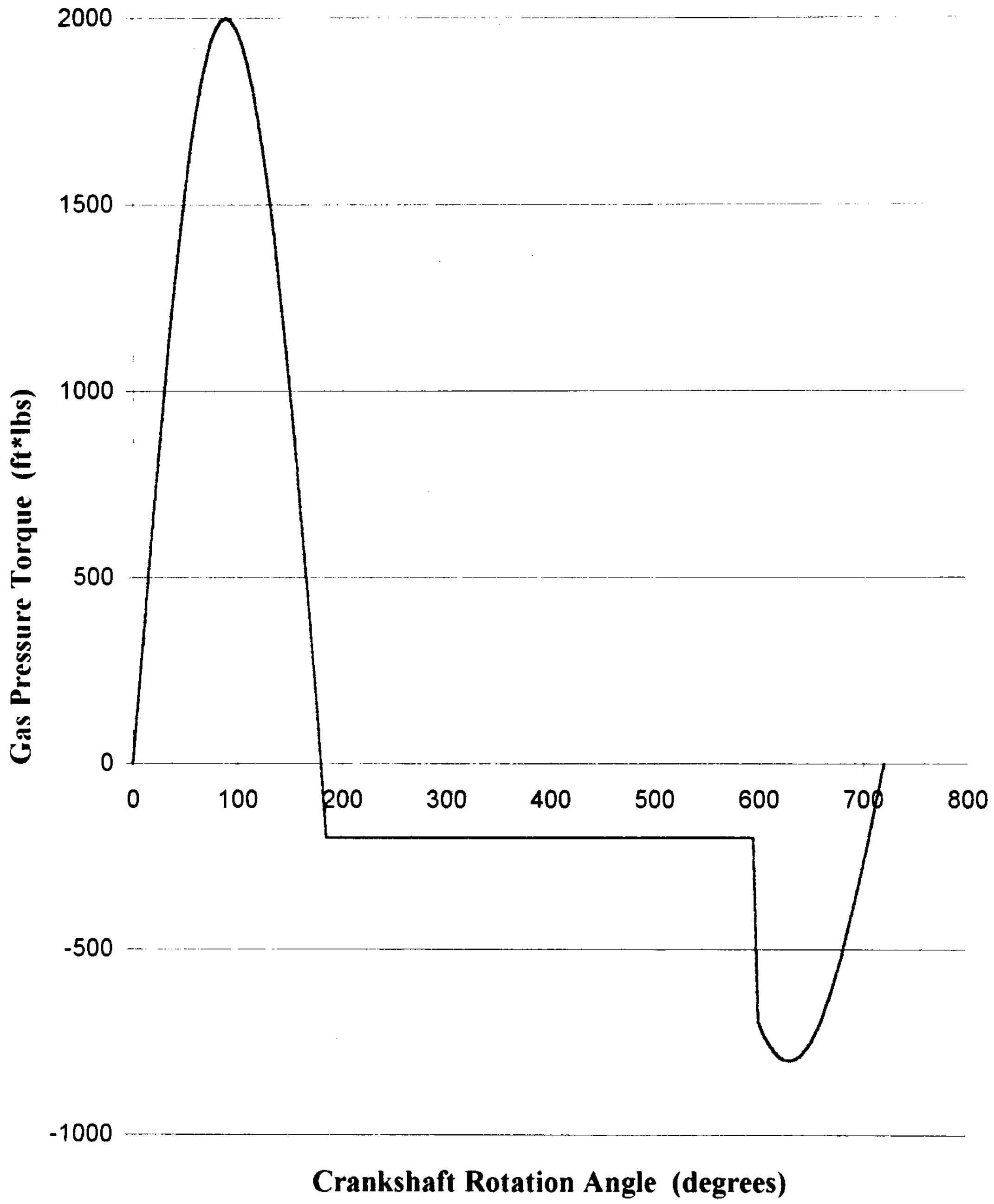

Figure 5. Simplified Gas Pressure Torque Curve

per cylinder. However, this is a mean torque, and a maximum torque is needed for the code. The maximum gas pressure torque used in the model was estimated as 2000 inch pounds.

Gas torque is transmitted through the connecting rod from the piston to the crankshaft. The connecting rod force causes the bending in the crankshaft. The connecting rod's force is derived through geometry,

$$F = \frac{T}{R \times \cos(\pi/2 - \phi - \theta)}$$

where F = gas pressure force,
T = torque,
R = crank distance,
ϕ= connecting rod angle,
θ = crankshaft angle.

Singularities occur in the model every time the crankshaft angle approaches a multiple of $\pi/2$. These functions had to be approximated ten degrees on both sides of the singularities. The gas pressure force function used in the code is plotted as Figure 6.

The firing order was taken from a Saturn four cylinder engine. The cylinders fire in a 4-1-3-2 order separated by 180 degrees of crankshaft rotation. Each cylinder follows the same piston force profile. The firing order in the code is referenced to the first cylinder's rotational position. Each cylinder has a phase angle of an integer multiple of π, based on the firing order. So, for every time step, each cylinder's force was calculated based on the new crankshaft angle and the cylinder's phase angle. The program that calculates the gas pressure forces acting on the crankshaft is provided in Appendix A.

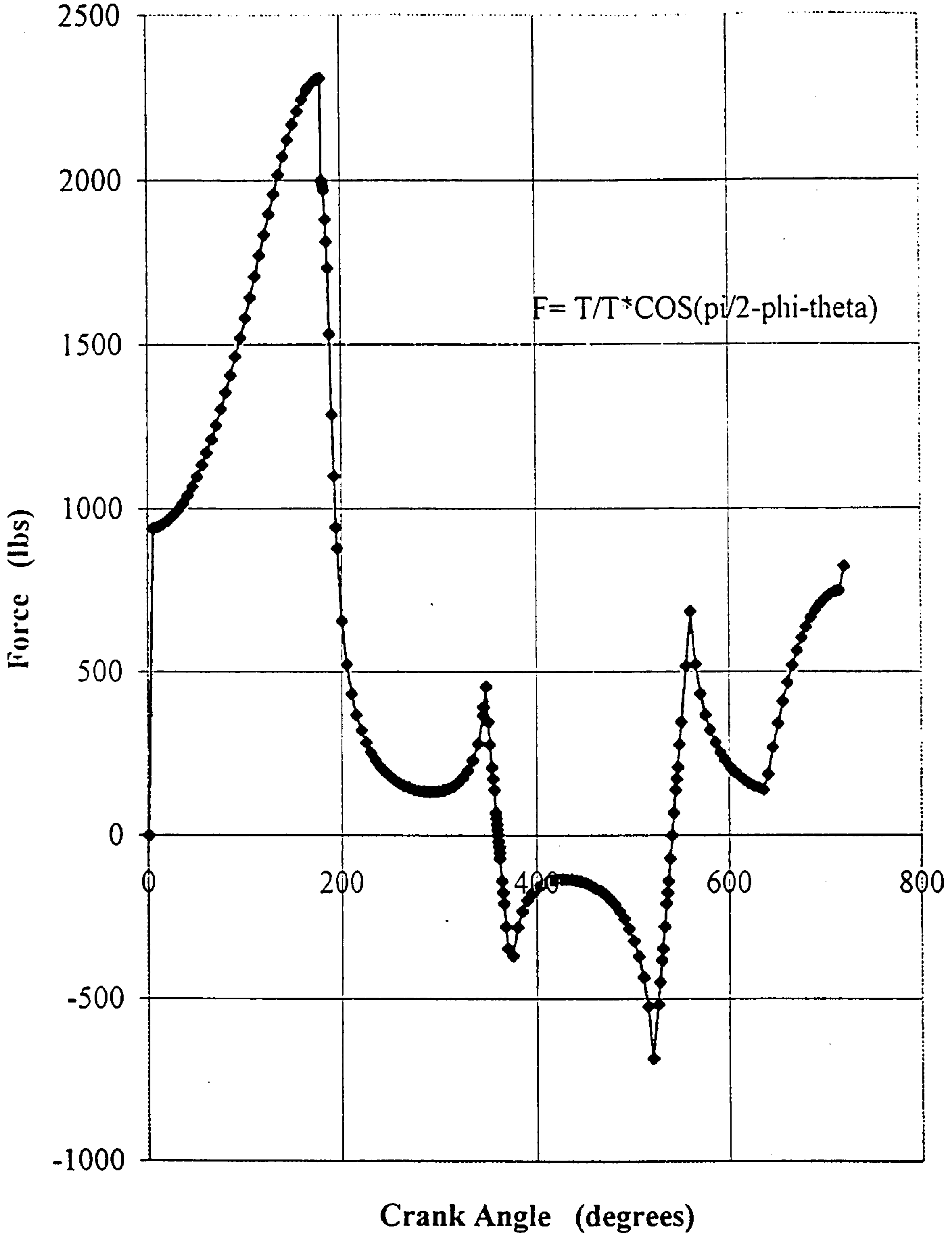

Figure 6 Single Cylinder Crank Force

Testing

With all the program's pieces in place, the testing began. The Runge-Kutta integration step size greatly affected the error in solving the equations. A smaller step size usually produces less error, but it increases the solution time of the program [10]. The crankshaft's integration step size was set at 1 microsecond. This size allowed the program to provide converging solutions in the least amount of time. If the step size was set larger, the forces from the springs at the bearings caused the program's results to diverge. The program's results were written to the screen and to data file every two hundred microseconds. This output time provided enough data for a smooth curve while minimizing the size of the needed data in the output file. The program's output created a data file containing a digital signal sampled at 5000 Hz. This sampling time was chosen because it is at least twice the maximum value in the frequency range of interest. The crankshaft program did not reach a steady state vibration until about 100 crankshaft revolutions depending on engine speed. Running the program this long took an excessive amount of time, so the program was converted to Fortran and run on a Sun workstation.

Results of previous experimental studies indicated that there was a resonant bending frequency in the 250 Hz to 400 Hz range [1, 3, 4]. The resonant frequencies are also integer and half multiples of the engine speed [3]. In the experimental tests, the vibrations were monitored by a strain gauge placed on the number four outside crank arm. This point corresponded to the seventeenth mass point in the bending vibration response model. For comparison, the deflection of this mass point was monitored. The bearing stiffness was adjusted until a resonant frequency in the 250 Hz to 400 Hz band occurred at an integer multiple of the engine speed. A resonant peak at 5400 RPM was calculated to be 374.53 Hz which is within 3.89% of the fourth order component and within 1.2% of reported data [3]. Changing the bearing stiffness greatly effected the amplitude of vibration. As bearing stiffness was increased the vibration amplitude decreased, and the response of the crankshaft decreased with increasing stiffness. The dampers at the bearing had an even larger effect on vibration amplitude. As the damping was increased, the vibrational amplitude decreased, but the crankshaft's response remained unchanged. In past experimental studies either sound pressure or crankshaft stress was monitored. Due to this, the amplitude of the vibration was not compared to experimental data.

The vibration of the crankshaft is complex. The vibration of the system is composed of as many as four different frequencies. A plot showing the analytical vibrational response of the crankshaft at 4000 RPM is provided as Figure 7. The largest peak is the half order component which is due to the firing of the fourth piston every other revolution. The harmonic order components are due to inertial forces of the firing of the other pistons.

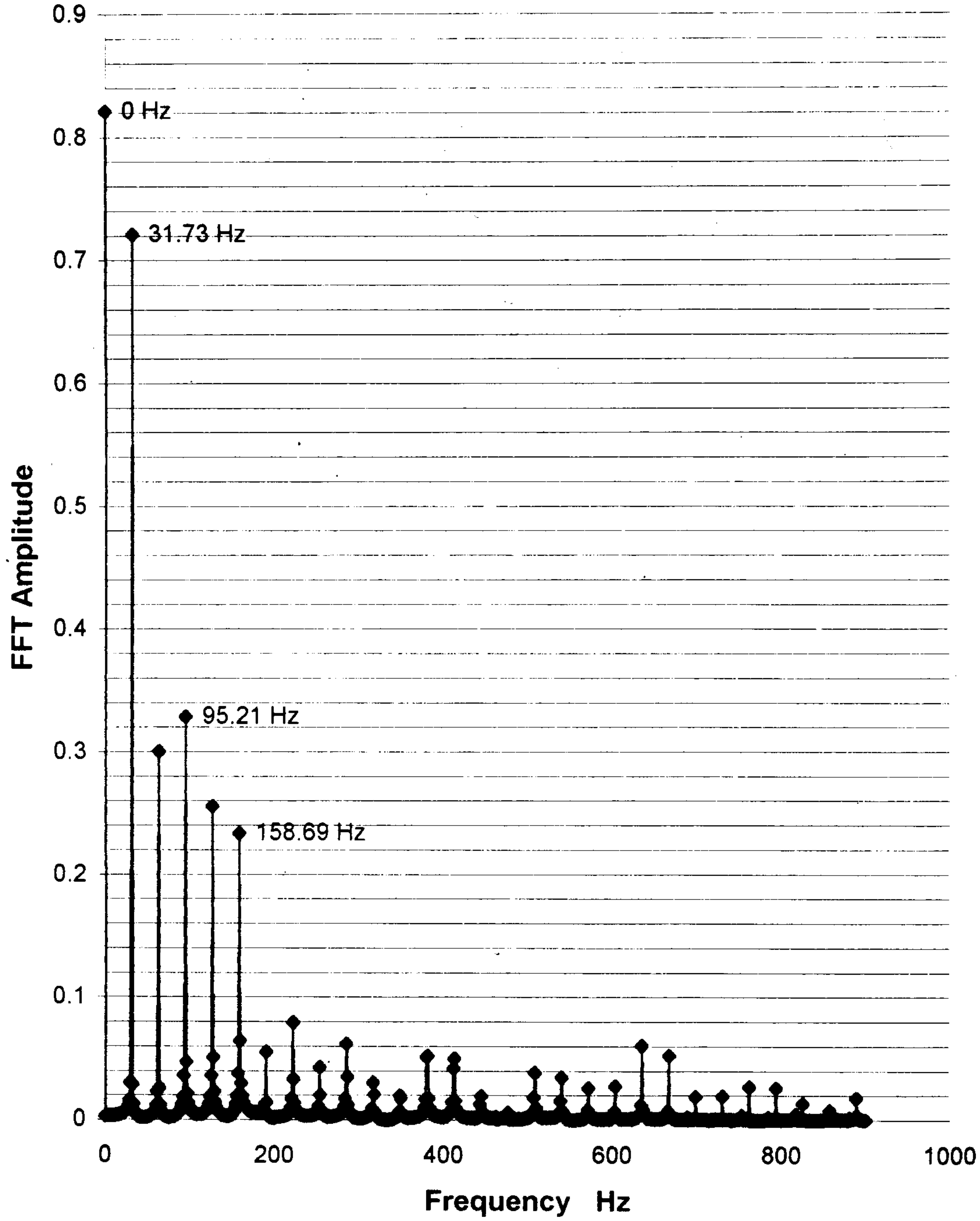

Figure 7. Crankshaft Bending Vibration Response at 4000 RPM with no Flywheel Damper

Chapter Three

Flywheel and Damper Designs

An engine's flywheel is mounted at the rear of the engine on the crankshaft. It is mounted between the engine and the transmission. The flywheel reduces the torsional vibration transmitted from the engine to the transmission. A related problem is the bending vibration of the crankshaft. By placing a damper on the crankshaft this bending vibration can be reduced. The installation location that least impacts existing engine design is the front or the rear of the crankshaft. On the front end of the crankshaft is the accessory pulley that drives the alternator, water pump, air conditioner, and other engine accessories. The proposed damper designs are to be used in place of the traditional flywheel, but the ideas could be used at the front of the crankshaft. This choice was made based on imposed size restrains at the front of the crankshaft. A larger damper can have more of an affect on the crankshaft's vibration than a smaller damper. Also, by placing a damper between the engine and transmission, wear and noise will be decreased.

Theoretical Damper

A theoretical damper is used to determine the effects of a damper on the vibration of the crankshaft. The damper is imaginary because it is connected to ground, which has no motion. In a real situation a damper is connected to some point of the vehicle which is vibrating itself. To model this damper, a damping term was added to the summation of forces and torques at the last mass point. The damping term was the product of the translational and rotational velocity components and a damping constant. This term provided a negative force or torque in the summation equations of the vibration response code. This theoretical damper acted on the nineteenth mass point. It absorbed energy from the crankshaft, reducing the amplitude of the vibration in the crankshaft which damper represented an ideal damping situation.

Solid Flywheel

Torsional vibration is typically the most important engine vibration problem. The conventional method of decreasing the torsional vibration in the crankshaft is a flywheel. Its added inertial mass reduces torsional gas pressure pulses that cause vibration. The effect on bending vibration from this type damper were explored. A round flywheel was added to the crankshaft model. The inertial mass was designed to combat torsional vibration, so this value would be held constant while optimizing the bending inertial mass.

The inertial mass of a Saturn inline four cylinder engine's flywheel was used as an ideal value. The geometric design constraints consisted of a maximum diameter of eight inches and a maximum thickness of one and a quarter inches. These constraints were used to enable comparison of the damper/absorber types given maximum volume.

Elastomer Damper

An elastomer damper is a damping system that is common in vibration control situations. The damper utilizes deformation of an elastomer. The viscoelastic behavior of the elastomer damps vibrations. This type of damper is also desirable for another reason, cost. Elastomer materials are inexpensive and easily processed into shapes.

The damper consists of a disk that is attached to the crankshaft. An inertial mass is then attached to the disk and separated by an elastomer. A diagram of the elastomer damper is provided as Figure 8.

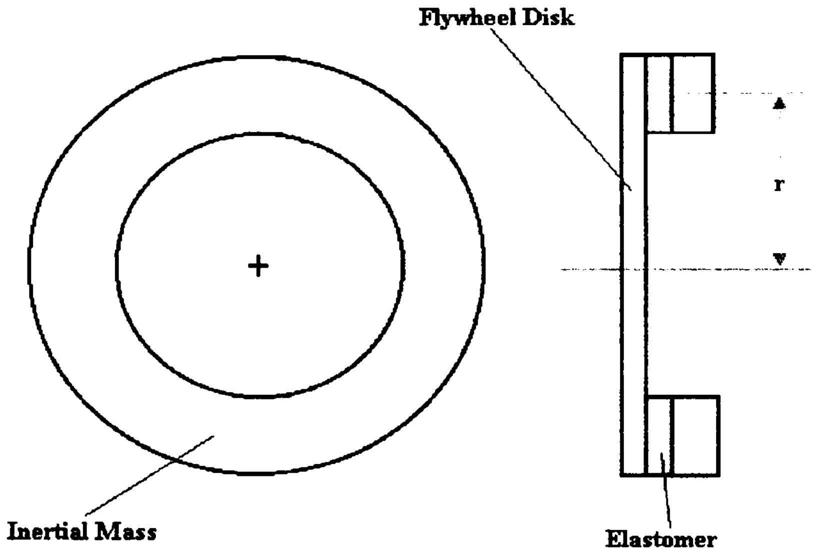

Figure 8. Elastomer Damper Model

When the crankshaft bends, the disk rotates about an axis perpendicular to the rotational axis. Angular momentum from the disk rotation opposes displacement of the inertial mass ring. So, as the disk rotates, the elastomer between the disk and ring is deformed, and a force is exerted on both the disk and the inertial mass. Along with the force the elastomer absorbs some of the energy of this encounter. A phase angle is created between the motion of the disk and the inertial mass. The phase angle is an important factor in increasing the effectiveness of the elastomer damper.

There are two models that represent dynamic elastomer damping. These models are described by spring and dashpot models. The Voigt model is used for finding stress while the Maxwell model is used to find strain. The models used to describe them use the effects of springs and dampers. The Voigt model utilizes a spring and a damper connected in parallel. The Maxwell model uses a spring and a damper connected in series. A mathematical representation of the Voigt model is

$$\sigma = \left(G'_{elastomer}\right)\varepsilon_{elastomer} + \mu\frac{d\varepsilon}{dt}$$

where σ = material's stress,
G'= modulus of elasticity,
ε = material's strain,
μ = damping factor.

The Maxwell model's mathematical representation is

$$\varepsilon = \left(E'_{elastomer}\right)\sigma_{elastomer} + \mu\frac{d\sigma}{dt}$$

where ε = strain,
E = modulus of rigidity,
σ = stress,
μ = damping coefficient.

The choice of the model used in a representation is based on what is known, stress or strain. Both of these models assume a linear stress-strain relationship during dynamic situations.

Since the strain in the material in the elastomer damper can be calculated, the Voigt model is used. The first term in the Voigt model equation behaves like a spring, and the second term behaves like a damper. The deformation of the elastomer is

$$\delta = r(\sin\theta_1 - \sin\theta_2)$$

where δ = material deformation,
r = distance from center of shaft to the material,
θ_1 = disk rotation angle,
θ_2 = elastomer ring rotation angle.

Strain in the elastomer material becomes

$$\varepsilon = \frac{\delta}{h} = \frac{r}{h}(\sin\theta_1 - \sin\theta_2)$$

where ε = material strain,
δ = material deformation,
h = material thickness.

By taking the first derivative with respect to time, t, the rate of strain is

$$\frac{d\varepsilon}{dt} = \frac{r}{h}\left(\frac{d\theta_1}{dt} - \frac{d\theta_2}{dt}\right)$$

The values of G' and μ are experimentally determined values. The test consists of a test specimen is placed in dynamic hysteresis. This is done by applying a load at a given test frequency. The results of the test are measures of elastic, G', and damping, G'', properties of the material. A damping coefficient is found from

$$\mu = \frac{G"}{\omega}$$

where μ = damping coefficient,
G''' = experimental value,
ω = test frequency.

Both of these values are temperature and frequency dependent. Therefore, the damper material must be matched or tuned to engine operating temperatures and vibration frequencies.

Mathematical Elastomer Model

With all the parts of the Voigt model and the elastic and damping coefficients known, the model could be added to the crankshaft response program. The stress at the elastomer-disk interface was calculated from the strain and the Voigt model. This stress exerts a force on both the disk and the inertial ring. This force is

$$F = \sigma \times A$$

where F = elastomer's force,
σ = stress,
A = interface area.

The force of the elastomer created a torque on the disk opposing the bending vibration torque. The equation for the torque is a product of the force and the moment arm. The relationahip is given by

$$T = F \times R$$

where T = torque,
F = elastomer force,
R = damper's torque arm.

For a ring shaped piece of elastomer, the torque arm is equal to its outer diameter minus one half of its width. The damper was added to the crankshaft model by introducing the disk as the nineteenth mass point , and the inertial mass served as the twentieth mass point. The torque created by the elastomer was added to both points' summation of torques equations.

Viscous Roller Damper

The device is an invention of Dr. Frank Speckhart. The record of invention which proposes this design is provided in Appendix B. It is intended for use with any size or type of internal combustion engine. The device is mounted to the rear of the crankshaft where size and therefore effectiveness can be maximized. Its design starts with a solid steel disk 8 inches in diameter and 1 1/4 inch thick. It is mounted to the crankshaft so that its axis of symmetry is aligned to the crankshaft's axis of rotation The cylinder has four holes, or cavities, perpendicular to the axis of rotation. Each sealed cavity contains a roller suspended in a viscous fluid. Each roller is weighted so that the center of mass and the center of rotation are not at the same point. The device is made with steel due to its weight, strength, and wear properties. The viscous roller device is shown in Figure 9.

During engine operation, damper rotation is induced by the crankshaft bending. Simultaneously the device is rotating at the engine speed, ϕ. Because the rollers are not symmetric in weight, the centrifugal force acting on the heavy side of the roller causes the

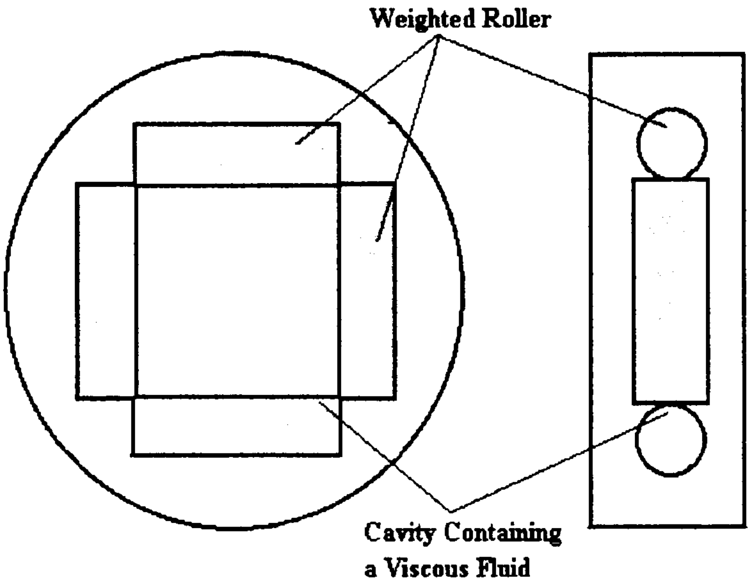

Figure 9. Viscous Roller Device

roller to rotate in the cavity. The centrifugal force and direction of roller rotation are in the opposite direction of the device's rotation, θ. A drawing of the device's exaggerated deflection and the roller position illustrates this in Figure 10. The viscous fluid allows the weighted roller to slide instead of roll. Relative motion of the roller and the cylinder produces a shear in the viscous fluid. The viscous shear of the fluid is the mechanism that dissipates energy.

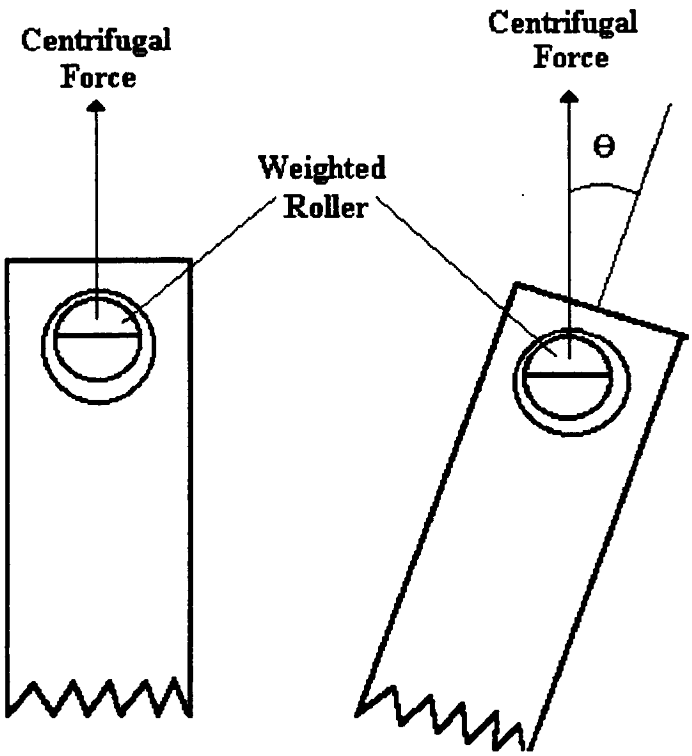

Figure 10. Exaggerated View of Viscous Roller Motion

Viscous Friction

If the fluid is imagined to be made of individual layers, the velocity gradient is dependent upon the friction between these layers. The fluid velocity at a surface is assumed to be the same as the surface's. The model in Figure 11 represents this idea.

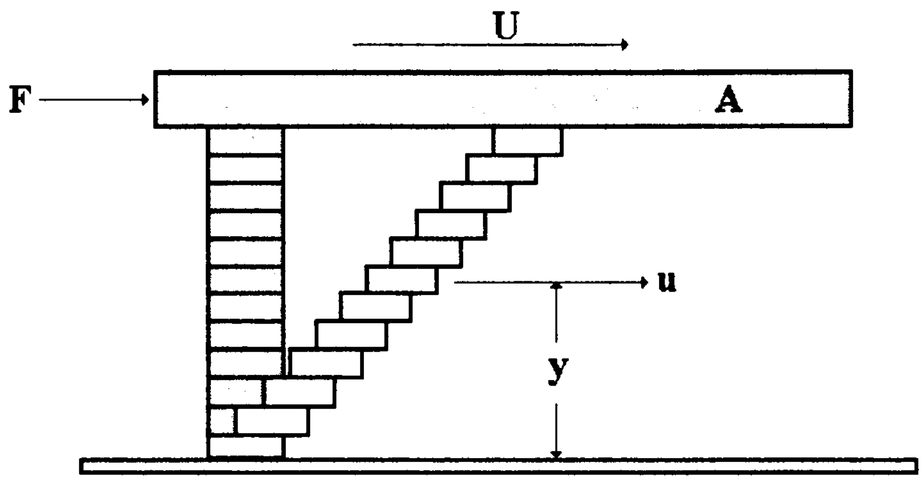

Figure 11. Viscous Shear Model

The shear in a fluid is governed by Newton's law of viscous flow that is represented by

$$\tau = \frac{F}{A} = \mu \frac{du}{dy}$$

where τ = fluid shear,
μ= dynamic viscosity of the fluid,
F = applied force,
A = interface area.

The viscosity can be thought of as a measure of the internal frictional resistance of the fluid [11]. In the case of the viscous roller damper, the cavity and the roller are modeled by the two surfaces. Viscous shear transmits energy from the outer cavity to the roller. The transmitted energy increases the kinetic energy in the roller. The viscous shear between two surfaces is a widely studied lubrication problem.

There are several different types of lubrication regimes each discerned by different frictional behavior. Each regime has its own theories to predict the coefficient of friction that is a dimensionless parameter that describes frictional characteristics. Boundary lubrication is the first to form. In this regime the lubricant film is only a few molecules in thickness. Because of the thin lubrication thickness, the choice of surface finish and fluid viscosity play an important role in determining the degree of contact between the two surfaces. As speed is increased, the lubricant film thickness increases. When the film is relatively thick, it is described by the hydrodynamic regime. In this regime, experimentally derived models predict the fluid's behavior. As the roller in the viscous roller device moves, its velocity changes from zero to some maximum. Because of this velocity variation and force fluctuations, it experiences both of these lubrication regimes.

Boundary lubrication is the first to form, and it typically describes low velocity, high temperature, or heavily loaded bearings. A fluid film has started to form, but surface contact occurs. In this regime the surface finish and fluid viscosity are important factors in determining the friction coefficient. Chemical composition of the fluid is more important than its viscosity in this regime. Wear and heat are important design considerations.

As speed, temperature, or load is decreased the lubrication enters a mixed regime. A film has developed, but it cannot provide full film lubrication. The mixed and boundary lubrication regimes are also unstable. The lack of stability exists due to the non-self correcting relationship between friction, temperature, and viscosity. Several theories have attempted to describe the frictional characteristics of this regime.

When the fluid film has fully formed, there is no surface to surface contact, and the stability can be explained by the laws of fluid mechanics. The fluid is in the hydrodynamic regime. In this regime, the fluid is pulled into the surfaces' interface with a high enough velocity to prevent contact. This regime is also called full film lubrication.

Journal Bearings

A journal bearing is a common mechanism that has a similar geometry and function as viscous roller device. The bearing's geometry is described in Figure 12. The outer cylinder of the damper is much the same as the bearing, and the roller is modeled as the journal. Journal force varies with time as the crankshaft vibrates. The distance h_o is the minimum film thickness for a given geometry, viscosity, journal speed, and load. The distance, e, is the eccentricity which is the distance between the centers of the roller and the bearing. Reynold's theorized the lubricant adhering to the bearing as well as the journal. The fluid is pulled between the journal and the bearing with enough intensity to support the bearing load. When this condition is established the bearing and the journal are a distance of h_o apart.

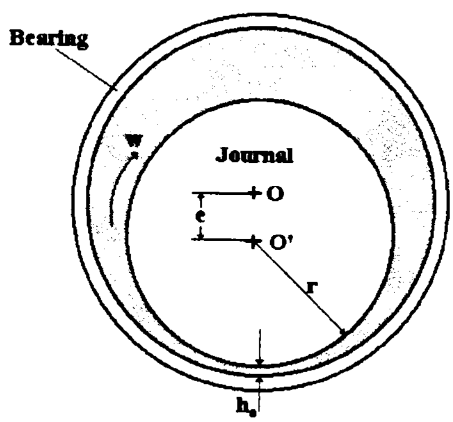

Figure 12. Journal Bearing Geometry

The basic premise of the journal bearing utilizes hydrodynamic lubrication. The theory of hydrodynamic lubrication originated in England in the 1880's by Beauchamp Tower. Tower experimented with friction and pressure of railroad journal bearings. His results had such regularity the Osborne Reynolds sought a law to relate friction, pressure, and velocity of the lubricant. The present mathematical hydrodynamic theory is based on Reynolds' work. The classical Reynolds equation for one dimensional flow is

$$\frac{\partial}{\partial x}\left(\frac{h^3}{\mu}\frac{\partial p}{\partial x}\right)-\frac{\partial}{\partial z}\left(\frac{h^3}{\mu}\frac{\partial p}{\partial z}\right)=-6U\frac{\partial h}{\partial x}$$

where x = the direction of rotation,
h_o = film thickness,
μ = viscosity,
p = pressure,
z = direction perpendicular to the direction of rotation.

There is no general solution to this equation. Approximate solutions have been obtained using relaxation methods, analogies, and other methods. One such approximation was performed by Sommerfield who noticed the following functional relationship,

$$\frac{r}{c}f=\Phi\left[\left(\frac{r}{c}\right)^2\mu\frac{N}{P}\right]$$

where r = journal radius,
c = radial clearance,
f = non dimensional friction factor,
μ = absolute viscosity,
N = significant speed,
P = load per unit of projected bearing area.

Sommerfield derived a dimensionless parameter that was given his name. This parameter is found by

$$S = \left(\frac{r}{c}\right)^2 \frac{\mu N}{P}$$

where S = Sommerfield's number,
r = journal radius,
c = radial clearance,
μ = lubricant viscosity,
N = journal speed,
P = bearing load.

In 1958, Albert Raymondi and John Boyd used an iteration technique to solve Reynolds equation using a computer. Their results were published in three papers containing 45 graphs and 6 tables of numerical results. These graphs and tables relate temperature, viscosity, film thickness, position angle, coefficient of friction, flow rate, film pressure, and Sommerfield's number [11]. These graphs and tables are the basis for most bearing design today.

Mathematical Roller Damper Model

As mentioned earlier, the damping effect of the device is derived from the viscous effects of the fluid which is similar to a journal bearing. As the damper is deflected, a centrifugal force acts on the center of mass of the roller. This force causes a torque around the geometric center of the roller. The torque rotates the roller in the fluid filled cavity. The roller rotation is opposite the case rotation. The key to modeling the viscous roller damper is correctly modeling the viscous friction between the roller and the cavity.

There are two equations of motion that describe the interaction between the damper case and the roller. Both of these equations come from summing the torques acting upon each. Summation of torques on the case provides

$$I_{case}\frac{d^2\theta}{dt^2} = T_{input} - T_{friction}$$

where I_{case} = mass moment of inertia,
θ = angular deflection,
T_{input} = input torque from the crankshaft,
$T_{friction}$ = viscous friction torque.

Summation of torques on the roller provides

$$I_{roller}\frac{d^2\theta}{dt^2} = T_{friction} - T_{centrifugal}$$

where I_{roller} = mass moment of inertia of the roller,
θ = angular deflection of the roller,
$T_{friction}$ = viscous friction torque,
$T_{centrifugal}$ = torque from the centrifugal force.

These second order coupled equations represent the damper system. As stated before, the damper and a journal bearing geometries are very similar. The results of past studies on journal bearing will be the basis of the modeling.

Since bearing data is tested using steady state conditions, the assumption of constant velocity and loading had to be used. Using this assumption and Raymondi and Boyd's data, the friction torque is a function of Sommerfield's number. The non-dimensional friction factor is found using Sommerfield's number. Torque is then found using the equation

$$T_{friction} = f \times W \times r$$

where $T_{friction}$ = viscous friction torque,
f = friction factor,
W = bearing load,
r = bearing radius.

The relationship between Sommerfield's number and the friction coefficient is very complicated. The relationship is linear on a log-log plot, and it is described for different length to diameter, l/d, ratios. Interpolation is used for any l/d ratio not published in Raymondl and Boyd's findings. To use this method, the instantaneous velocity at each time step or an average velocity and constant load is used to calculate Sommerfield's number and the friction factor. With the friction factor, the torque on both surfaces caused by viscous friction can be calculated.

However if the load is light enough, the speed is high enough, or the viscosity is high enough, the oil film can be assumed to be uniform around the bearing [11, 13]. Petroff used the assumption that the journal and bearing geometric centers were concentric. Petroff's work can be used to describe the viscous friction torque relationship. Because the radial clearances between the cavity and the roller are a few thousandths of an inch this assumption is used. The friction force used to derive the torque is derived from

$$F = \tau \times A$$

where F = friction force,
τ = viscous shear in the fluid on the bearing surface,
A = area of the bearing surface.

Newton's law of viscous flow provides the relationship,

$$\tau = \mu \frac{U}{h}$$

where τ = viscous shear in the fluid on the bearing surface,
μ = viscosity of the fluid,
U = the significant velocity of the surface,
h = the film thickness.

Combining these equations, describing the significant velocity in terms of RPM's, and substituting the equation for the bearing's surface area provides

$$F = \frac{\mu}{c}\frac{4\pi^2 r^2 NL}{60}$$

where F = viscous frictional force,
μ = viscosity of the fluid,
c = bearing radial clearance,
r = bearing radius,
N = journal speed,
L = bearing length.

The friction torque , or moment of friction, is then

$$T = F \times r = \frac{\mu}{c}\frac{4\pi^2 r^2 NL}{60}$$

where T = friction torque,
F = friction force,
r = torque arm or bearing radius,
μ = viscosity of the fluid,
N = journal speed,
L = bearing length.

The friction torque is substituted into the two governing differential equations for the damper, and they are solved with the Runge-Kutta solver.

Chapter Four

Discussion of Results

A crankshaft undergoes a bending vibration due to the gas pressure pulses of engine firing. The crankshaft bending response code generated the vertical and angular displacements and velocities of all nineteen mass points in the model. Due to the volume of data generated by the code only two mass points were monitored. These points were the tenth and nineteenth mass points. By monitoring only two points the data file size was kept under 1.44 megabytes. To find the vibration's frequencies, a fast Fourier Transform, FFT, was performed on the displacement data. To do this PSPlot was used. PSPlot is a department licensed data analysis program. The FFT produced the frequency, amplitude, and phase of the displacement data. The amplitude is a representation of the relative energy of the vibration at a particular frequency. The amplitude plotted verses frequency data provides a FFT spectral representation of the vibration. PSPlot performs an FFT on a power of two data points no greater than 4096. To get the maximum resolution in the spectral analysis this maximum number was used. These data points were taken from the steady state crankshaft vibration. The crankshaft speed was increased by 500 RPM from 1500 RPM to 6000 RPM. This speed range encompasses the typical operating range of an engine. As stated before and reported in earlier studies, the problem bending vibration range was between 200 Hz and 500 Hz.

Each of the test cases consisted of 4096 points ranging in frequency from 0 Hz to 1283 Hz. Comparison of the FFT spectral analysis is tedious and confusing without the use of a statistic. So, for the purpose of data comparison, the sum and the maximum of the FFT amplitude in the problem frequency band were used. The band extended 50 Hz past the reported problem area to provide more insight into the problem. The sum is simply the addition of all the FFT amplitudes in the 150 Hz to 550 Hz frequency band. The sum provides the relative amount of vibrational energy in the band. The maximum describes any peaks or spikes in the band which skew the comparison of the amplitude sums. These spikes need to be identified because they are the cause of noise and even failure of engine components. In combination these statistics were simple to obtain and provided the needed means of comparison.

PSplot test

To test the accuracy of the spectral analysis, a FFT was performed on a signal consisting of known components. The sampled signal was created by a simple QuickBASIC program, and it sampled a signal composed of superimposed 20 Hz, 60 Hz, 100 Hz, 140 Hz, and 180 Hz signals with the same amplitude. The signal generating program is provided in Appendix A. Figure 13 is a frequency analysis plot of the sampled test signal data. The plotted peak's frequencies were within +/-0.53 Hz of the known test signal frequencies. The difference in the amplitude of each signal's peak, even though they were equal in the input signal, were caused by the interference of the different waves composing the signal. Because of the nature this superposition, individual amplitudes were added or subtracted as the test signal is created. Signal leakage caused the difference in

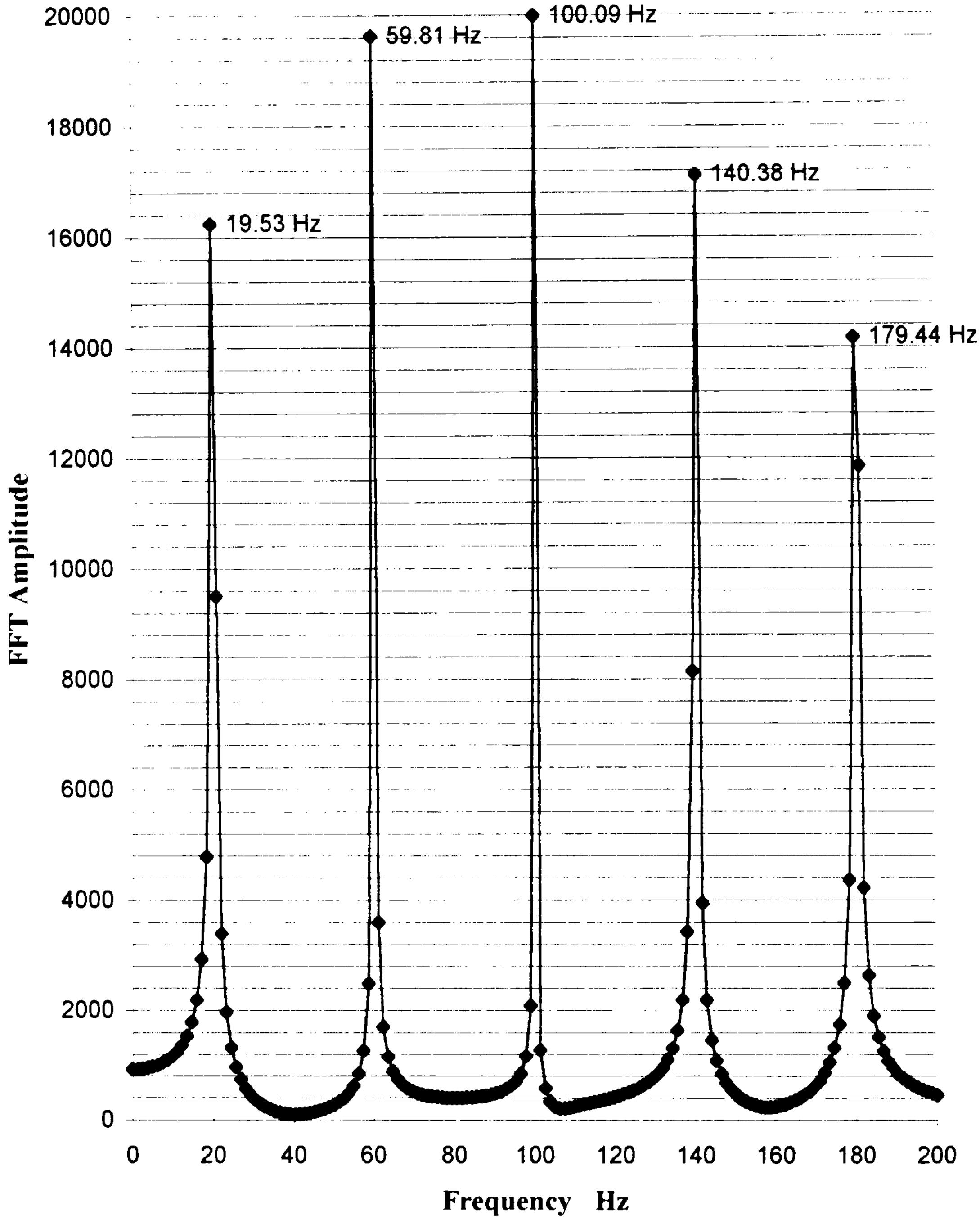

Figure 13. PSPlot FFT Analysis of a Known Input Signal

the width of the base of the component frequency peaks. This signal leakage was caused by the digital sampling of the test signal and the FFT's smoothing effect. Increasing the sampling frequency decreased the leakage.

Free End

A baseline for the crankshaft vibration was first established. This baseline was established by running the program without a flywheel. The tenth mass point modeled the portion of the crankshaft at the center crankshaft bearing. The nineteenth mass point modeled a 2.25 inch diameter 1.25 inch long portion of crankshaft hanging freely past the last engine bearing. Plots of the displacement verses time for the tenth and nineteenth mass points at 4000 RPM are provided in Figure 14 and 15. Vibrational amplitude of the tenth mass point at 4000 RPM was between 0.000441 inch and -0.00172 inch with a mean amplitude of -0.0005. The vibrational amplitude at the same speed of the nineteenth mass point was between 0.000595 inch and -0.00144 inch with a mean amplitude of -0.0002. The negative mean of both the vibrations came from the firing of a cylinder every 180 degrees of crank rotation. This firing placed the crankshaft in a constant deflection causing the negative mean amplitude of both mass points.

Using PSPlot, the FFT spectrum analysis for the tenth and nineteenth mass points are plotted as Figure 16 and 17, respectively. At the tenth mass point, the first peak at 0 Hz occurs because the crankshaft was modeled as a rigid body. The second peak is the half order component of engine speed at 31.73 Hz. The other peaks occur a half order

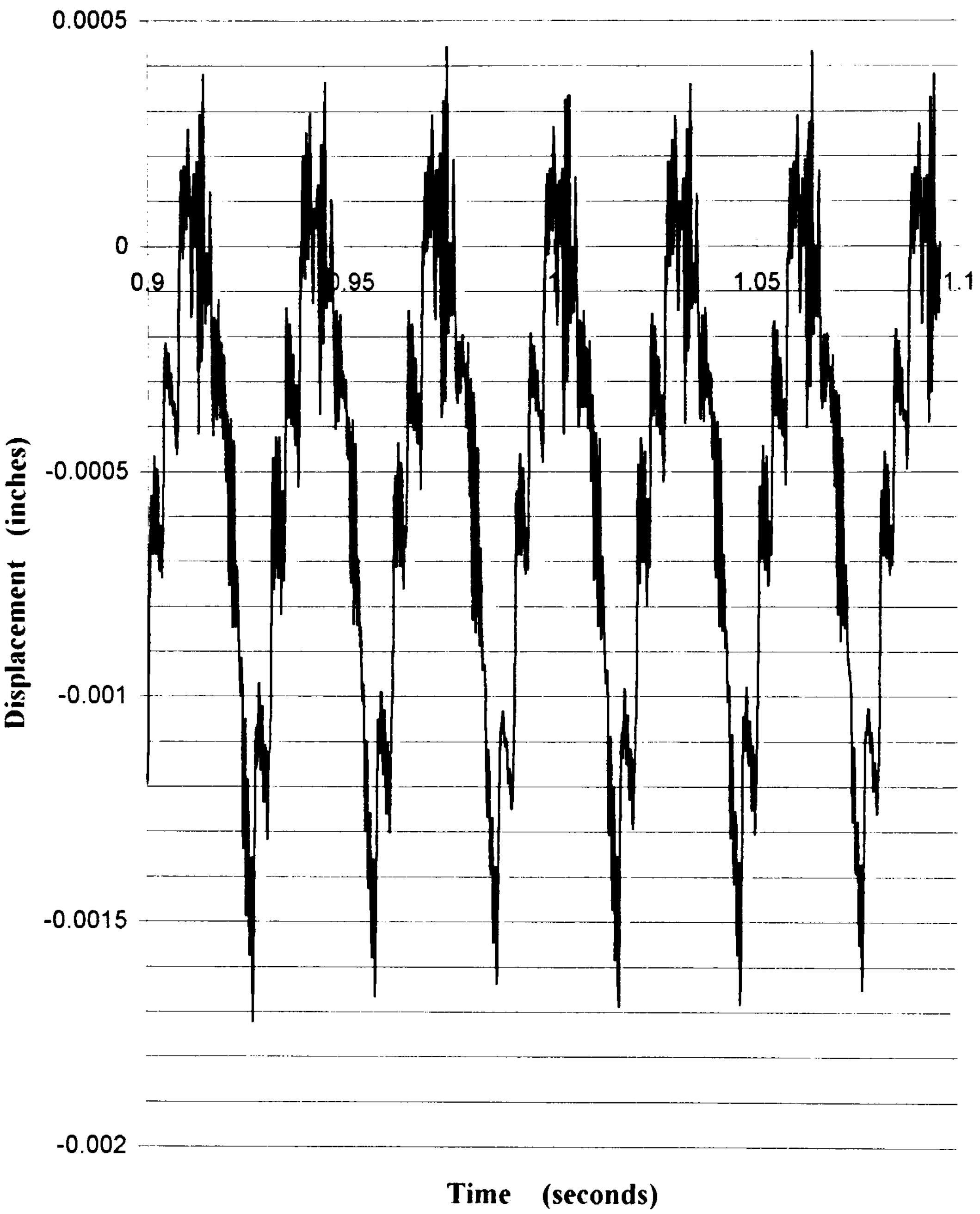

Figure 14. Displacement verses Time for the Tenth Mass Point at 4000 RPM for the Free End Configuration

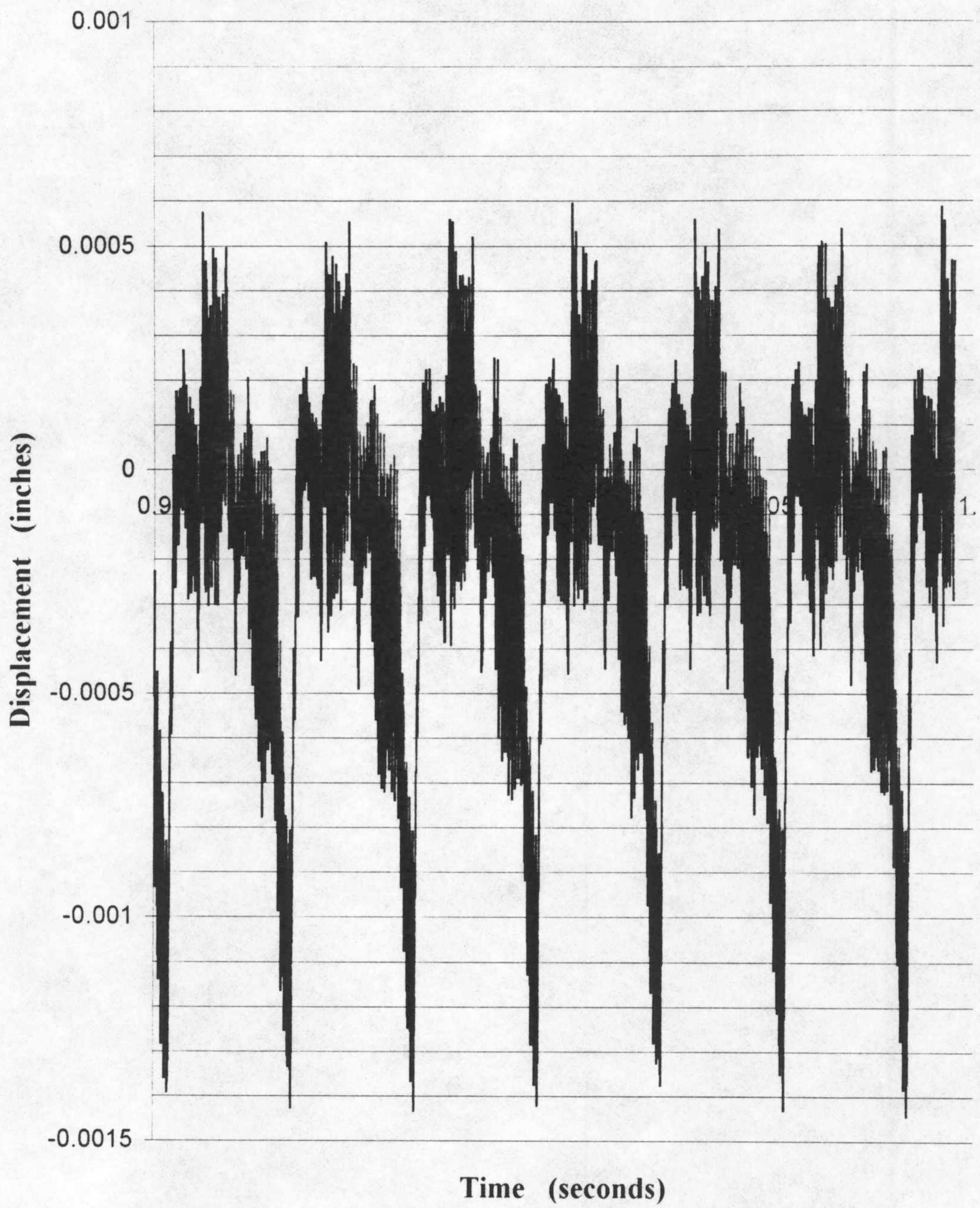

Figure 15. Displacement verses time for the Nineteenth Mass Point at 4000 RPM for Free End Configuration

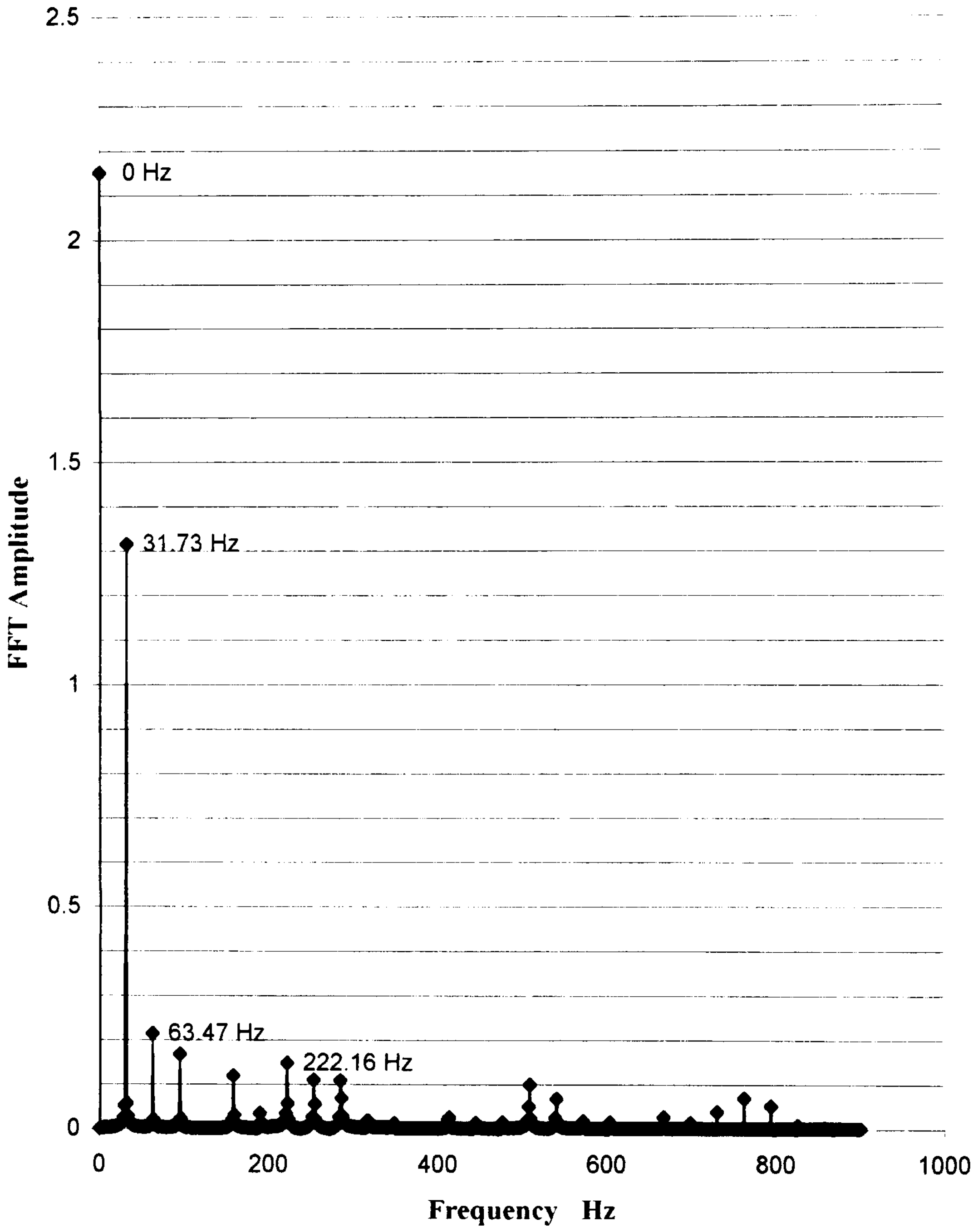

Figure 16. FFT Spectrum Analysis for the Tenth Mass Point at 4000 RPM for Free End Configuration

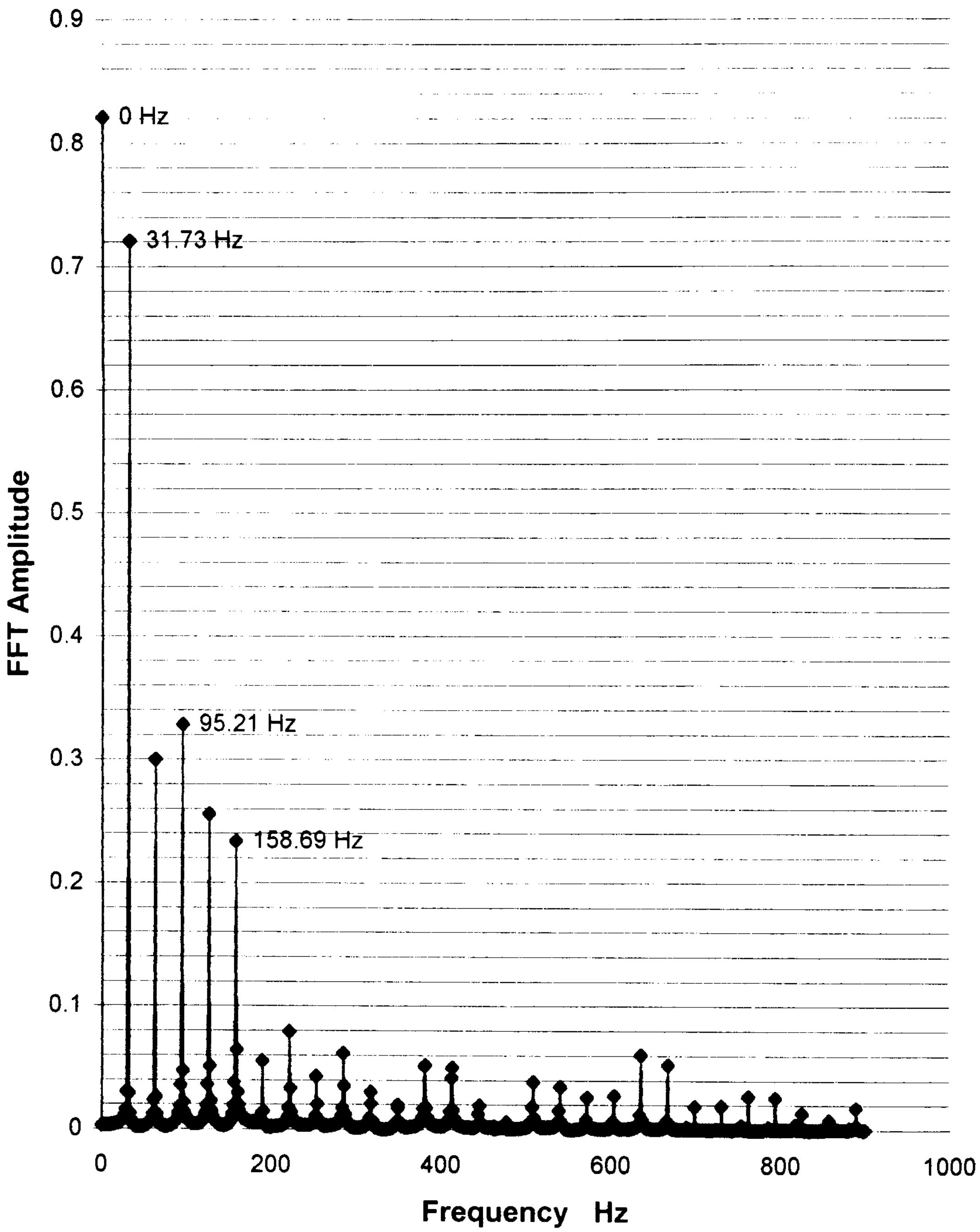

Figure 17. FFT Spectrum Analysis for the Nineteenth Mass Point at 4000 RPM for Free End Configuration

multiples of engine speed. The same 31.73 Hz peak was in the nineteenth mass point's plot. The other peaks are again multiples of the half order component of engine speed.

Figure 18 shows just the problem frequency band of the FFT analysis for the tenth mass point. Several of the peaks are identified for reference. At the tenth mass point the majority of the vibrational energy was lower than 285.64 Hz and greater than 509.03 Hz. The problem range of the FFT analysis for the nineteenth mass point is plotted in Figure 19. Several peaks occur at the same peak frequencies as the tenth mass point. The 285.64 Hz to 509.03 Hz range of the nineteenth mass point analysis was no longer void of significant peaks.

To show the differences in vibrational energy at 4000 RPM between the two mass points, Figure 20 plots the peaks of the FFT analysis in the problem band for both mass points. The nineteenth mass point contained more energy between 150 Hz and 200 Hz. The tenth mass point had more energy in the 200 Hz to 300 Hz range, but the nineteenth mass point had more in the 300 Hz to 500 Hz range. Finally, the tenth mass point had more energy in the 500 Hz to 550 Hz frequency range.

The frequency and amplitude of the FFT peaks were affected by engine speed. To illustrate this fact, Figure 21 plots the FFT analysis peaks at the nineteenth mass point for different speeds. All the speeds were not included in the interest of clarity. As speed was increased the number of peaks is decreased, but the amplitude of the peaks was increased. The greatest increase was the 250.2 Hz peak at 219 Hz. There were as many as 28 peaks at 1500 RPM, and as few as 9 peaks at 5500 RPM.

For the purpose of comparison the sum and maximum of all the FFT amplitudes

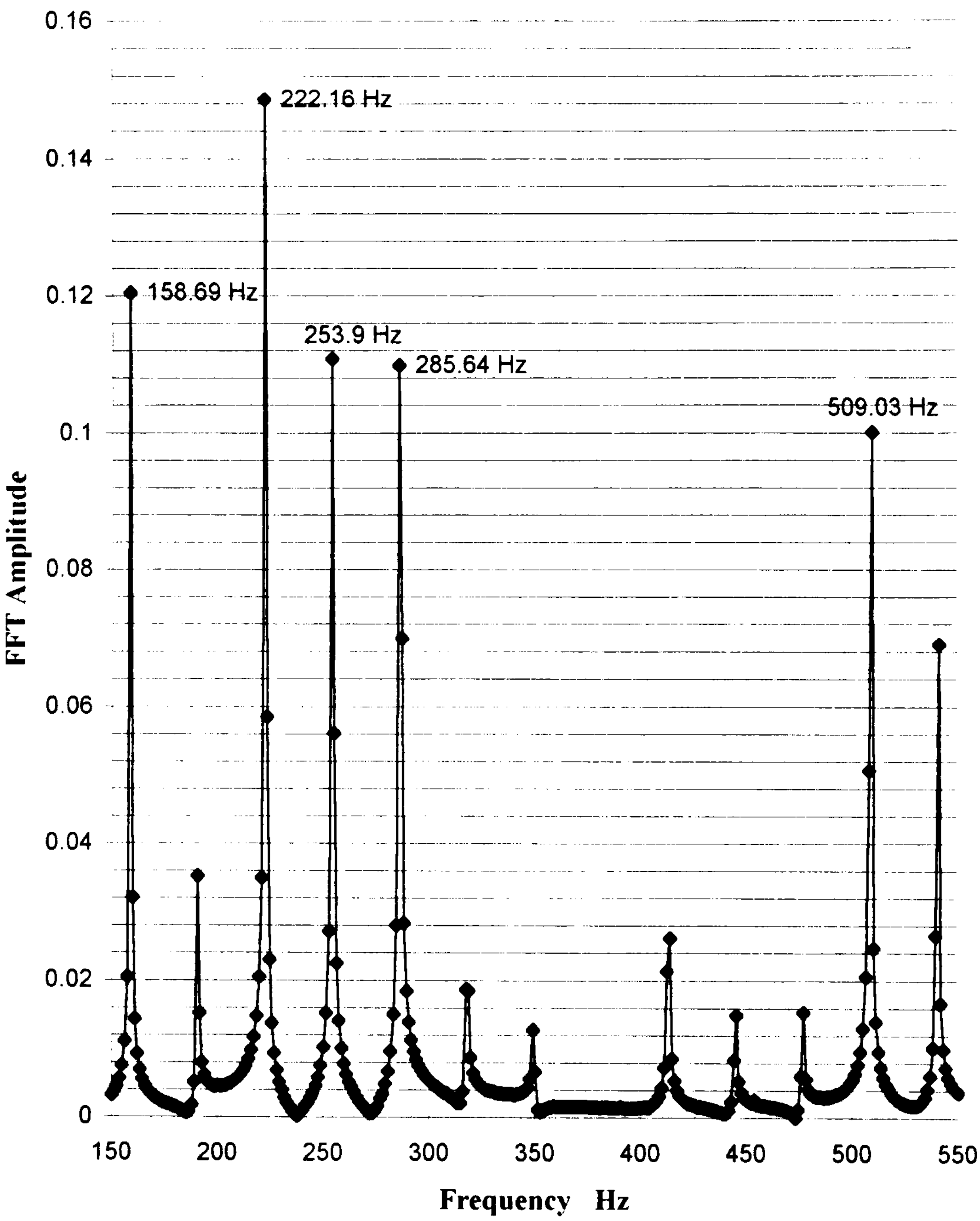

Figure 18. FFT Analysis of Problem Frequency Band of Tenth Mass Point at 4000 RPM for Free End Configuration

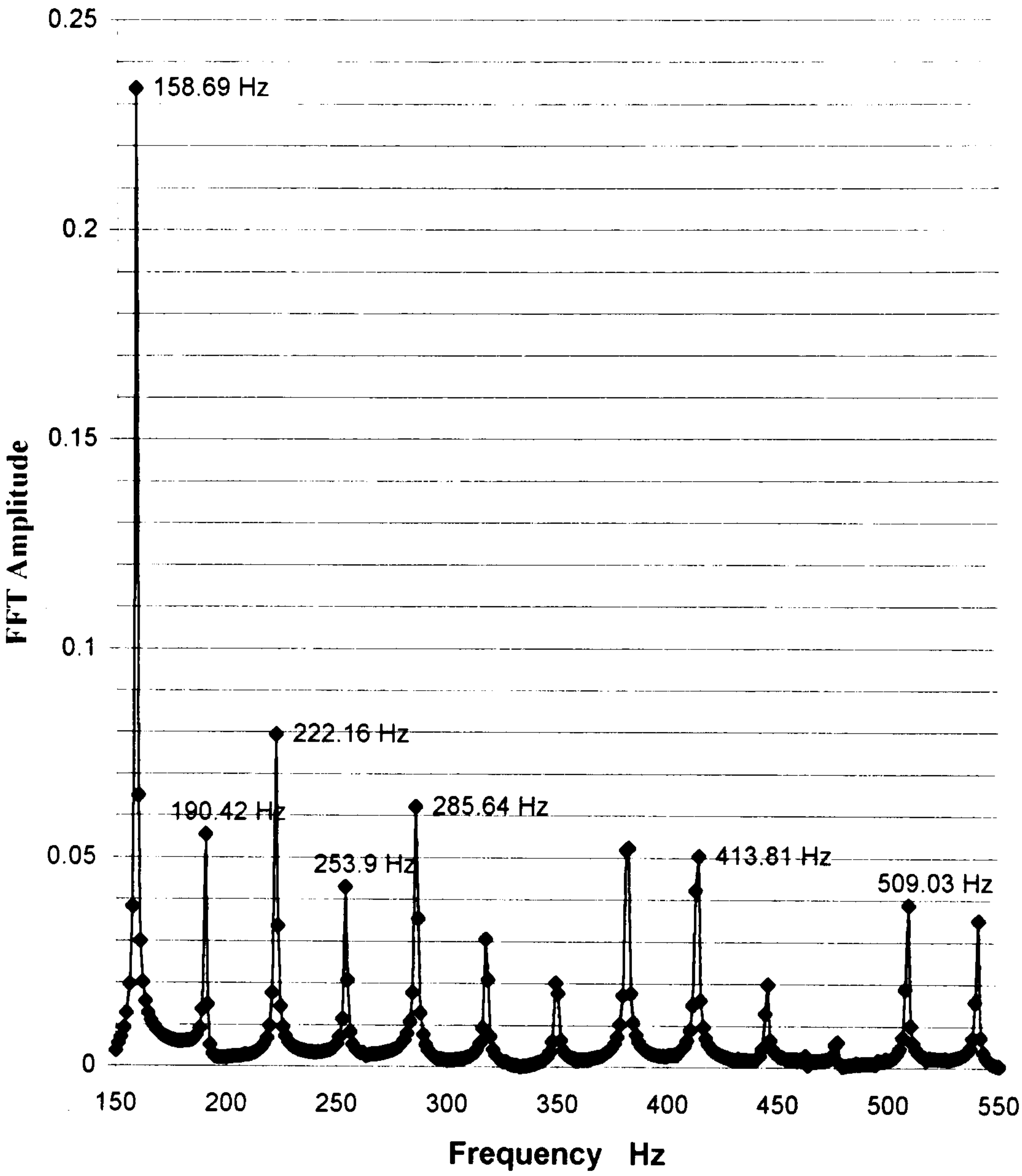

Figure 19. FFT Analysis of Problem Frequency Band of Nineteenth Mass Point at 4000 RPM for Free End Configuration

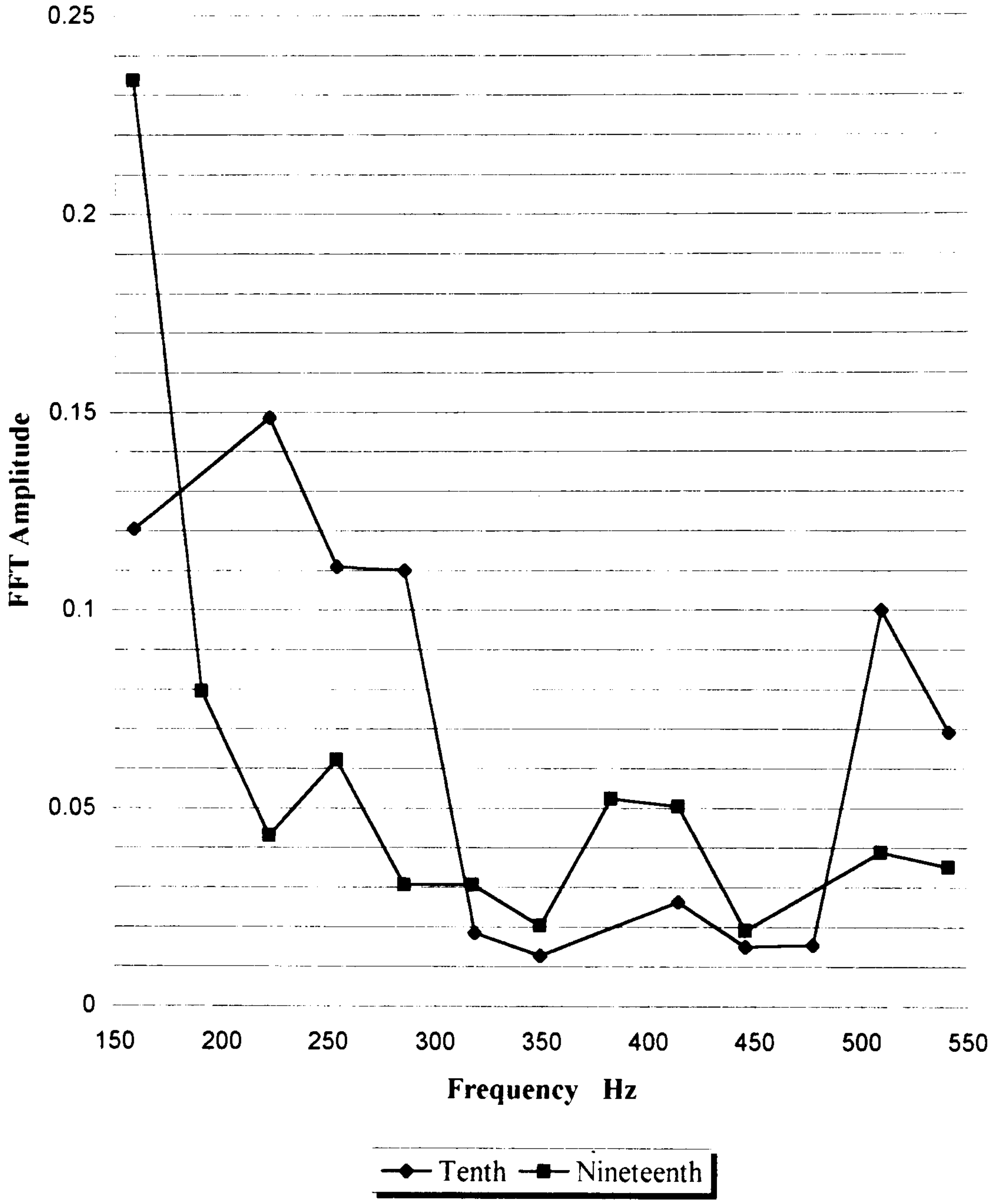

Figure 20. FFT Amplitude Peaks at 4000 RPM for Both Mass Points in the Free End Configuration

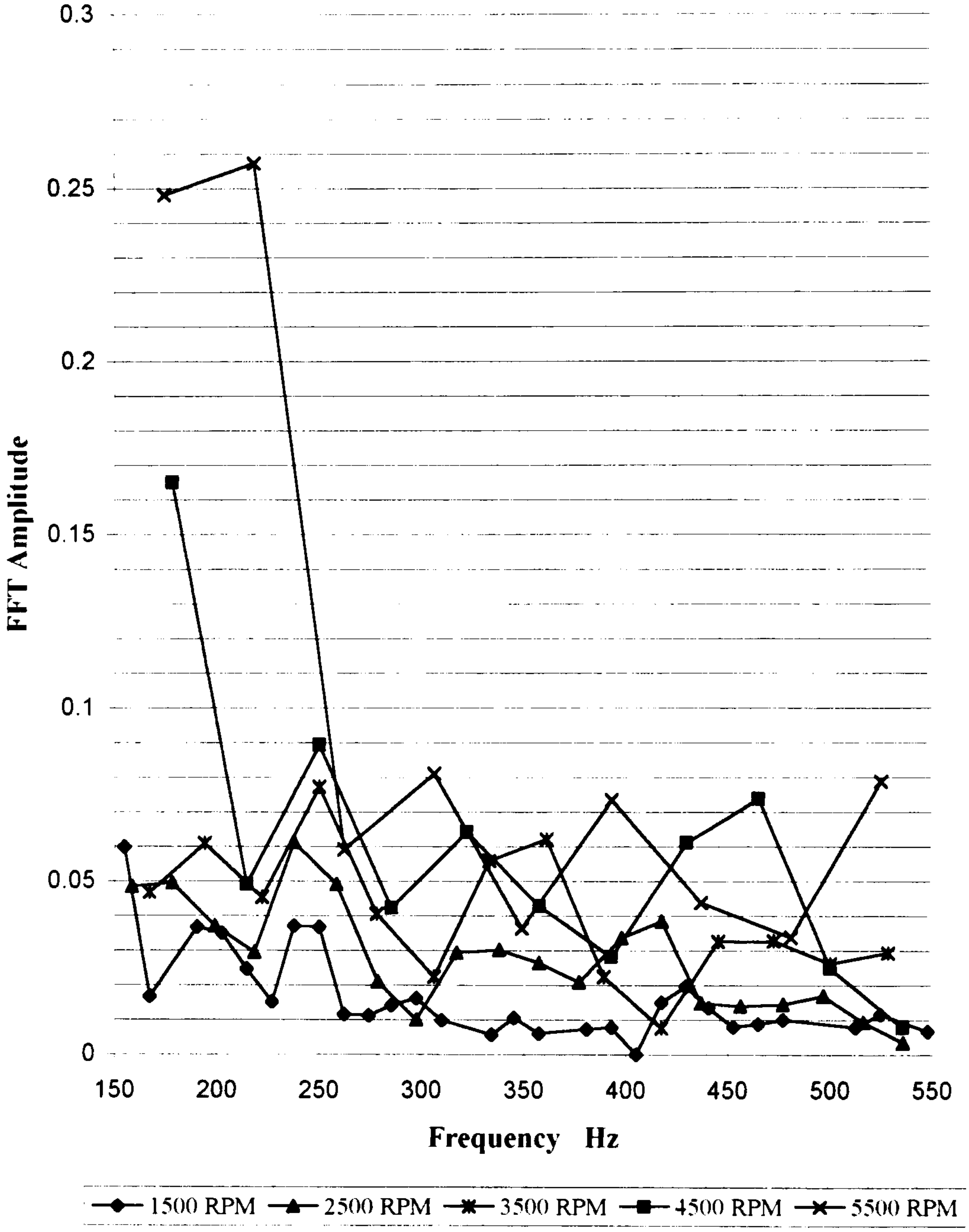

Figure 21. FFT Amplitude Peaks at Nineteenth Mass Point verses Frequency for Different Engine Speeds and Free End Configuration

between 150 Hz and 550 Hz for each speed were calculated. Figure 22 shows the FFT sum as a function of engine speed for both mass points. The FFT sum for the tenth mass point peaked at the 4000 RPM engine speed. The sum for the nineteenth mass point occurred at 5000 RPM. The tenth point had more vibrational energy within the test frequency band until the engine speed passes 4500 RPM. Figure 23 shows the FFT amplitude maximums as a function of speed for both mass points. The FFT amplitude of the tenth mass point reached a maximum when the engine speed is 4500 RPM. The maximum of the nineteenth mass point continued to climb through the typical engine operating speed range. The FFT maximum fell off sharply at 4500 RPM, then continued to climb at its previous rate. The tenth mass point had a greater FFT amplitude maximum until 3500 RPM when there is a dramatic rise in the nineteenth mass point's maximum amplitude at 4000 RPM. The sum and maximum of the FFT amplitude for the free end crankshaft model provided the basis for comparison for the vibrational damper designs.

Theoretical Damper

Theoretical Damper Test Design Specifications

To model an ideal damping situation at the rear of the crankshaft, a theoretical damper was added to the model. A damping term was added to the summation of rotational moments equation of the nineteenth mass point. The damping term consisted of a negative damping constant multiplied by the rotational velocity of the mass point. The only damping introduced to the model was in the rotational term because that is the

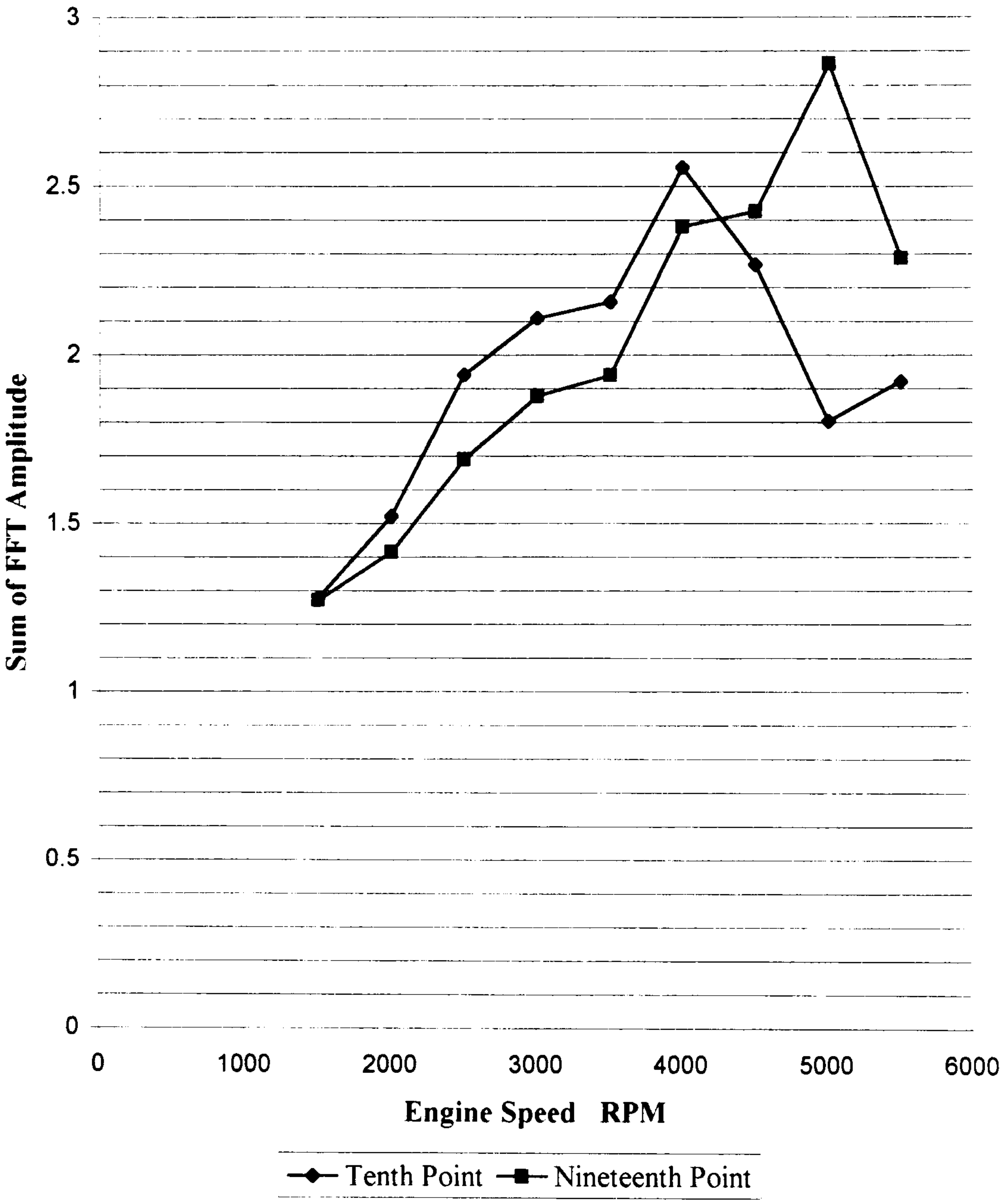

Figure 22. FFT Amplitude Sums verses Engine Speed at the Tenth and Nineteenth Mass Points for Free End Configuration

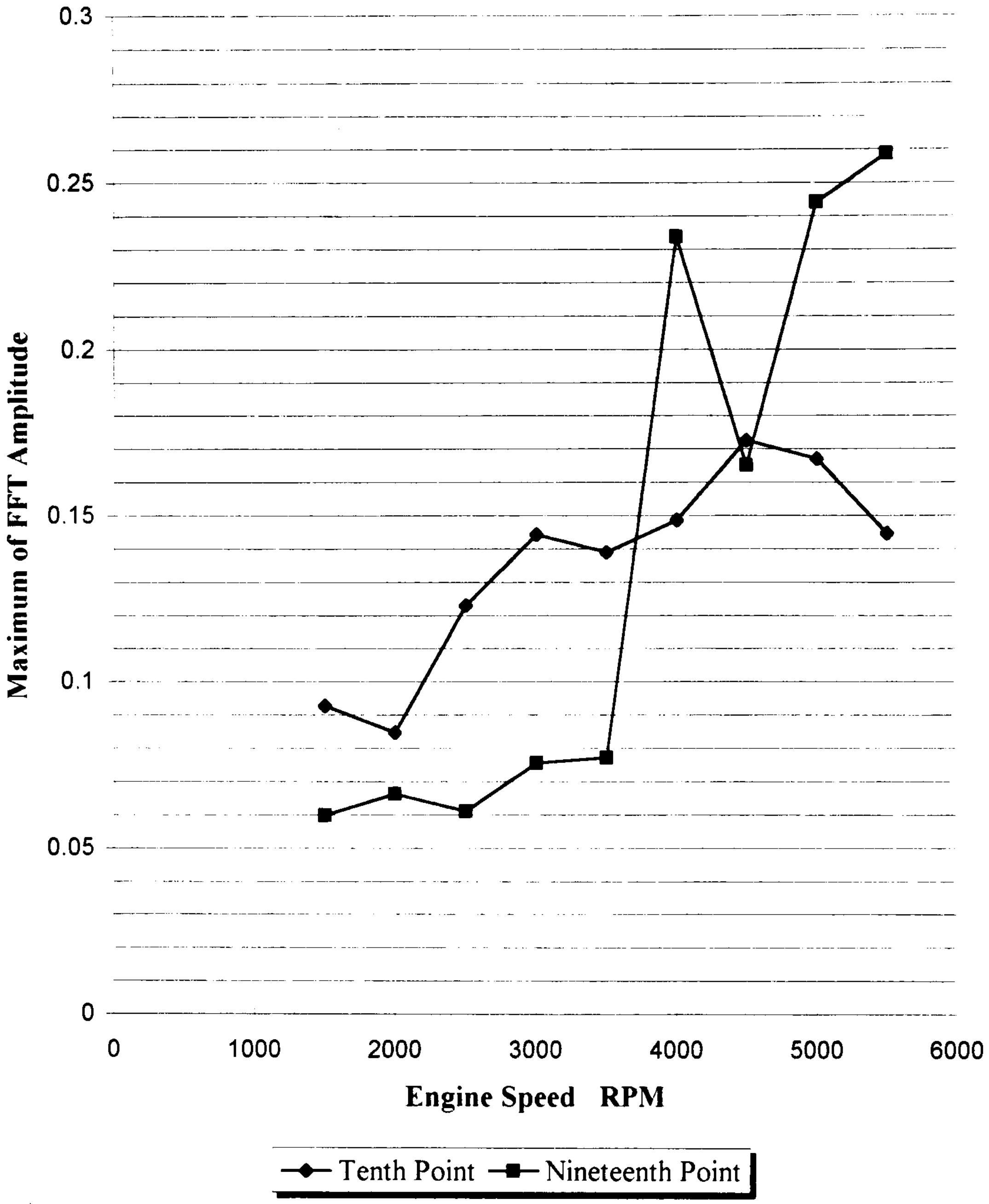

Figure 23. FFT Amplitude Maximums verses Engine Speed for the Tenth and Nineteenth Mass Points for Free End Configuration

premise of the roller and elastomer damper designs. All of these designs combat angular deflection. Damping constants of 1, 10, and 100 were used. For each damping constant the model created data for the test speed range. An example of this program is contained in Appendix A.

Bending Response Code Test Results

After performing the FFT analysis, the sum and maximum statistics were tabulated in Table 3. The sum of the FFT amplitudes of the nineteenth mass point in the problem frequency band is plotted verses the engine speed in Figure 24. Vibration was reduced as the theoretical damper value is increased. This relationship was valid for speeds equal to or less than 3000 RPM. For speeds greater than 3000 RPM the dampers all performed within +/- 0.002988 or +/-0.134% of each other. All three values affected the FFT sum between -0.336572 at 5000 RPM and +0.275294 at 5500 RPM.

Figure 25 shows the FFT maximum of the nineteenth mass point as a function of engine speed. The different values acted alike above 3000 RPM again. The largest difference occurred at 1500 RPM. The theoretical damper of 100 decreased the maximum FFT amplitude by 0.013852. The theoretical damper of 10 decreased the maximum amplitude 0.001934 at 1500 RPM. The theoretical damper of 1 increased the FFT maximum amplitude by 0.06359 at 1500 RPM. The maximums of the dampers converged and followed a single line, +/-0.001173 or +/-0.473%, as the crankshaft speed was increased. They increased the amplitude between 4000 RPM and 5000 RPM by as much as 0.00391 at 5000 RPM.

Free End

Speed	sum 10th	max 10th	sum 19th	max 19th
1500	1.27782	0.09277	1.27184	0.05983
2000	1.52111	0.08472	1.41496	0.06616
2500	1.94109	0.12292	1.68995	0.06112
3000	2.10947	0.14431	1.87741	0.07561
3500	2.1563	0.13892	1.93978	0.07712
4000	2.55505	0.14863	2.38084	0.23383
4500	2.2676	0.17249	2.42537	0.16513
5000	1.80442	0.16708	2.86256	0.24424
5500	1.92122	0.14466	2.28704	0.25872
6000				

Ideal Damper=10

Speed	sum 10th	max 10th	sum 19th	max 19th
1500	1.459433	0.074448	1.053335	0.057896
2000	1.587218	0.079121	1.356874	0.064699
2500	2.100856	0.119198	1.605225	0.062005
3000	2.130540	0.144589	1.870000	0.075000
3500	2.178799	0.139787	1.670752	0.075686
4000	2.488000	0.145000	2.294000	0.236800
4500	1.903000	0.168000	2.229000	0.168700
5000	1.790000	0.167000	2.526000	0.248000
5500	2.196000	0.139000	2.558000	0.257900
6000	2.468000	0.127500	2.824000	0.245600

Ideal Damper=1

Speed	sum 10th	max 10th	sum 19th	max 19th
1500	1.435499	0.086471	1.083012	0.066189
2000	1.313703	0.082324	1.410710	0.066143
2500	2.423392	0.116648	1.699060	0.061552
3000	2.130093	0.144587	1.873699	0.075650
3500	2.178338	0.139576	1.670230	0.075939
4000	2.488572	0.145226	2.295153	0.236897
4500	1.899481	0.168313	2.231054	0.168824
5000	1.794711	0.167684	2.525988	0.248250
5500	2.200530	0.139076	2.557360	0.258051
6000	2.467669	0.127594	2.823989	0.245612

Ideal Damper=100

Speed	sum 10th	max 10th	sum 19th	max 19th
1500	1.480689	0.064776	1.028277	0.045978
2000	1.835307	0.074724	1.297358	0.063400
2500	1.861422	0.121698	1.551939	0.062994
3000	2.132605	0.144548	1.868890	0.076173
3500	2.179244	0.139693	1.670948	0.075180
4000	2.488485	0.144159	2.290877	0.236389
4500	1.915261	0.168085	2.228066	0.168382
5000	1.788843	0.167584	2.534853	0.248150
5500	2.184951	0.139074	2.562334	0.257238
6000	2.482940	0.127383	2.833324	0.245566

Table 3. Theoretical Damper FFT Amplitude Sums and Maximums

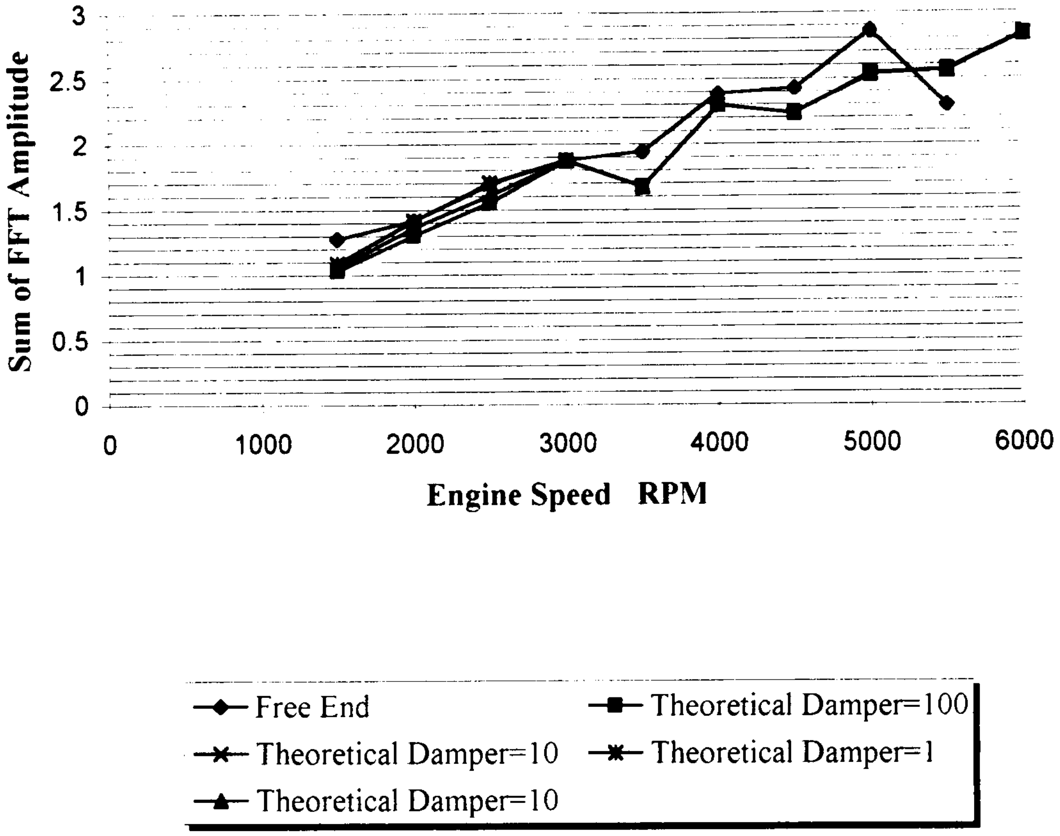

Figure 24. Theoretical Damper FFT Sum verses Engine Speed at the Nineteenth Mass Point

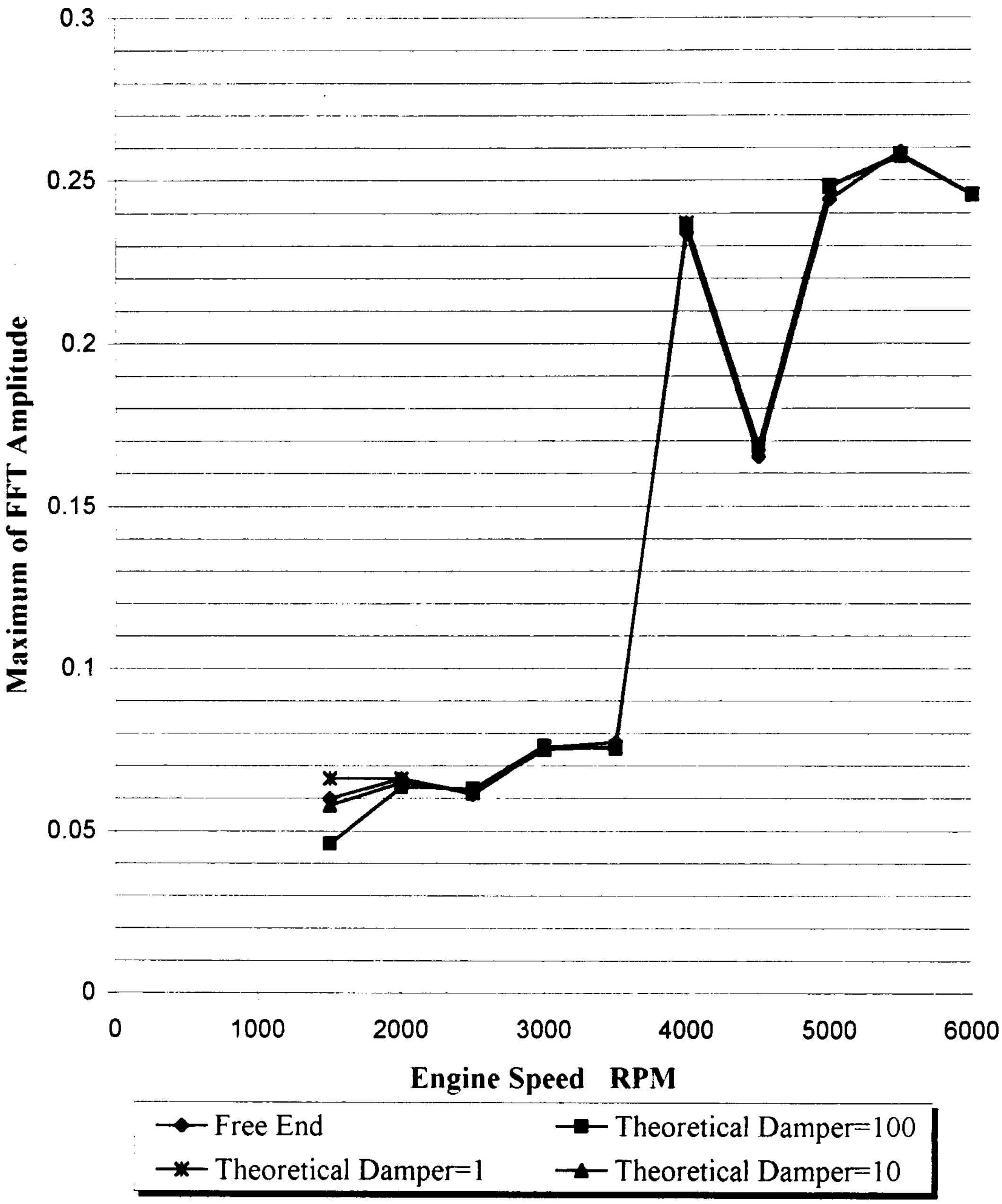

Figure 25. Theoretical Damper FFT Amplitude Maximum verses Engine Speed at the Nineteenth Mass Point

As the end of the crankshaft was restricted by the damper the vibrational characteristics of the tenth mass point were altered. Figure 26 shows the FFT amplitude sum of the tenth mass point as a function of engine speed. The three damper values created similar reactions in the tenth mass point from speeds greater than or equal to 3000 RPM. In this range, the FFT sum was reduced only between 4000 RPM and 5000 RPM by as much as 0.368119. At 3000 RPM, 3500 RPM, 5500 RPM, and 6000 RPM, the FFT sum was increased. The different damper values created different responses by the crankshaft system in the 3000 RPM and below range. The theoretical damper of 1 changed the free end vibration between -0.207407 at 2000 RPM to 0.482302 at 2500 RPM. The theoretical damper of 10 altered the vibration between -0.066108 at 2000 RPM to 0.159766 at 2500 RPM, and the theoretical damper of 100 altered the vibration between -0.079668 at 2500 RPM to 0.314197 at 2000 RPM. As the damping value was increased the FFT sum at the tenth mass point was closer to the free end data at 3000 RPM and below. For speeds greater than 3000 RPM the damping value did not significantly change the FFT sum data. The theoretical dampers reduced the FFT amplitude maximum at every speed except at 4000 RPM and 5000 RPM. The two greatest differences between the different damping values occurred at 1500 RPM and 2000 RPM. A plot of the FFT amplitude maximums at the tenth mass point as a function of engine speed is provided as Figure 27. Again the different dampers followed the same trend at speeds greater than 2500 RPM. The 100 damper provided the most damping followed by the 10 and then the 1.

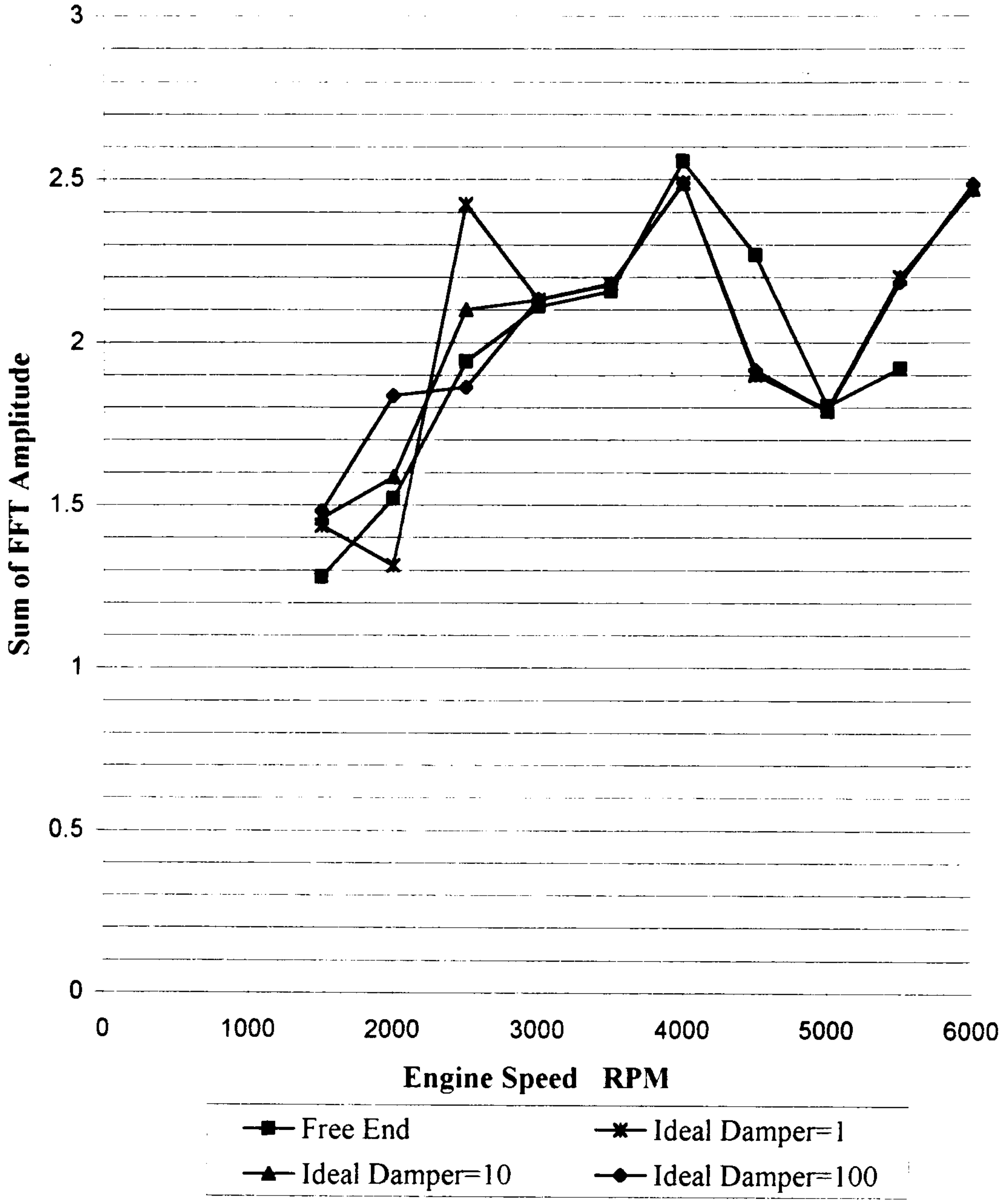

Figure 26. Theoretical Damper FFT Amplitude Sum verses Engine Speed at the Tenth Mass Point

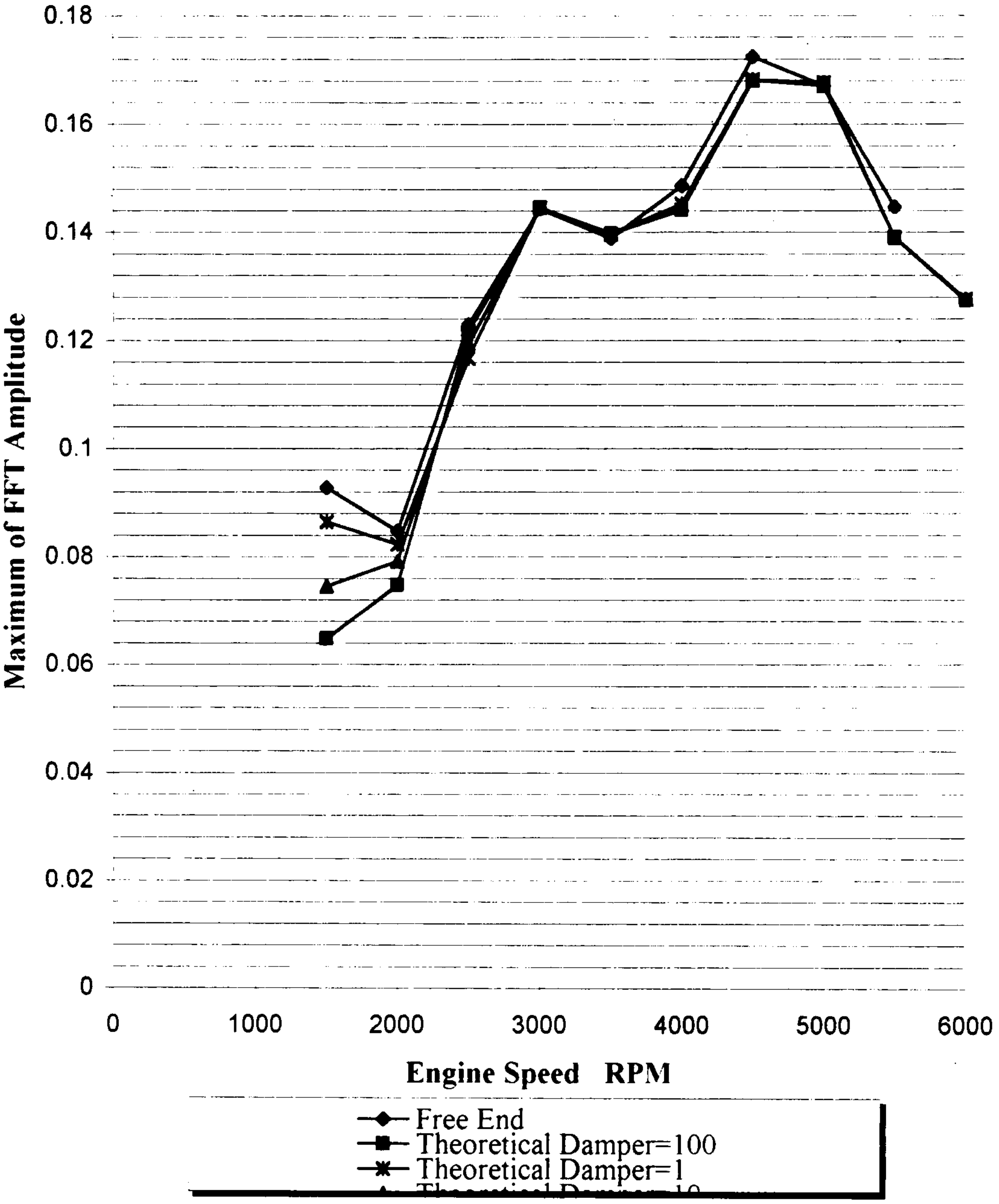

Figure 27. Theoretical Damper FFT Amplitude Maximum verses Engine Speed at the Tenth Mass Point

The theoretical damper of 100 created the most energy dissipation in the crankshaft system. A plot of the FFT amplitude peaks at 2500 RPM and 5500 RPM is presented in Figure 28. Any damping that occurs was done below 300 Hz or above 450 Hz at 2500 RPM. Damping at 5500 RPM occurred at 174.4 Hz, 218.5 Hz, and 349.1 Hz. The theoretical damper of 100 created the most damping of the three values tested, and the greatest difference was in the 3000 RPM and below range. This affected the below 300 Hz range the most at the nineteenth mass point.

Flywheel

Flywheel Test Design Specifications

As stated earlier, the flywheel is the conventional method of combating torsional vibration. Several flywheel geometries were tested for comparison against the other types of dampers. The first and second geometries conformed to the 8 inch x 1.25 inch proposed viscous roller design specifications. The designs took advantage of the known torsional rotational inertia of a Saturn four cylinder engine, 434.77 inch pounds. The first flywheel design was a solid disk with a 7.92 inch diameter and a 1.00 inch thickness. The second flywheel design was a solid disk with a 7.50 inch diameter and 1.25 inch thickness. The third flywheel design was a solid disk with a 6.7 inch diameter and a 2 inch thickness.

Bending Vibration Code Test Results

The three flywheel designs were evaluated with the bending response code. The results of the FFT analysis for these different flywheel configurations are in Table 4.

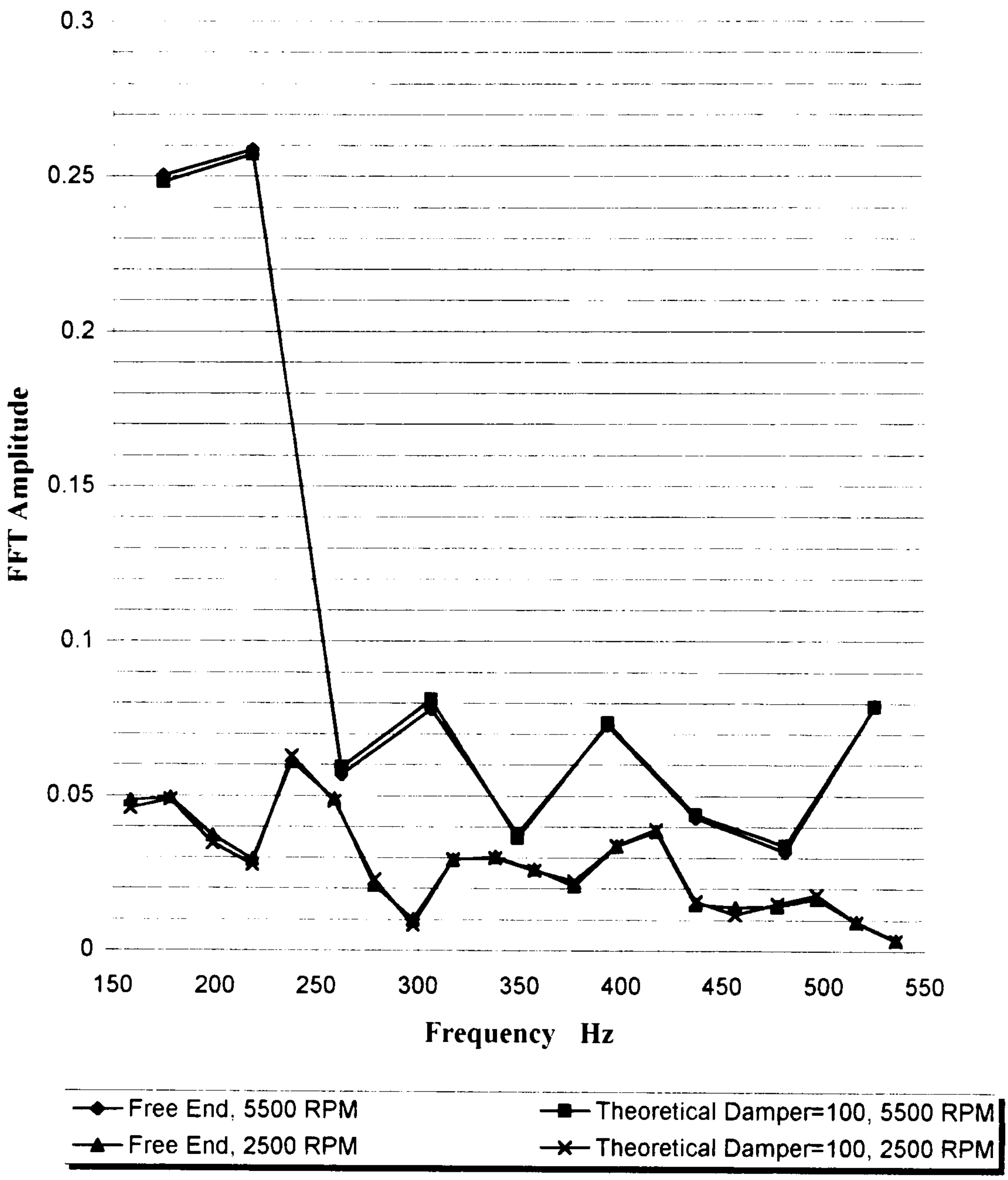

Figure 28. FFT Amplitude Peaks for Theoretical Damper Designs and Free End at 2500 RPM and 5500 RPM

Free End

Speed	sum 10th	max 10th	sum 19th	max 19th
1500	1.27782	0.09277	1.27184	0.05983
2000	1.52111	0.08472	1.41496	0.06616
2500	1.94109	0.12292	1.68995	0.06112
3000	2.10947	0.14431	1.87741	0.07561
3500	2.1563	0.13892	1.93978	0.07712
4000	2.55505	0.14863	2.38084	0.23383
4500	2.2676	0.17249	2.42537	0.16513
5000	1.80442	0.16708	2.86256	0.24424
5500	1.92122	0.14466	2.28704	0.25872
6000				

Flywheel Design 2

Speed	sum 10th	max 10th	sum 19th	max 19th
1500	1.495967	0.086586	1.341791	0.068546
2000	1.332803	0.082240	1.719899	0.069573
2500	2.190471	0.115391	2.195614	0.066431
3000	2.117266	0.144331	2.250579	0.078932
3500	2.215054	0.140162	2.105550	0.082847
4000	2.508272	0.145257	2.853501	0.245943
4500	1.901036	0.168666	3.128507	0.180479
5000	1.856941	0.167891	3.682286	0.259111
5500	2.225607	0.138477	3.151325	0.278465
6000	2.782844	0.131487	3.339649	0.259018

Flywheel Design 1

Speed	sum 10th	max 10th	sum 19th	max 19th
1500	1.434657	0.086631	1.693596	0.068958
2000	1.314498	0.082501	1.836732	0.070119
2500	2.293845	0.115398	1.974464	0.068014
3000	2.140931	0.144541	2.350009	0.087345
3500	2.219680	0.137430	2.263608	0.083750
4000	2.560909	0.145070	3.048194	0.247240
4500	1.914389	0.168806	3.471292	0.181861
5000	1.804293	0.167882	3.321790	0.258468
5500	2.243863	0.139731	3.362798	0.281072
6000	2.328463	0.129241	3.508348	0.260895

Flywheel Design 3

Speed	sum 10th	max 10th	sum 19th	max 19th
1500	1.480133	0.086609	1.969681	0.122757
2000	1.327810	0.082620	2.898374	0.116537
2500	2.294699	0.115265	2.806967	0.075808
3000	2.164348	0.144638	3.464469	0.251256
3500	2.325686	0.139924	5.252797	0.234086
4000	2.482014	0.145234	4.411098	0.367232
4500	1.899044	0.168933	3.449651	0.195790
5000	1.959417	0.167855	5.638470	0.402079
5500	2.290758	0.139577	5.344341	0.485800
6000	2.412809	0.128502	4.790649	0.268291

Table 4. FFT Amplitude Statistics for Flywheel Designs

Figure 29 shows the sum of the FFT amplitude in the test frequency band as a function of engine speed at the nineteenth mass point. The second design performed best at idle, and it had the same general shape as the free end curve. The second design added as little as 0.06995 at 1500 RPM and as much as 0.819726 at 5000 RPM to the free end vibration. The first flywheel design added between 0.2845 and 1.075758 to the FFT amplitude sum. As the graph shows, the third design performed the worst adding between 0.202313 and 3.313017 to the FFT amplitude sum.

The FFT amplitude maximum for the nineteenth mass point is plotted verses engine speed in Figure 30. The second flywheel design performed the best adding between 0.003322 and 0.019745 at 3000 RPM and 5500 RPM respectively. The first design added between 0.003959 at 2000 RPM and 0.022352 at 5500 RPM. The first two designs differed between 0.000472 and 0.008413 at 1500 RPM and 3000 RPM respectively. The third design added between 0.04688 and 0.22708 at 2500 RPM and 5500 RPM respectively. All three designs added vibrational energy to the maximum throughout the engine speed range. None of the flywheel designs performed better than the free end at the nineteenth mass point.

The FFT amplitude sum at the tenth mass point plotted verses the engine speed is provided as Figure 31. The second flywheel design added between 0.007796 at 3000 RPM and -0.366564 at 4500 RPM. This design decreased the vibrational energy at 2000 RPM, 4000 RPM, and 4500 RPM. The first flywheel design added between -0.000127 and -0.35321 at 5000 RPM and 4500 RPM respectively. The vibrational energy was decreased at 2000 RPM, 4500 RPM, and 5000 RPM by the second design The third

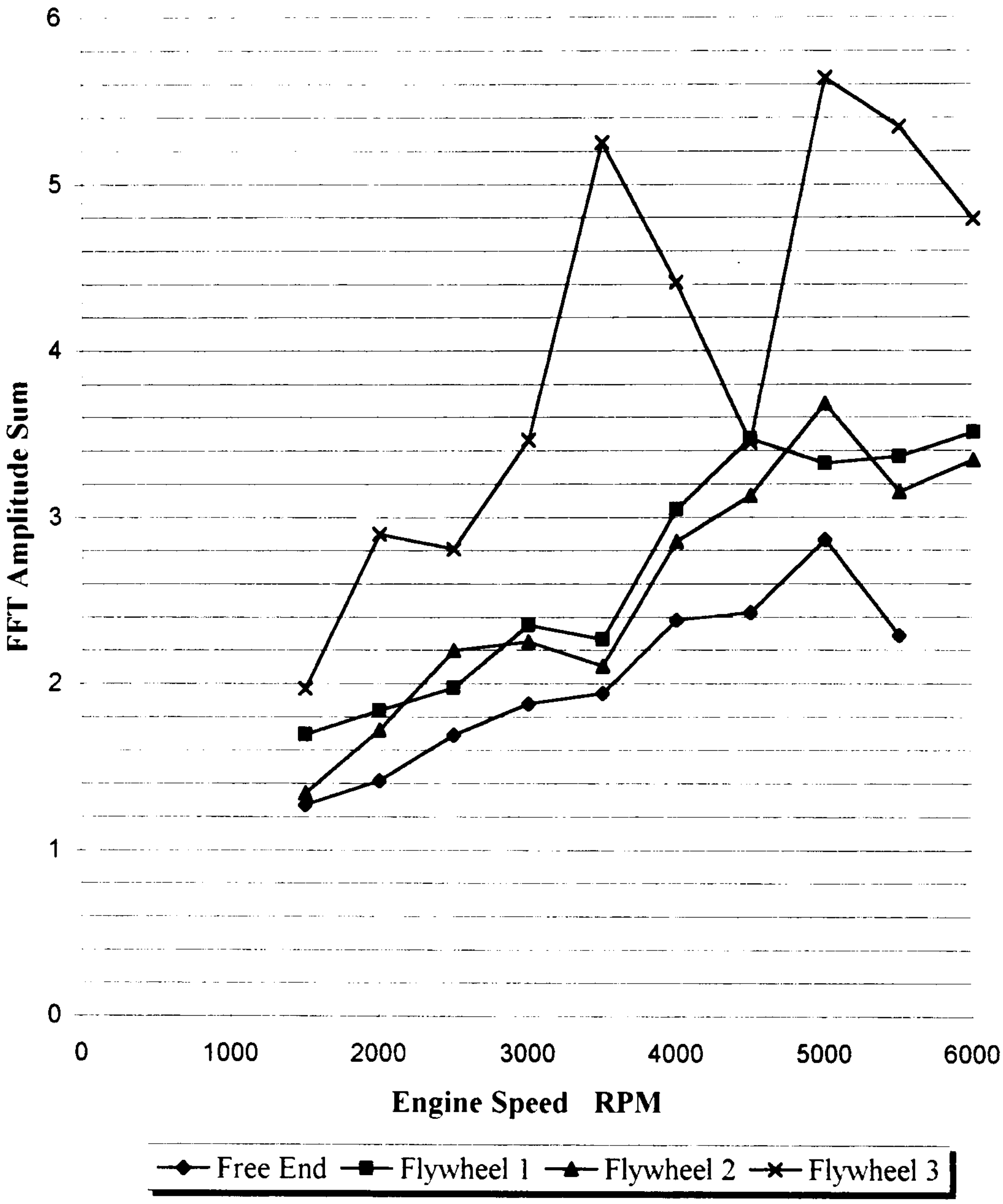

Figure 29. Flywheel Design FFT Amplitude Sums verses Engine Speed at the Nineteenth Mass Point

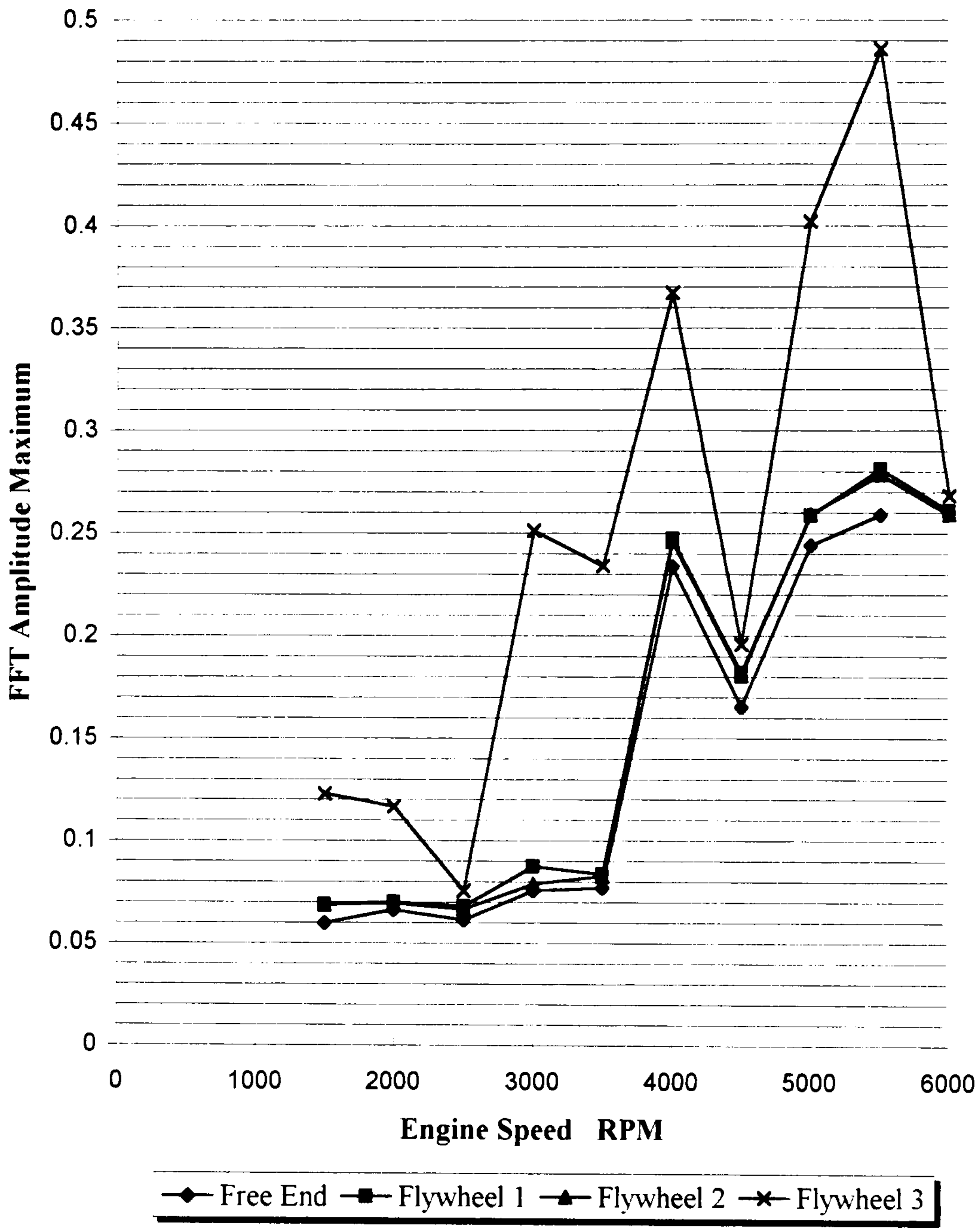

Figure 30. Flywheel Design FFT Maximum verses Engine Speed at the Nineteenth Mass Point

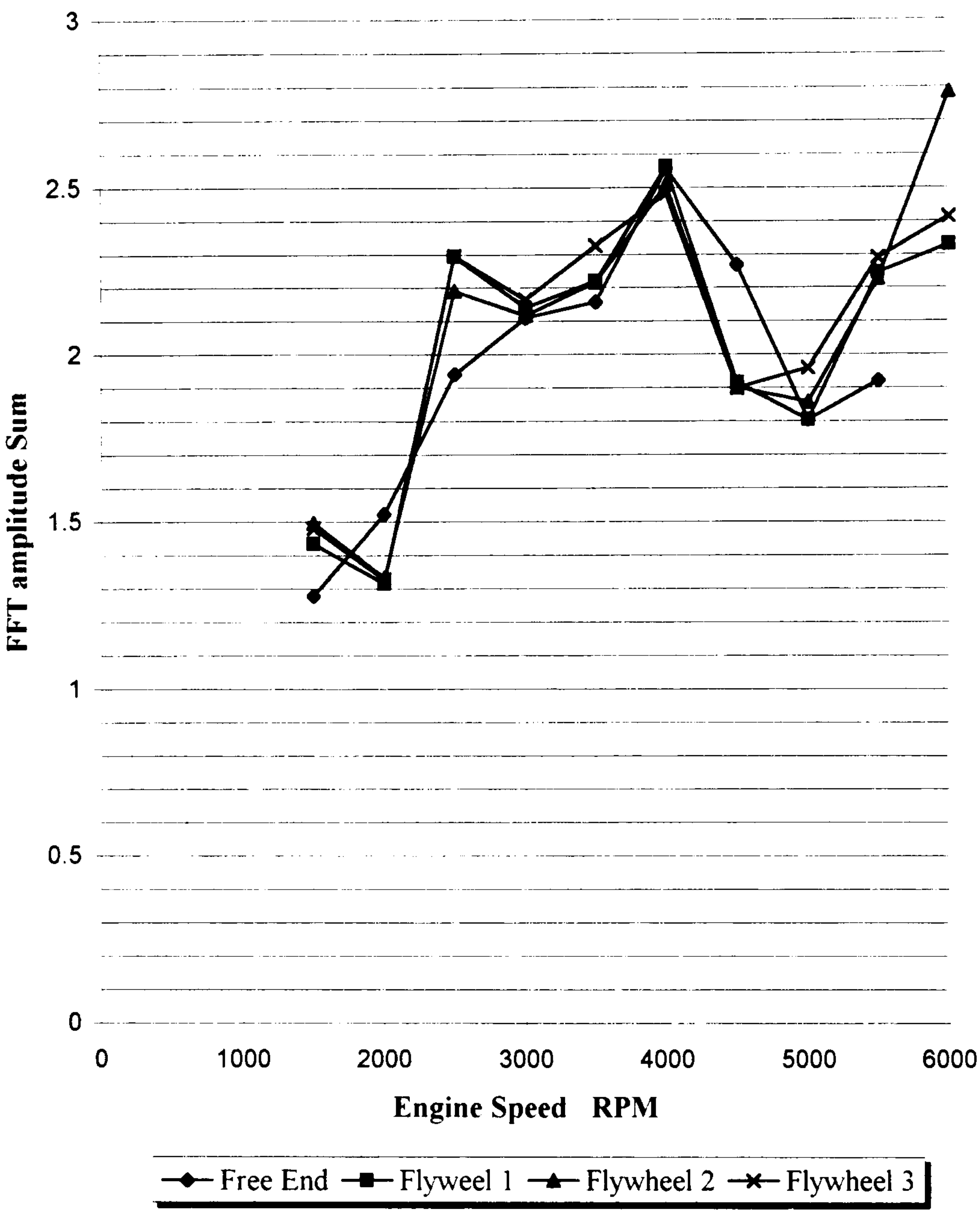

Figure 31. Flywheel Design FFT Amplitude Sum verses Engine Speed at the Tenth Mass Point

design added between 0.054878 and 0.369538 at 3000 RPM and 5500 RPM respectively. The third design decreased the vibrational energy at 2000 RPM and 4500 RPM.

Figure 32 is a plot of the FFT maximum amplitude verses engine speed for the tenth mass point. The first flywheel design added between -0.000231 at 3000 RPM and -0.007552 at 2500 RPM. The first design decreased the FFT amplitude maximum within the problem range at every speed tested except 5000 RPM. The second design added between -0.000021 and -0.007529 at 3000 RPM and 2500 RPM respectively. The third design added between 0.000328 at 3000 RPM and -0.007655 at 2500 RPM. 3500 RPM and 5000 RPM were the only engine speeds which the FFT maximum was not decreased by the second and third flywheel designs.

Elastomer Damper

Elastomer Damper Test Design Specifications

The elastomer damper works on the premise that an elastomer ring will absorb energy as it is deformed between two inertial disks. The original design geometry limits were set by the proposed viscous roller design. Each of the designs was composed of three parts, a disk, an elastomer, and an inertial ring. The first elastomer damper design had an 8 inch diameter and is 1.3 inch thick. The flywheel disk had an 8 inch diameter and 0.5 inch thick. The elastomer is 0.05 inch thick and covered the face of the inertial ring. The inertial ring had an 8 inch outside diameter, 2.25 inch inside diameter, and 0.75 inch length.

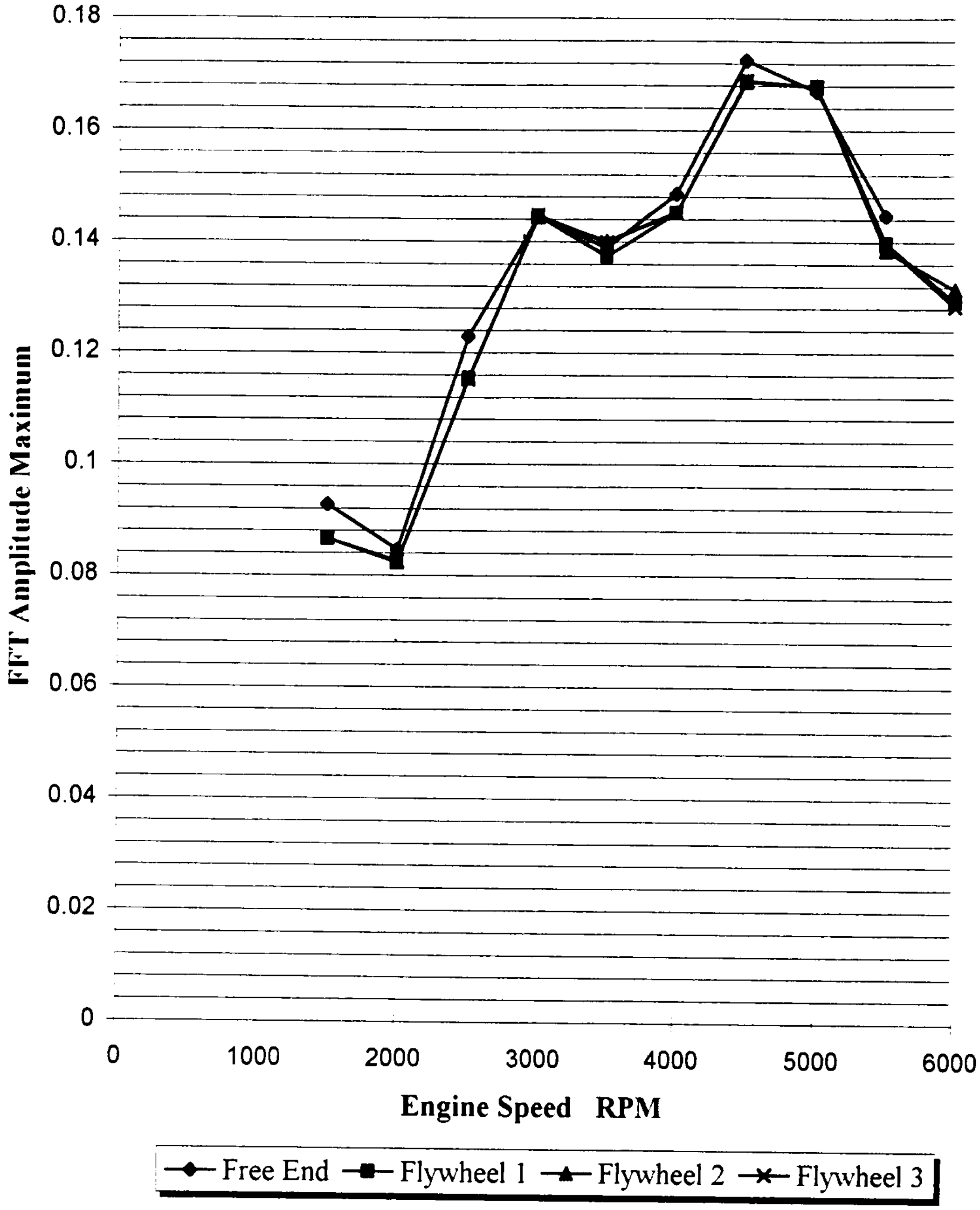

Figure 32. Flywheel Design FFT Amplitude Maximum verses Engine Speed at the Tenth Mass Point

To again take advantage of measured flywheel inertial values for a Saturn four cylinder engine, a second elastomer damper design was created. A spreadsheet program was used to optimize the rotational inertia in the bending direction while maintaining the rotational inertia in the torsional direction. Saturn reported a flywheel inertial of 434.77 inch pounds. The second elastomer damper design had a 10 inch diameter. The flywheel disk had a solid diameter and is 0.15 inch thick. The inertial ring had a 10 inch outside diameter and a 2.25 inch inside diameter, and It was 1.25 inch thick.

Steel was used for the flywheel disk and inertial ring because of its strength and wear characteristics. The dynamic behavior of elastomers has a strong temperature and frequency dependence. Dupont fluoro rubber or Vitron A was the elastomer used. This elastomer's published viscoelastic moduli describe a 0 to 100 degrees Celsius operating temperature range. The values, G'=2.00 and G''=1.60, represent the 100 Hz frequency range [14].

Bending Response Code Test Results

FFT amplitude sums and maximums for the free end, elastomer design 1, and elastomer design 2 are tabulated in Table 5. The summation of the FFT amplitudes at the nineteenth mass point is presented in Figure 33. The first elastomer design decreased the sum by 0.113271 at 1500 RPM and 0.114732 at 3500 RPM. This design increased the sum at every other speed from between 0.002788 at 5000 RPM to 1.182978 at 4500 RPM. The second elastomer design consistently increased the sum throughout the entire speed range. This design increased the sum from 0.31385 at 1500 RPM to 0.919295 at

Free End

Speed	sum 10th	max 10th	sum 19th	max 19th
1500	1.27782	0.09277	1.27184	0.05983
2000	1.52111	0.08472	1.41496	0.06616
2500	1.94109	0.12292	1.68995	0.06112
3000	2.10947	0.14431	1.87741	0.07561
3500	2.1563	0.13892	1.93978	0.07712
4000	2.55505	0.14863	2.38084	0.23383
4500	2.2676	0.17249	2.42537	0.16513
5000	1.80442	0.16708	2.86256	0.24424
5500	1.92122	0.14466	2.28704	0.25872
6000				

Elastomer Design 1

Speed	sum 10th	max 10th	sum 19th	max 19th
1500	1.46806	0.08667	1.15857	0.06702
2000	1.47826	0.08318	1.49837	0.06857
2500	2.26024	0.11634	1.77326	0.0641
3000	2.13334	0.14473	2.01089	0.07717
3500	2.28451	0.1397	1.82505	0.07658
4000	2.51156	0.14557	2.48877	0.24204
4500	2.51005	0.16948	3.60835	0.3307
5000	1.80436	0.1681	2.86535	0.25228
5500	2.18986	0.13901	2.85616	0.26999
6000	2.41402	0.1276	3.04685	0.25225

Elastomer Design 2

Speed	sum 10th	max 10th	sum 19th	max 19th
1500	1.50051	0.08791	1.49354	0.07017
2000	1.29836	0.0819	2.00587	0.07077
2500	2.28642	0.11659	2.14617	0.0692
3000	2.14195	0.14585	2.60262	0.11157
3500	2.22553	0.13946	2.60444	0.1095
4000	2.5112	0.14293	3.30014	0.25303
4500	1.88877	0.16574	3.04106	0.18453
5000	1.85533	0.16507	3.63124	0.26036
5500	2.18639	0.13845	3.79455	0.27907
6000	2.33185	0.1273	3.75849	0.26385

Table 5. FFT Amplitude Statistics for Elastomer Damper Designs

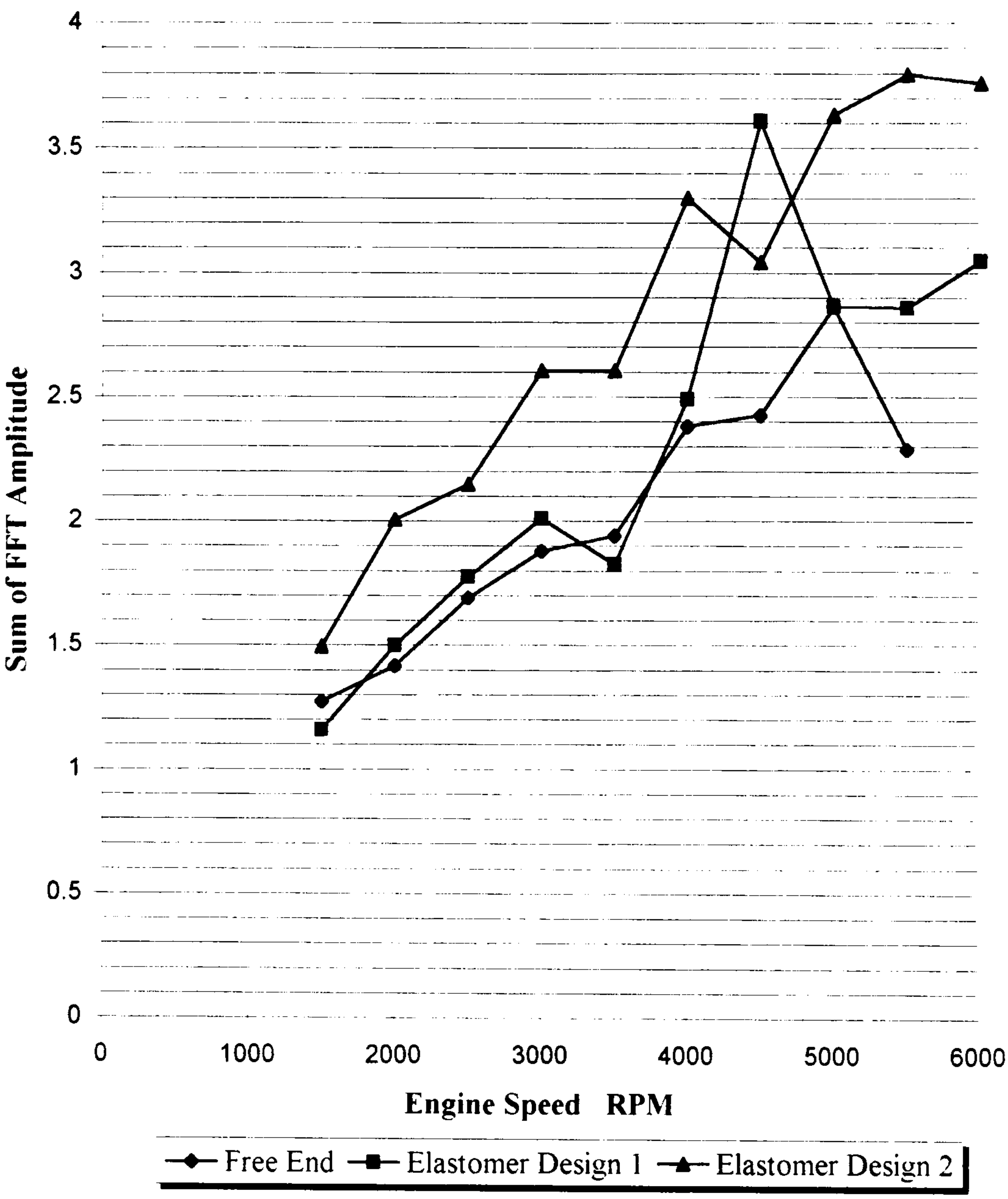

Figure 33. Elastomer Damper FFT Amplitude Sum verses Engine Speed at Nineteenth Mass Point

4000 RPM. The first elastomer damper design added the least to the amplitude except at 4500 RPM.

Figure 34 presents the FFT amplitude maximum for the nineteenth mass point as a function of engine speed for the free end and both elastomer damper designs. The first design changed the free end amplitude maximum from -0.000536 at 3500 RPM and 0.165568 at 4500 RPM. This design reduced the maximum amplitude at 3500 RPM. The first elastomer damper design added the least to the maximum throughout the speed range except for one point, 4500 RPM. The second design added between 0.004614 at 2000 RPM and 0.034403 at 3000 RPM. Again the resonant sixth order component of engine speed caused the higher maximum at 4500 RPM for the first elastomer damper design.

Changes of the vibrational characteristics at the tenth mass point are presented in Table 5. The FFT amplitude sums at the tenth mass point as a function of engine speed are plotted in Figure 35. Elastomer design 1 added between -0.000065 at 5000 RPM and 0.31915 at 2500 RPM. This design lowered the FFT sum at 2000 RPM, 4000 RPM, and 5000 RPM, however these decreases were minimal. The greatest increases occurred at 2500 RPM and 4500 RPM.

To illustrate the difference in the FFT amplitude maximum for the tenth mass point, Figure 36 is provided from amplitude maximum data in Table 5. The first elastomer damper design increased the maximum by 0.000421 at 3000 RPM to -0.006584 at 2500 RPM. This damper slightly increased the maximum at 3000 RPM and 5000 RPM. The second elastomer design decreased the FFT maximum amplitude by 0.000535 at 3500 RPM to 0.006753 at 4500 RPM. This design decreased the maximum at every speed

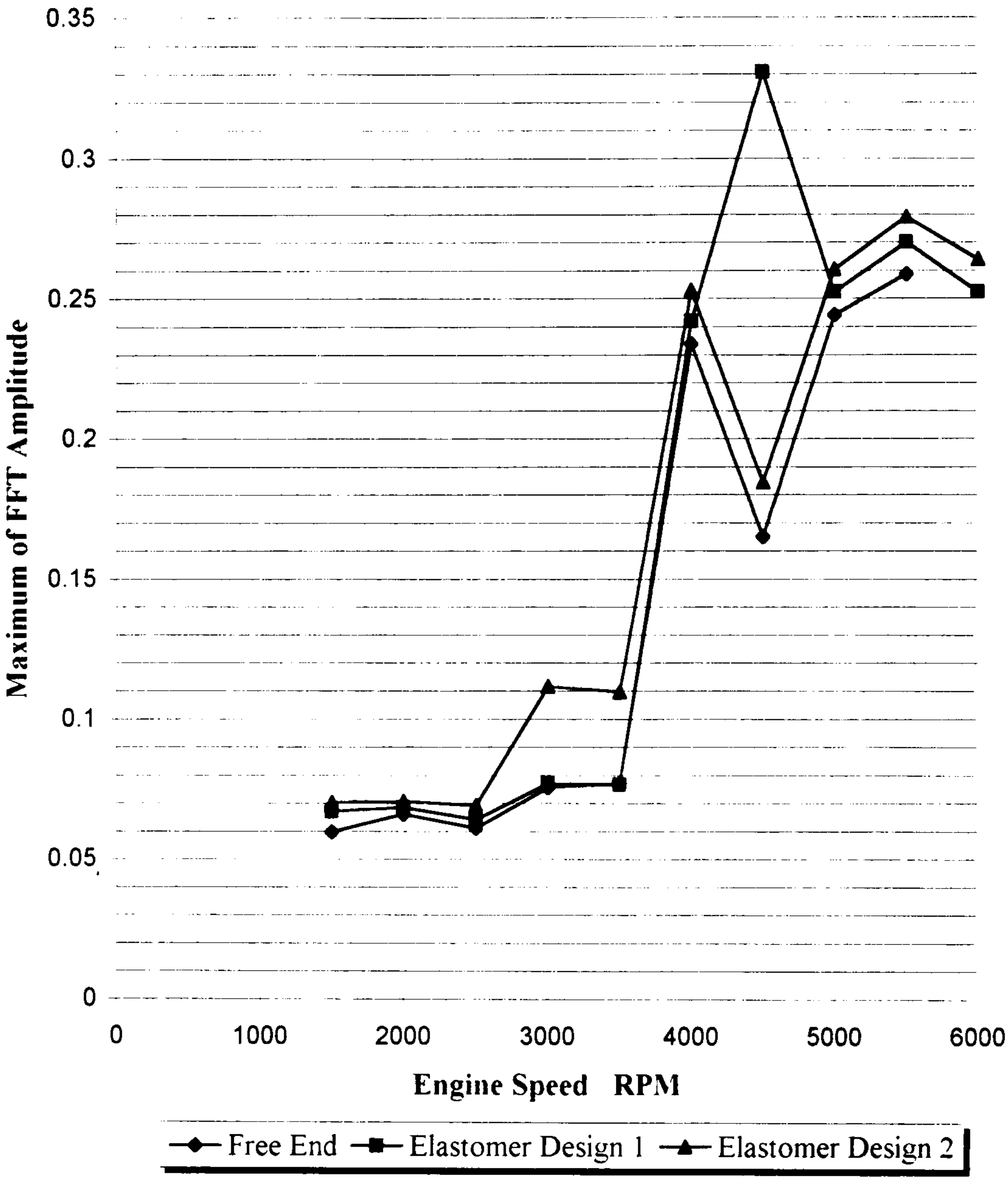

Figure 34. Elastomer Damper FFT Amplitude Maximum verses Engine Speed at Nineteenth Mass Point

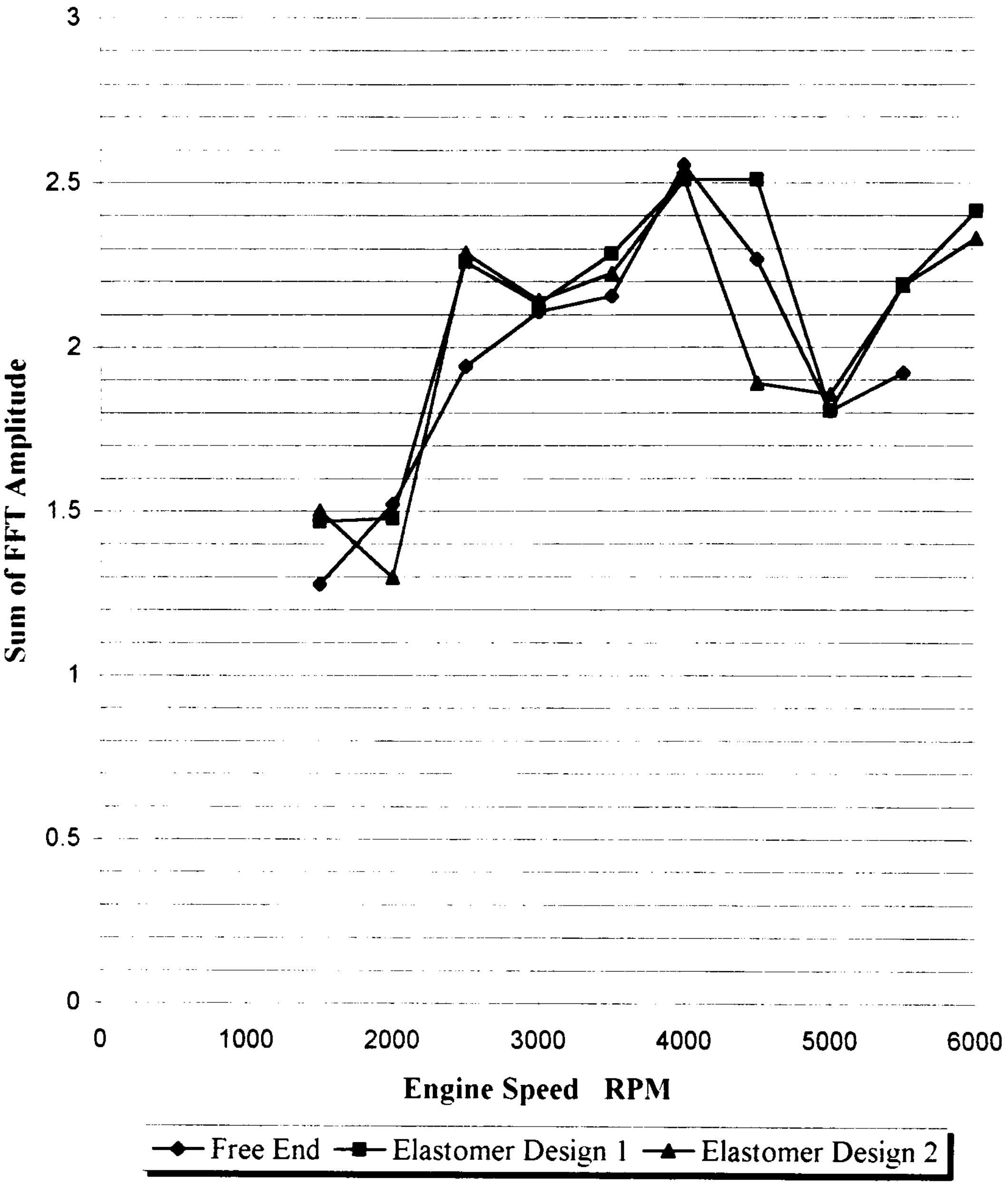

Figure 35. Elastomer Damper FFT Amplitude Sum verses Engine Speed at Tenth Mass Point

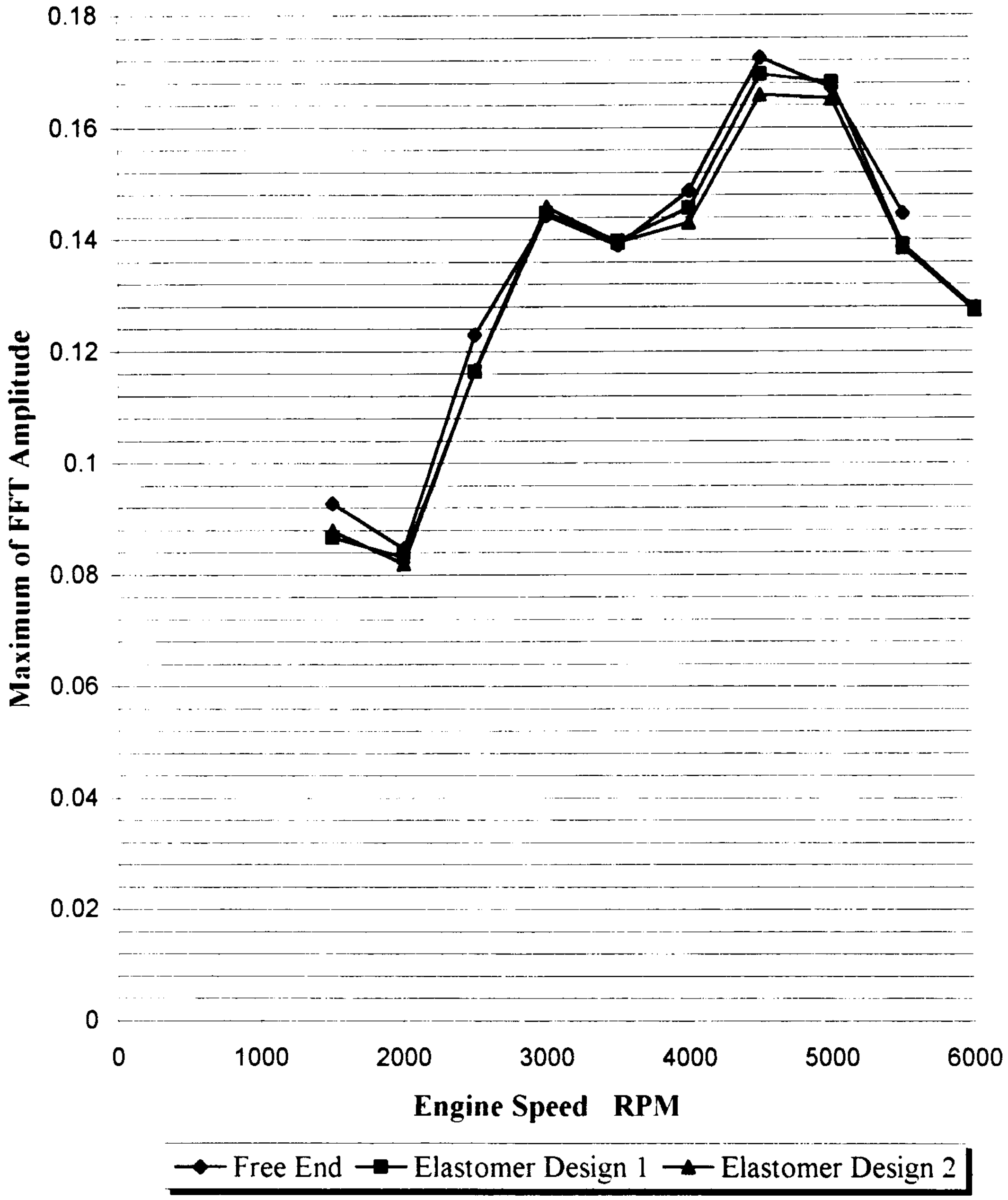

Figure 36. Elastomer Damper FFT Amplitude Maximum verses Engine Speed at Tenth Mass Point

except 3000 RPM, where it was only increased slightly.

To provide insight into the behavior of this damper design at 4500 RPM, the peak amplitudes of both of the mass points were isolated and charted. Table 6 provides the frequency and amplitude of the peaks as well as the difference in the amplitudes for the first elastomer damper design at 4500 RPM. The peaks in FFT amplitude sum at both mass points as a function of frequency is presented in Figure 37. The largest peaks at the nineteenth mass point occurred at 250.2 Hz and 322.3 Hz. At the tenth mass point, 178.2 Hz and 465.1 Hz were the largest peaks. Figure 38 is a plot of the difference in amplitude between the free end and elastomer design 1 at corresponding mass points. The largest increases in the nineteenth mass point's amplitude were at 178.22 Hz and 465.09 Hz. These increases did not occur at the greatest amplitude peaks. The nineteenth mass point's amplitude was decreased at 285.64 Hz. At the tenth mass point, the largest peak, 178.2 Hz, was the largest decrease. The tenth mass point's FFT amplitude was also decreased at 429.68 Hz and 537.11 Hz. The increase peak of the nineteenth mass point and a corresponding increase at the tenth mass point suggested a resonance occurring within the damper at 465 Hz at 4500 RPM.

FFT Sum at the Tenth Mass Point

Frequency (Hz)	Free End	Elastomer Design 1	Difference
178.2	0.086069	0.082769	-0.003300
214.8	0.039042	0.039588	0.000546
250.2	0.169482	0.172494	0.003012
285.6	0.107005	0.108276	0.001271
322.3	0.121253	0.123332	0.002079
357.6	0.029090	0.032766	0.003676
393.1	0.013939	0.013673	-0.000266
465.1	0.038465	0.039381	0.000916
500.1	0.018814	0.020666	0.001852
535.9	0.012688	0.012169	-0.000519

FFT Sum at Nineteenth Mass Point

Frequency (Hz)	Free End	Elastomer Design 1	Difference
178.22	0.165125	0.173975	0.008850
250.24	0.089176	0.096472	0.007296
285.64	0.042197	0.041430	-0.000767
322.27	0.064156	0.066809	0.002653
357.66	0.042660	0.044768	0.002108
393.06	0.028085	0.032333	0.004248
429.68	0.061070	0.070857	0.009787
465.09	0.073684	0.089527	0.015843
500.48	0.024740	0.033266	0.008526
537.11	0.007781	0.008504	0.000723

Table 6. Elastomer Design 1's FFT Amplitude Sum Increases for the Tenth and Nineteenth Mass Point at 4500 RPM

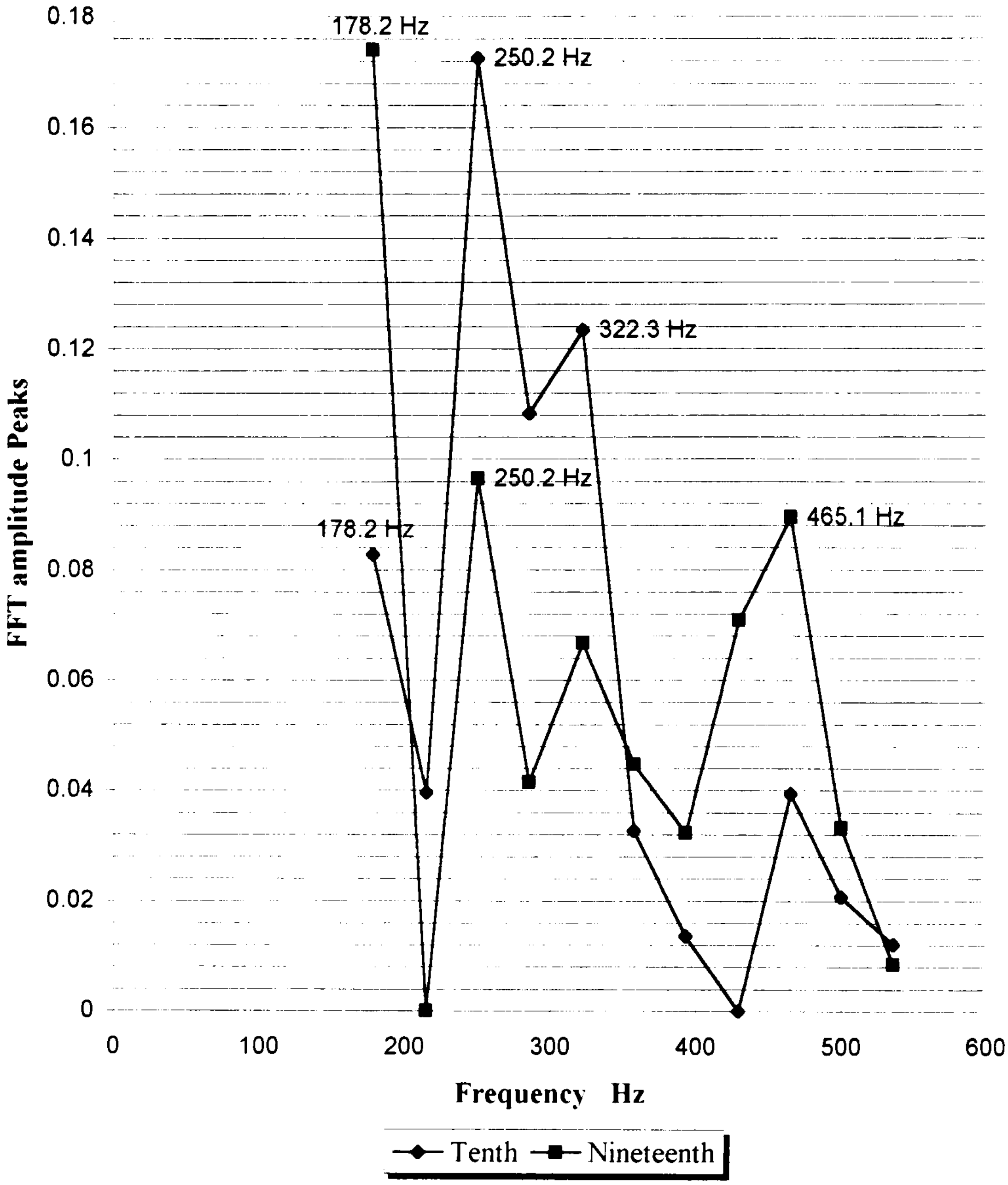

Figure 37. FFT Amplitude Sum Peaks for Elastomer Design 1 at 4500 RPM

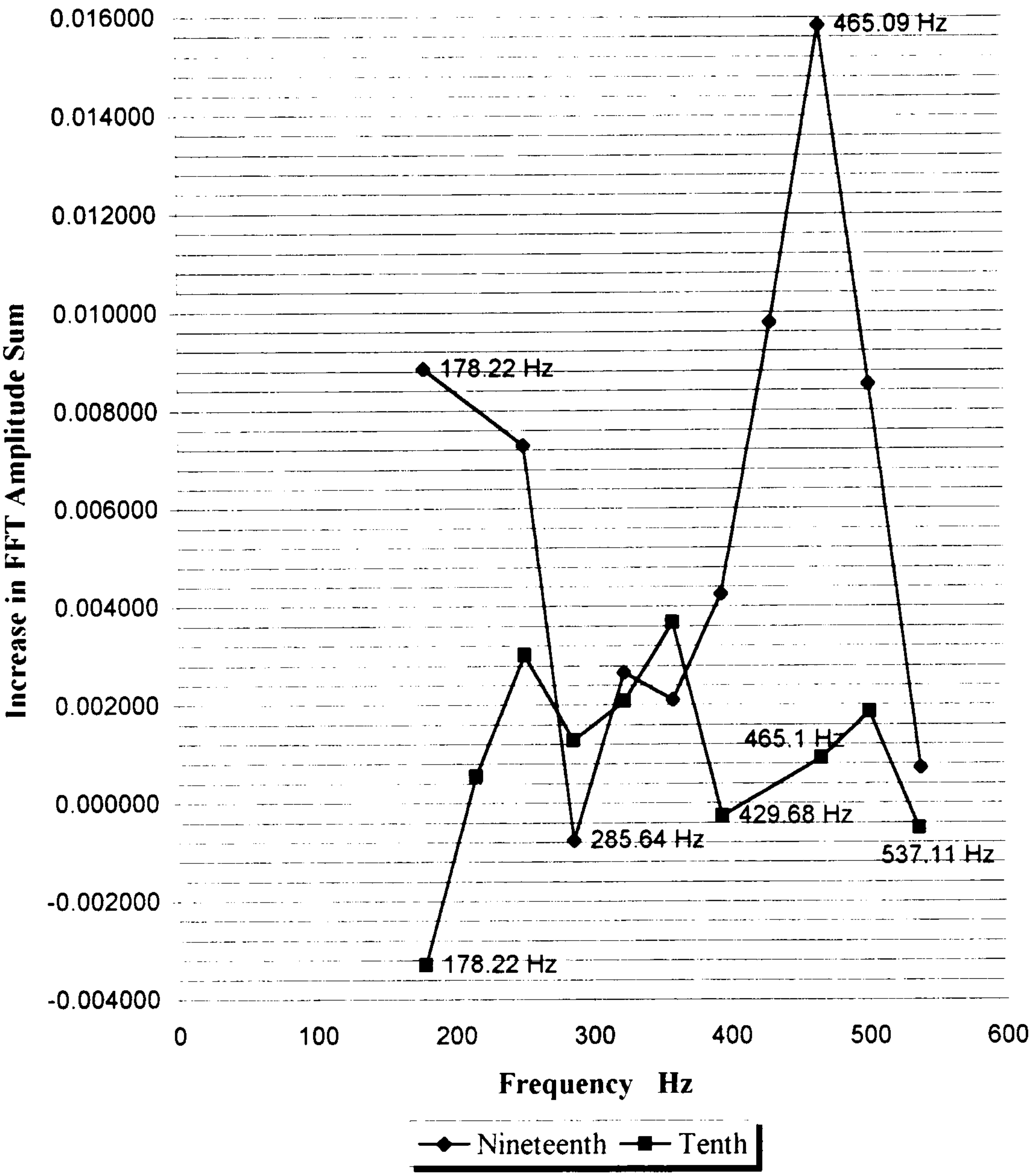

Figure 38. Increase in FFT Amplitude Sum at 4500 RPM for Both Mass Points of Elastomer Design 1

Viscous Roller Damper

Viscous Roller Test Design Specifications

The size of these designs was set at the onset of the project. The proposed design allowed for 8 inches by 1.25 inch cylinder of any material capable of operating in an internal combustion engine's operating environment. Again this design utilized steel because of the strength, wear resistance, and machineability. The four roller cavities are perpendicular to the crankshaft's rotational axis. The roller cavity diameters were set at 0.75 inch. This size allowed 0.25 inch of structure on either side of the cavity. The cavities were four inches long, centered 7 inches from the dampers rotational axis. With these design characteristics set, the roller diameter and the viscosity of the fluid were set based on their performance.

Theoretical Viscous Roller Analysis

The clearance and the viscosity dictated the designs ability to dissipate energy. To evaluate the roller diameter and viscosity, a quantitative means of comparison was created. This tool also acted to check the results of the bending response code. The relationship between the cavity wall and the roller surface was described by two coupled second order differential equations. Summation of torques acting on the cavity wall provides

$$I_C \frac{d^2\Theta_C}{dt^2} + c_{damping}\left(\frac{d\Theta_C}{dt} - \frac{d\Theta_R}{dt}\right) = T\sin(wt)$$

where I_C = rotational inertial of the case,
Θ_C= angular position of the case,

$c_{damping}$ = damping factor created by viscous fluid,
Θ_R= angular position of the roller,
T = input torque of the excitation,
w = angular velocity of the excitation torque,
t = time.

A second equation describes the summation of torques acting on the roller,

$$I_R \frac{d^2\Theta_R}{dt^2} + c_{damping}\left(\frac{d\Theta_R}{dt} - \frac{d\Theta_C}{dt}\right) + k\Theta_R = 0$$

where I_R = roller's rotational inertia,
Θ_R= roller's angular position,
Θ_C= case's angular position
$c_{damping}$ = damping factor created by the viscous fluid,
k = spring constant created by the spinning of the entire damper.

The damping factor created by the viscous fluid was modeled as a lightly loaded journal bearing. The damping factor is

$$c_{damping} = \left(\frac{r}{c}\right)^2 \frac{\mu \Pi}{60l}$$

where r = roller radius,
c = radial clearance,
μ = fluid viscosity,
l = roller length.

Centrifugal force acts on the roller and caused a spring constant factor to arise in its description. The spring constant factor is described by

$$k = R m_{roller} w_{engine}{}^2 \sin(\Theta_R)$$

where R = distance from roller's center to crankshaft center,
m_{roller} = mass of the roller,
w_{engine} = engine speed,
Θ_R = roller's angular position.

The equations are coupled by the viscous term acting on both surfaces. To evaluate the effect of radial clearance and viscosity, the work absorbed by the damper was calculated. The definition of work per cycle for the damper is

$$Work = \int_{0}^{2\pi w} T d\Theta$$

where $2\pi/w$ = time for one cycle,
T = torque,
Θ = relative speed of the surfaces.

The work was done by the viscous interaction of the two surfaces. Before this relation can be used a transformation was made,

$$Work = \int_{0}^{2\pi w} T \frac{d\Theta}{dt} dt = \int_{0}^{2\pi/w} c \frac{d\Theta}{dt} \frac{d\Theta}{dt} dt = c \int_{0}^{2\pi/w} \left(\frac{d\Theta}{dt}\right)^2 dt .$$

So, the work, or absorbed energy is the product of the viscous damping constant and the relative velocity of the surfaces squared integrated over one cycle. To find the velocities of the surfaces two substitutions into the differential equations were made,

$$\Theta_C = \overline{\Theta_C}\, e^{-wti} \quad and \quad \Theta_R = \overline{\Theta_R}\, e^{-wti} .$$

Using Kramer's rule, the solutions were put in the form

$$\Theta_C = \overline{\Theta_C} \sin(wt + \Phi_C) \quad and \quad \Theta_R = \overline{\Theta_R} \sin(wt + \Phi_R) .$$

The derivatives of both solutions were then used to solve for the damper's work. A QuickBASIC program was written to calculate the work for a given damper design. This program is provided in Appendix A.

Using repetitive running of this program a best value for C was chosen. It was chosen because it performed the most work. The value of the work was very small, on the order of $1x10^{-4}$. The optimum c value is 0.025. By doing back calculation, the best clearance for each fluid was found given the same geometry. For the caster oil, the best tested clearance was 0.01 inch. For the other two fluids, the 0.001 inch clearance was the best.

Bending Response Code Test Results

Using the bending response code and FFT analysis, different viscous roller damper designs were tested. The first two designs utilized caster oil which has a viscosity of 145 x 10^{-6} reyn. The first roller had a radial clearance of 0.001 inch, and the second design had a radial clearance of 0.005 inch. Using the data obtained in the testing, Table 7 was created for the first two viscous roller damper designs. The FFT amplitude sum verses the engine speed for the nineteenth mass point is plotted in Figure 39. The first design increased the sum between 0.342363 at 2500 RPM to 1.23231 at 4500 RPM. The second design performed very much the same increasing the sum between 0.342497 at 2500 RPM to 1.23238 at 4500 RPM.

The FFT amplitude maximum for the nineteenth mass point is plotted verses engine speed in Figure 40. The first design increased the maximum between 0.004637 at 2000 RPM to 0.024649 at 5500 RPM. Again the second design performed much the same as the first. The second design increased the maximum between 0.004638 at 2000 RPM to 0.024653 at 5500 RPM. The increases in the maximum by these design rise at 5500 RPM, but they were relatively constant throughout the speed range.

Free End

Speed	sum 10th	max 10th	sum 19th	max 19th
1500	1.27782	0.09277	1.27184	0.05983
2000	1.52111	0.08472	1.41496	0.06616
2500	1.94109	0.12292	1.68995	0.06112
3000	2.10947	0.14431	1.87741	0.07561
3500	2.1563	0.13892	1.93978	0.07712
4000	2.55505	0.14863	2.38084	0.23383
4500	2.2676	0.17249	2.42537	0.16513
5000	1.80442	0.16708	2.86256	0.24424
5500	1.92122	0.14466	2.28704	0.25872
6000				

Roller Design 1

Speed	sum 10th	max 10th	sum 19th	max 19th
1500	1.457259	0.086387	1.87041	0.069492
2000	1.668739	0.080219	1.914663	0.070797
2500	2.263986	0.115937	2.032313	0.069059
3000	2.13182	0.144407	2.424252	0.091172
3500	2.190447	0.139148	2.345289	0.08572
4000	2.497757	0.145057	3.18006	0.248125
4500	1.916734	0.168312	3.65775	0.182574
5000	1.796743	0.16733	3.458274	0.260155
5500	2.200943	0.138822	3.48525	0.283369
6000	2.420023	0.127498	3.642346	0.263249

Roller Design 2

Speed	sum 10th	max 10th	sum 19th	max 19th
1500	1.457642	0.086388	1.871813	0.0695
2000	1.671355	0.080209	1.914334	0.070798
2500	2.26416	0.115939	2.032447	0.069058
3000	2.137205	0.144408	2.423988	0.091176
3500	2.190445	0.139147	2.345282	0.085723
4000	2.497982	0.145057	3.179789	0.248127
4500	1.916734	0.168312	3.65775	0.182574
5000	1.796743	0.16733	3.458274	0.260155
5500	2.201131	0.138821	3.48522	0.283373
6000	2.420266	0.127498	3.642348	0.263249

Table 7. FFT Amplitude Statistics for Roller Designs 1 and 2

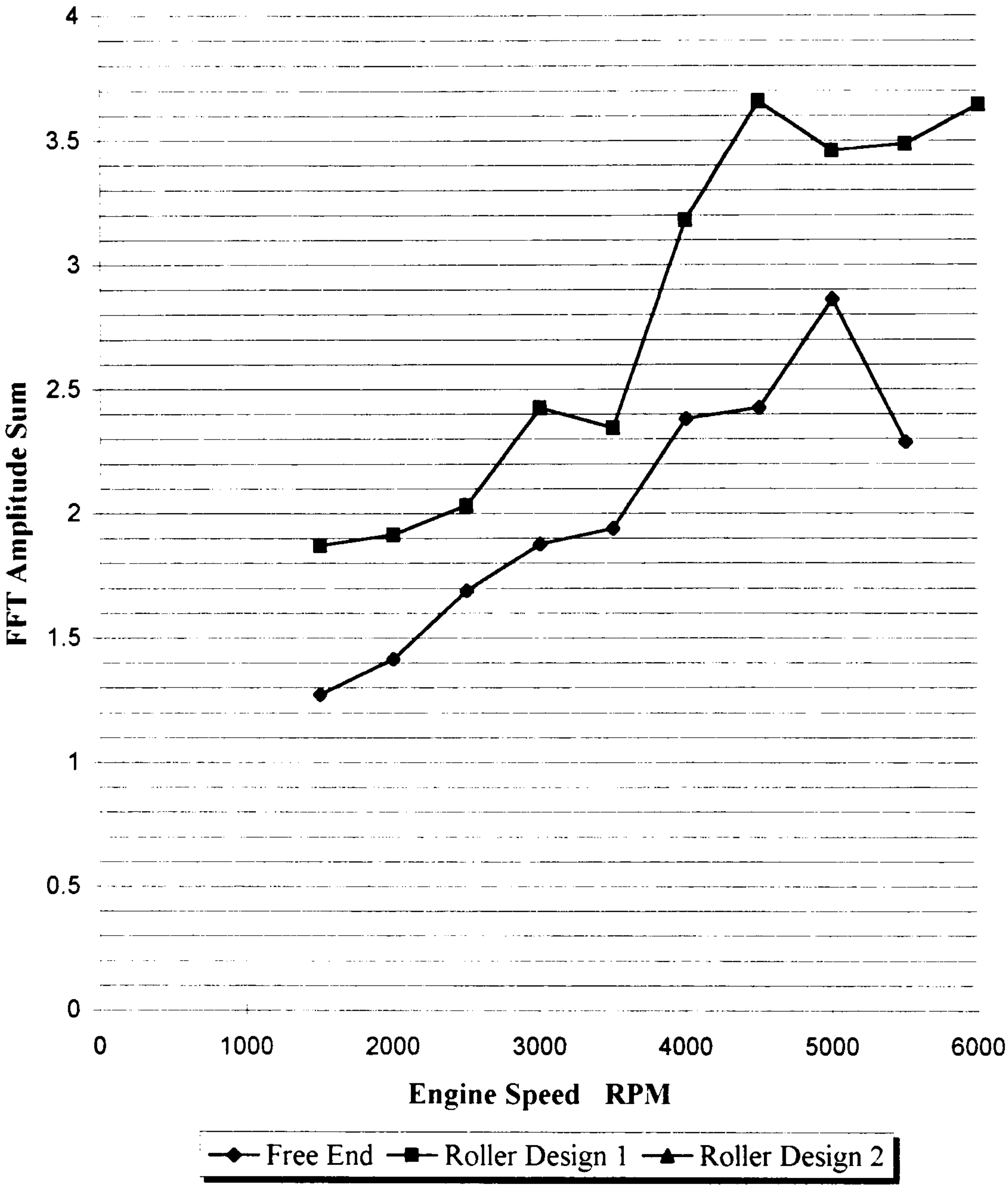

Figure 39. Roller Design 1 and 2 FFT Amplitude Sum verses Engine Speed at the Nineteenth Mass Point

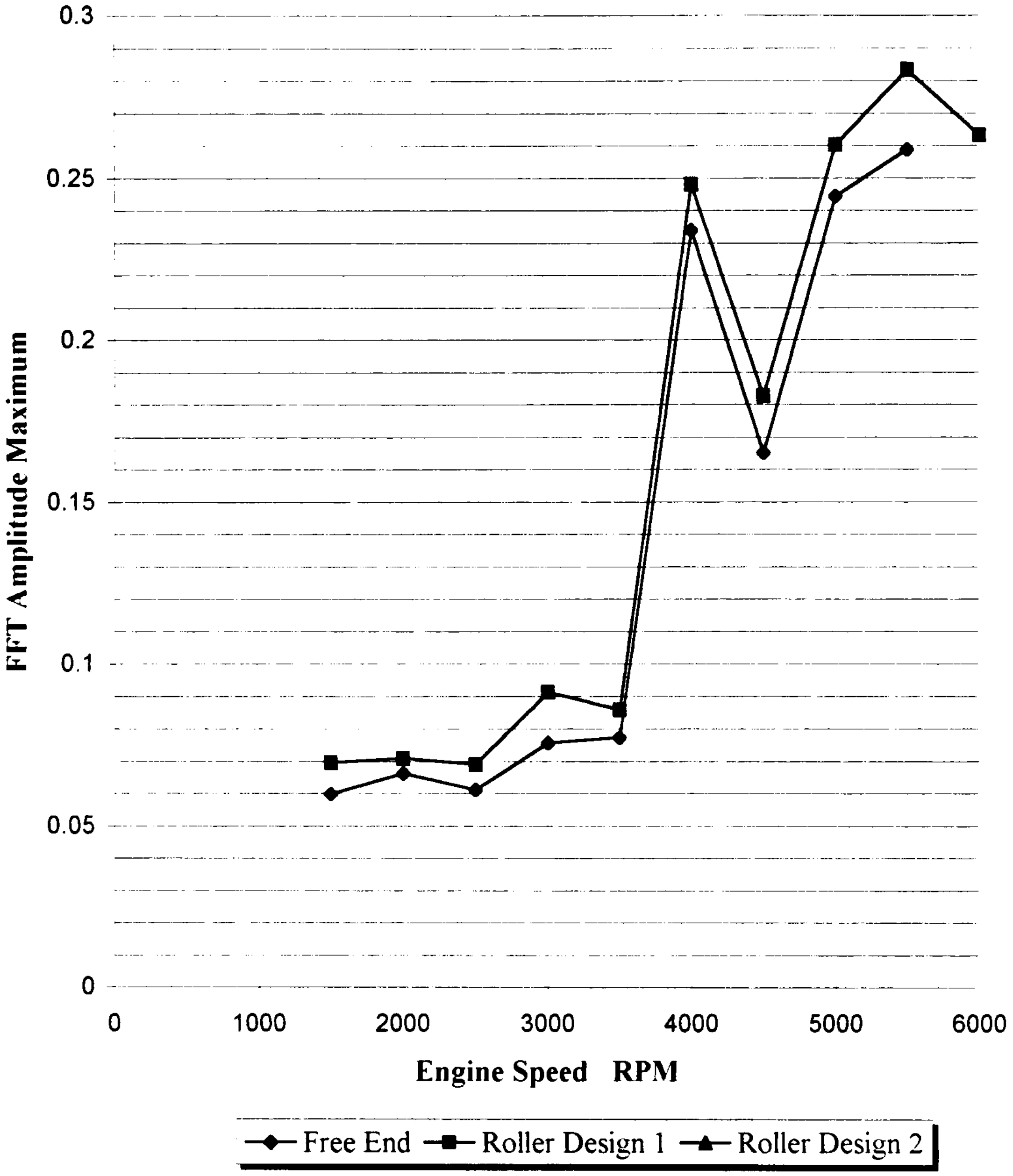

Figure 40. Roller Design 1 and 2 FFT Amplitude Maximum verses Engine Speed at the Nineteenth Mass Point

Figure 41 presents the FFT amplitude sum at the tenth mass point as a function of engine speed. The first design added between -0.066445 at 4500 RPM to 0.322896 at 2500 RPM. The second roller design performed the same as the first design +/- 0.000002. The sum was lowered in the 4000 RPM to 5000 RPM engine speed range, and the reduction peaked at 4500 RPM.

In Figure 42, the FFT amplitude maximum for the tenth mass point is plotted verses engine speed. The first roller design altered the maximum from 0.00025 at 5000 RPM to -0.006383 at 1500 RPM. The second roller damper design was within +/- 0.00001 of the first design's maximum values. The maximums decreased except at 3000 RPM, 3500 RPM, and 5000 RPM where the increases were less than 0.00025.

The next three designs utilized SAE-AN-06 oil with a viscosity of 3.5×10^{-6}. These designs were tested and tabulated in Table 8. Roller Design 4 had a radial clearance of 0.01 inch. Roller Design 5's radial clearance was 0.005 inch, and Roller Design 6 had a radial clearance of 0.001 inch. The FFT amplitude sum for the nineteenth mass point as a function of engine speed is provided as Figure 43. The graph shows the three different designs affecting the sum within +/-0.000328 or 0.017% of each other. The designs increased the sum between 0.342513 at 2500 RPM to 1.234436 at 4500 RPM.

Figure 44 provides the FFT amplitude maximum for the nineteenth mass point. The designs all followed perform relatively the same except at 5500 RPM. At 5500 RPM, the fourth roller design increased the amplitude maximum by 0.001913 more than the other two designs. The three roller designs increased the FFT amplitude maximum

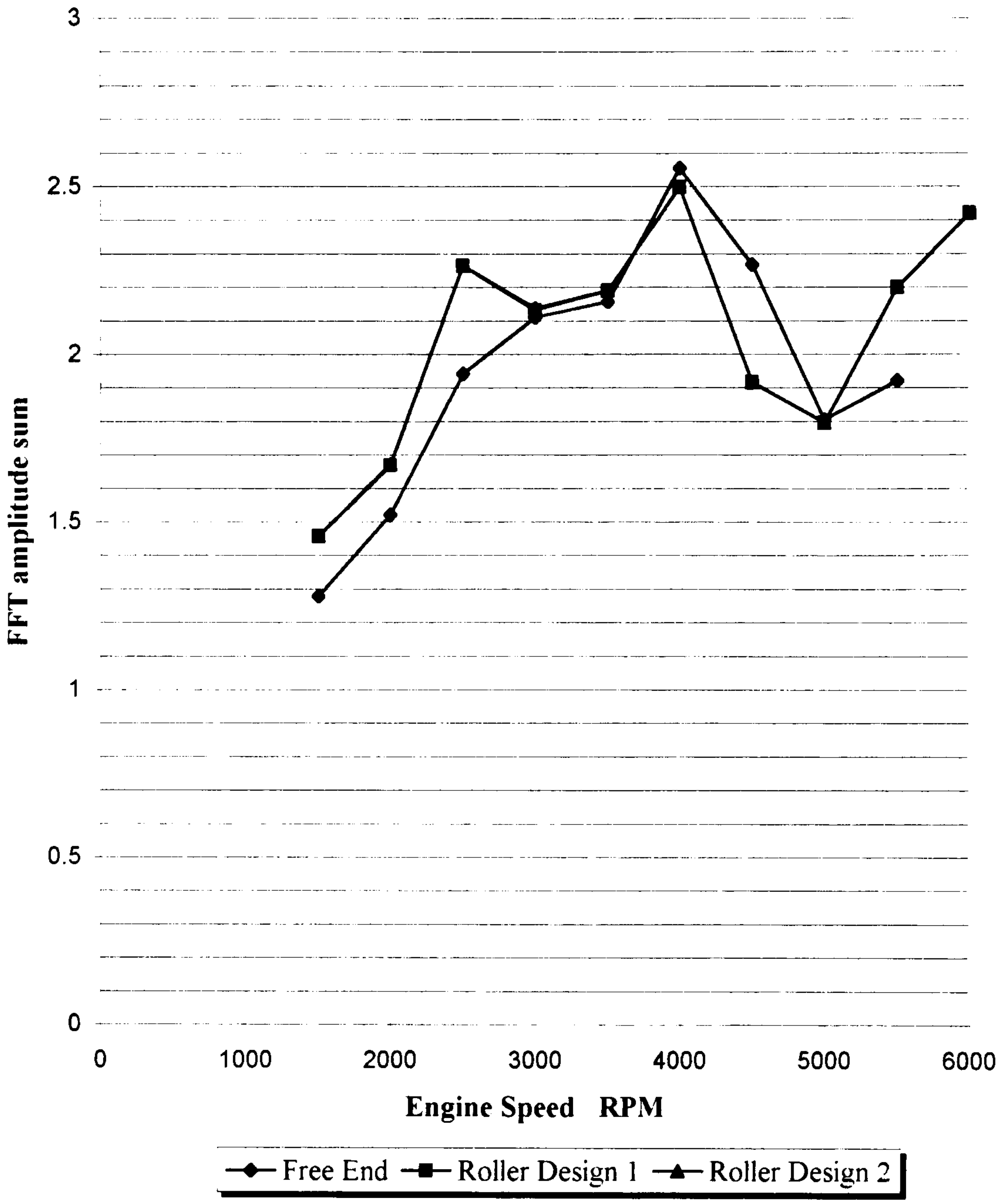

Figure 41. Roller Design 1 and 2 FFT Amplitude Sum verses Engine Speed at the Tenth Mass Point

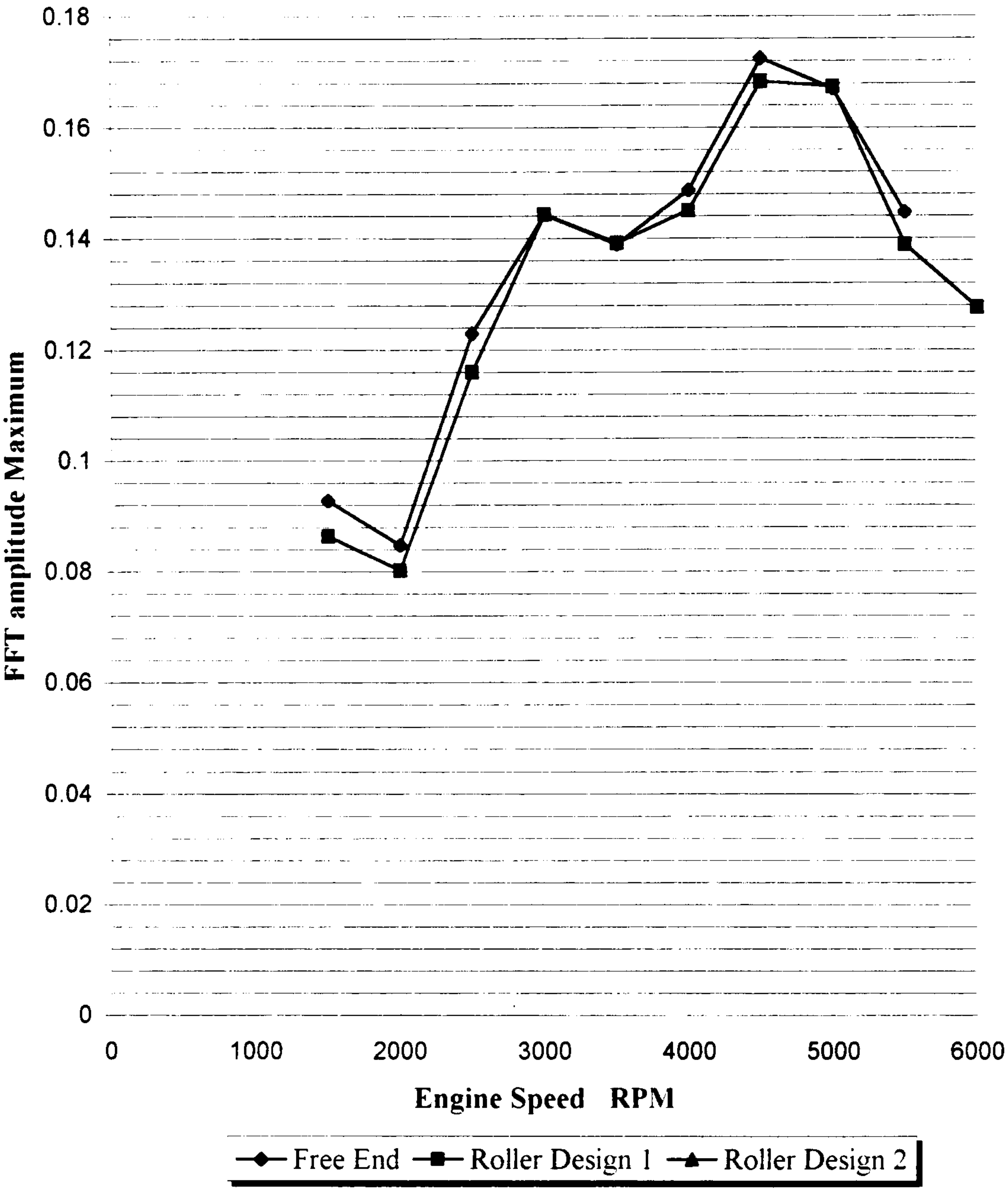

Figure 42. Roller Design 1 and 2 FFT Amplitude Maximum verses Engine Speed at the Tenth Mass Point

Free End

Speed	sum 10th	max 10th	sum 19th	max 19th
1500	1.27782	0.09277	1.27184	0.05983
2000	1.52111	0.08472	1.41496	0.06616
2500	1.94109	0.12292	1.68995	0.06112
3000	2.10947	0.14431	1.87741	0.07561
3500	2.1563	0.13892	1.93978	0.07712
4000	2.55505	0.14863	2.38084	0.23383
4500	2.2676	0.17249	2.42537	0.16513
5000	1.80442	0.16708	2.86256	0.24424
5500	1.92122	0.14466	2.28704	0.25872
6000				

Roller Design 5

Speed	sum 10th	max 10th	sum 19th	max 19th
1500	1.457605	0.086388	1.876253	0.069506
2000	1.673779	0.080200	1.914308	0.070798
2500	2.264141	0.115938	2.032463	0.069059
3000	2.137268	0.144408	2.423745	0.091180
3500	2.190450	0.139148	2.344801	0.085726
4000	2.498054	0.145057	3.179408	0.248127
4500	1.916850	0.168313	3.659806	0.182571
5000	1.796764	0.167330	3.458244	0.260155
5500	2.201142	0.138821	3.485306	0.283376
6000	2.420331	0.127498	3.642381	0.263250

Roller Design 4

Speed	sum 10th	max 10th	sum 19th	max 19th
1500	1.457629	0.086388	1.876319	0.069507
2000	1.674045	0.080198	1.914358	0.070798
2500	2.264128	0.115938	2.032453	0.069059
3000	2.137271	0.144409	2.423750	0.091180
3500	2.190444	0.139148	2.344831	0.085398
4000	2.498044	0.145057	3.179403	0.248128
4500	1.916869	0.168313	3.660004	0.182573
5000	1.796731	0.167331	3.458186	0.260155
5500	2.201140	0.138821	3.485289	0.285289
6000	2.420352	0.127498	3.642368	0.263250

Roller Design 6

Speed	sum 10th	max 10th	sum 19th	max 19th
1500	1.457602	0.086388	1.875814	0.069509
2000	1.673779	0.080200	1.914308	0.070798
2500	2.264132	0.115939	2.032459	0.069059
3000	2.137253	0.144408	2.423734	0.091180
3500	2.190460	0.139147	2.344866	0.085726
4000	2.498047	0.145058	3.179378	0.248128
4500	1.916804	0.168312	3.658407	0.182567
5000	1.796753	0.167331	3.458151	0.260155
5500	2.201133	0.138821	3.485252	0.283376
6000	2.420327	0.127498	3.642351	0.263251

Table 8. FFT Amplitude Statistics for Roller Designs 4, 5 and 6

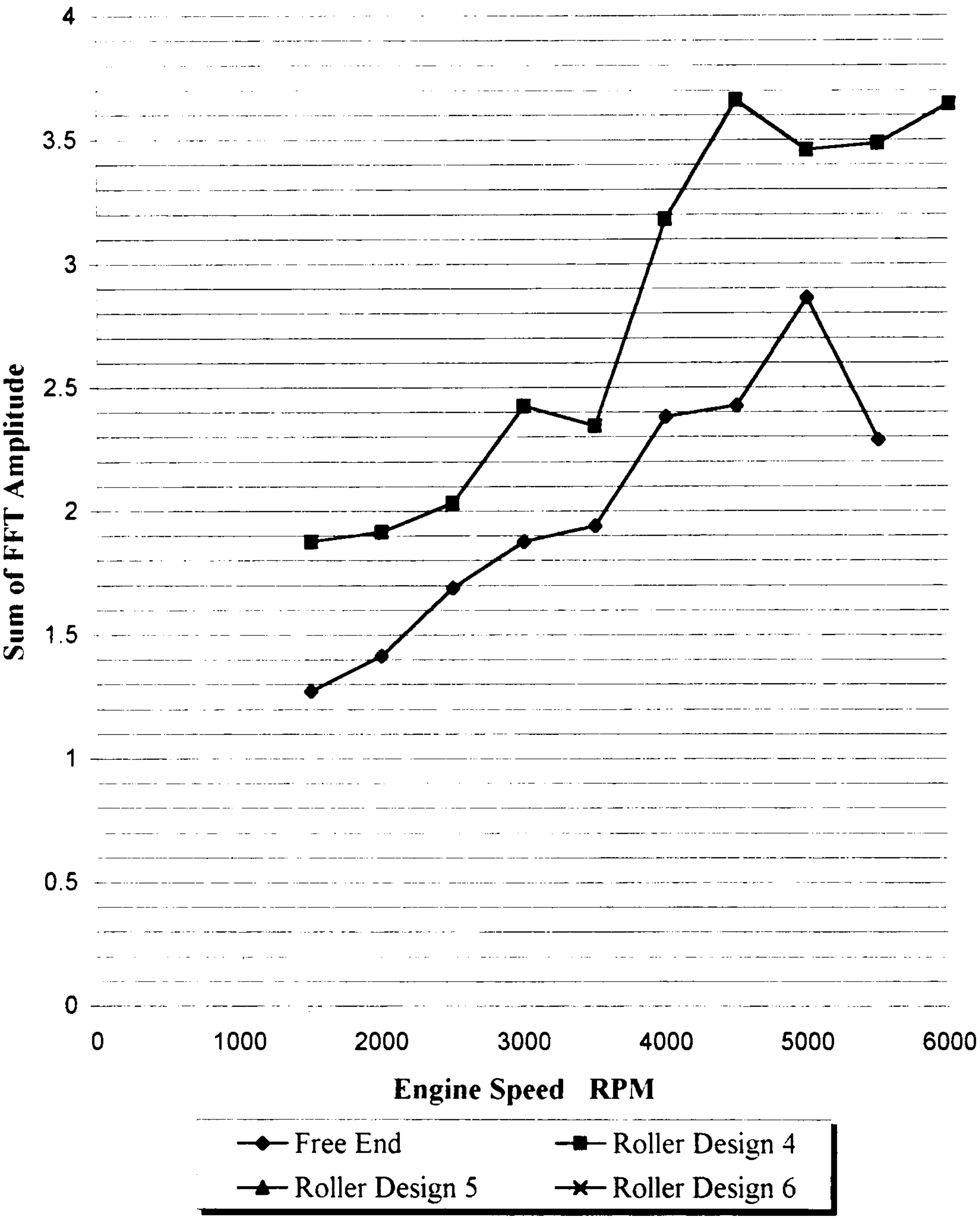

Figure 43. Roller Design 4, 5, and 6 FFT Amplitude Sum verses Engine Speed at the Nineteenth Mass Point

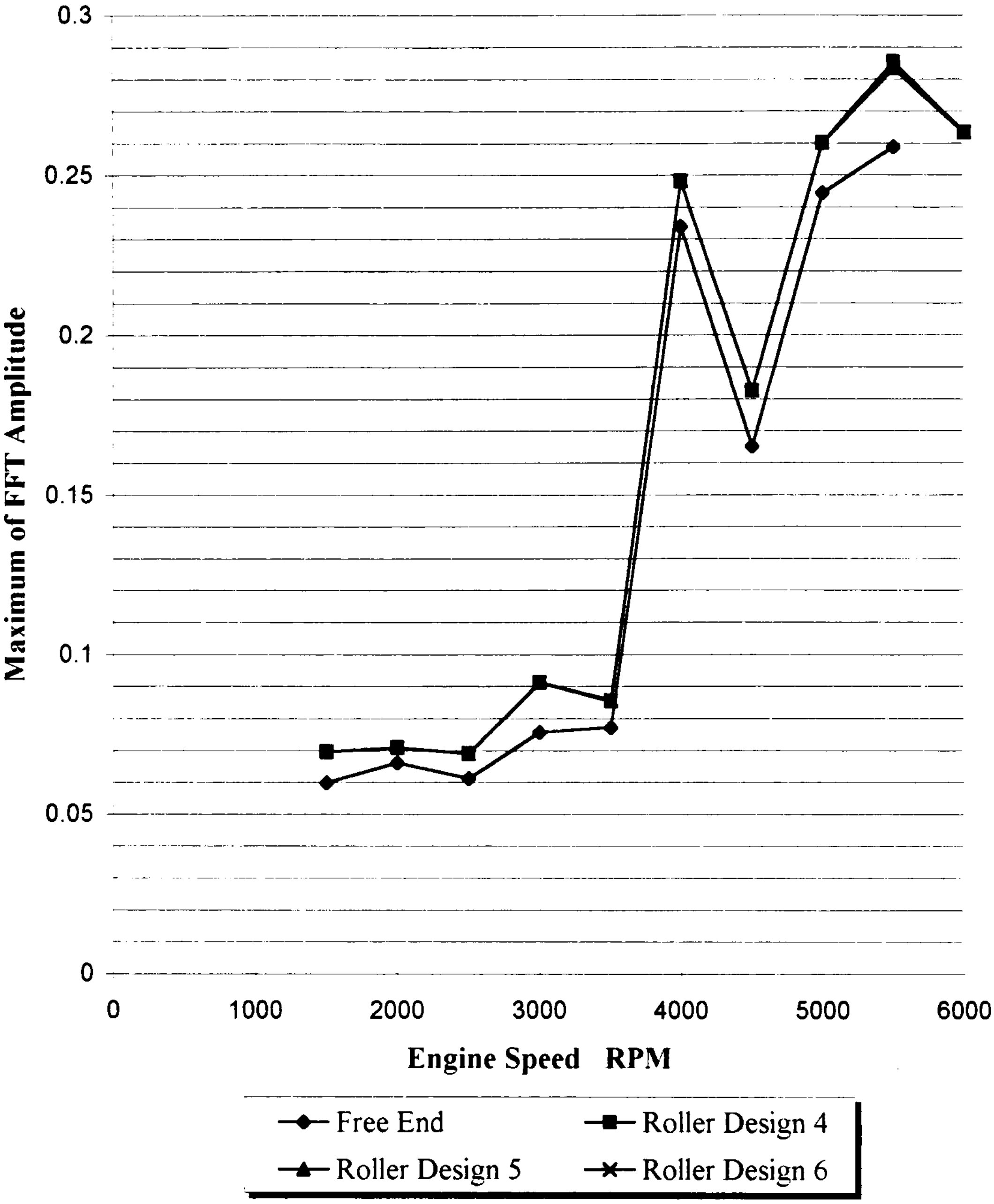

Figure 44. Roller Design 4, 5, and 6 FFT Amplitude Maximum verses Engine Speed at the Tenth Mass Point

between 0.004638 at 2000 RPM to 0.024656 at 5500 RPM.

To describe the damper designs' performance, Figure 45 shows the sum of the FFT amplitudes for the tenth mass point as a function of engine speed. The three SAE oil roller damper designs all performed within +/-0.000025 or +/-0.0017% of each other. The designs altered the free end FFT sums between -0.35075 at 4500 RPM and 0.0323051 at 2500 RPM. These designs lowered the sum in the 4000 RPM to 5000 RPM range.

The maximum of the FFT amplitudes plotted verses engine speed is presented in Figure 46. The three designs performed within +/-0.000002 of each other. They affected the maximum FFT amplitude between -0.006982 at 2500 RPM to 0.000098 at 3000 RPM. The designs lowered the amplitude everywhere in the speed range except at 3000 RPM, 3500 RPM, and 5000 RPM where it was only slightly increased.

There were no discernible differences in the statistics in the designs of the first two fluid types. This lack of variation in the results supports the idea that the viscous effects of the fluid are not seen. The damper design acted like a flywheel, only adding inertia to the system. These roller designs followed the general shape of the free end curve. This suggests there is no resonant behavior or need for tuning the inertial mass of the damper design.

The last three damper design utilized water, which has a viscosity of 0.145×10^{-6} reyn as the damping fluid. The seventh roller design had a radial clearance of 0.001 inch, and the eighth design's clearance was 0.05 inch. The ninth roller design had a radial clearance of 0.01 inch. A table of the bending response code's FFT analysis of the three designs is provided as Table 9. The sum of the FFT amplitudes for the nineteenth mass

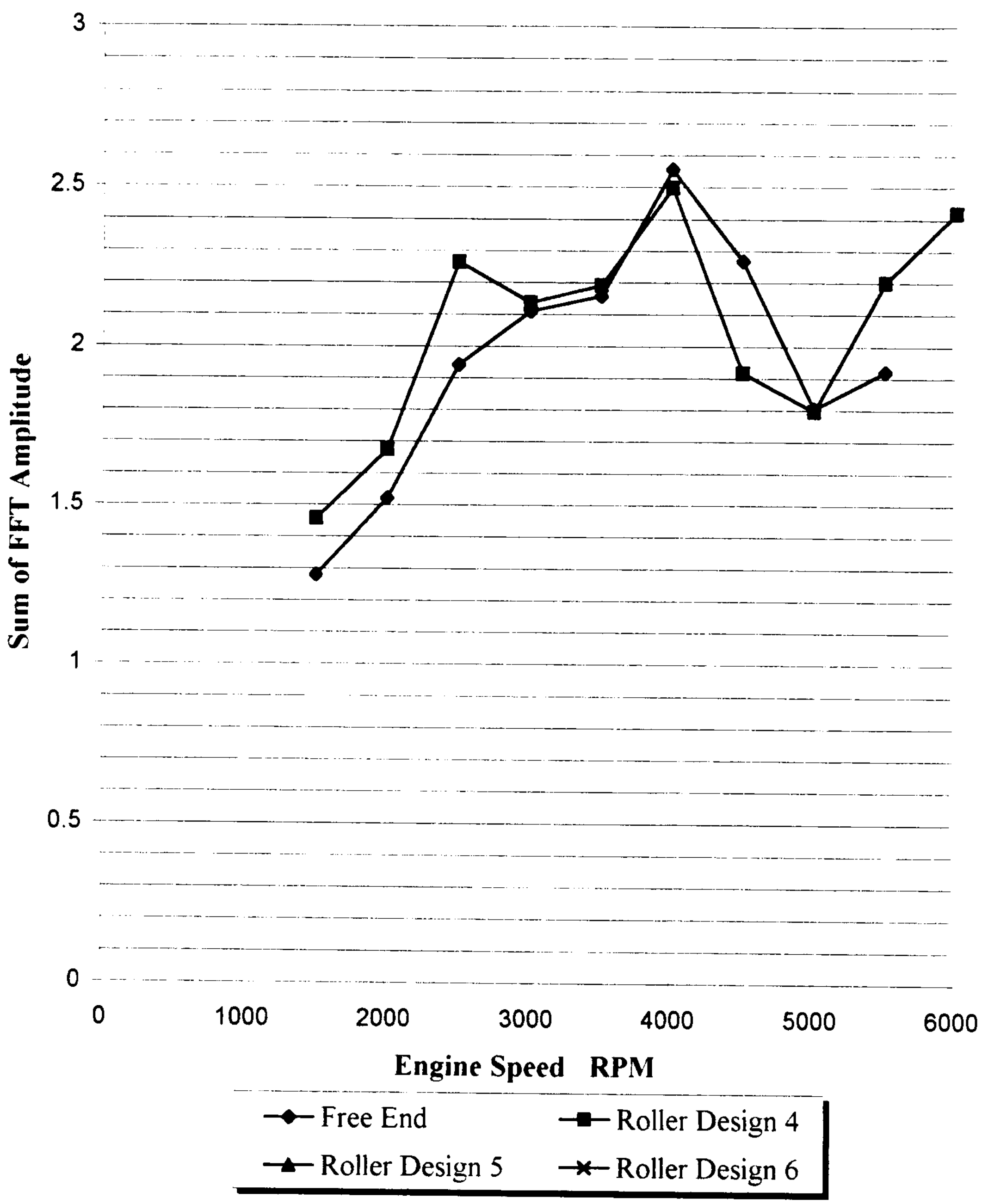

Figure 45. Roller Design 4, 5, and 6 FFT Amplitude Sum verses Engine Speed at the Tenth Mass Point

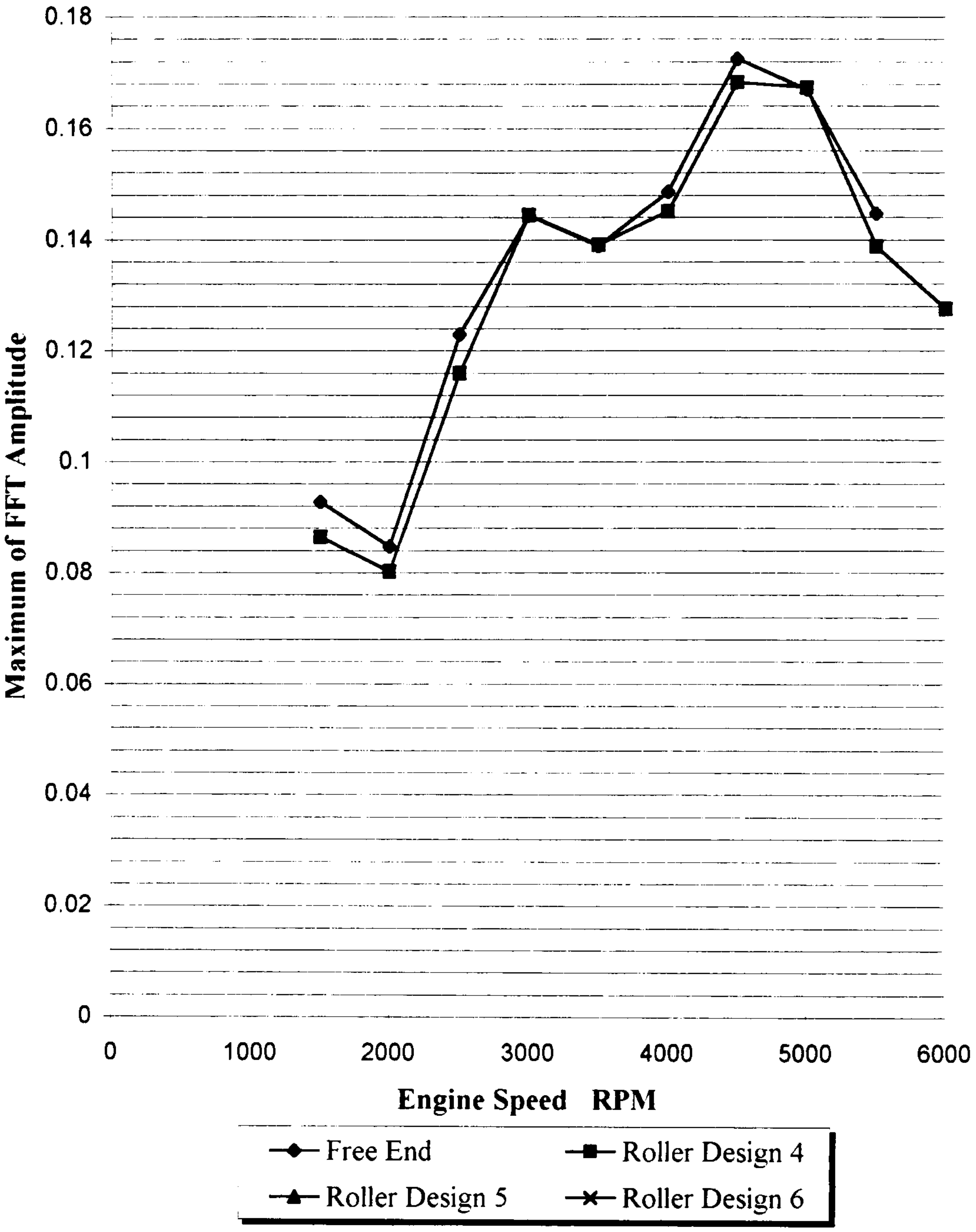

Figure 46. Roller Design 4, 5, and 6 FFT Amplitude Maximum verses Engine Speed at the Tenth Mass Point

Free End

Speed	sum 10th	max 10th	sum 19th	max 19th
1500	1.27782	0.09277	1.27184	0.05983
2000	1.52111	0.08472	1.41496	0.06616
2500	1.94109	0.12292	1.68995	0.06112
3000	2.10947	0.14431	1.87741	0.07561
3500	2.1563	0.13892	1.93978	0.07712
4000	2.55505	0.14863	2.38084	0.23383
4500	2.2676	0.17249	2.42537	0.16513
5000	1.80442	0.16708	2.86256	0.24424
5500	1.92122	0.14466	2.28704	0.25872
6000				

Roller Design 7

Speed	sum 10th	max 10th	sum 19th	max 19th
1500	1.222943	0.088343	2.232610	0.069719
2000	1.565302	0.085000	1.823628	0.072640
2500	1.862466	0.119533	1.965108	0.069760
3000	2.263815	0.143257	2.360885	0.094184
3500	2.306860	0.140334	2.330478	0.084571
4000	2.544228	0.145825	3.343309	0.247235
4500	2.299346	0.166596	3.714160	0.181017
5000	2.409369	0.167188	3.412368	0.262495
5500	1.942180	0.144307	3.101623	0.284037
6000				

Roller Design 7

Speed	sum 10th	max 10th	sum 19th	max 19th
1500	1.222934	0.088343	2.232550	0.069720
2000	1.565294	0.085000	1.823629	0.072640
2500	1.862473	0.119533	1.965102	0.069760
3000	2.263816	0.143257	2.360873	0.094184
3500	2.306860	0.140334	2.330474	0.084571
4000	2.544233	0.145824	3.343303	0.247234
4500	2.299356	0.166597	3.714083	0.181017
5000	2.409366	0.167188	3.412359	0.262495
5500	1.942190	0.144307	3.101628	0.284038
6000				

Roller Design 9

Speed	sum 10th	max 10th	sum 19th	max 19th
1500	1.312729	0.09301	1.890584	0.062004
2000	1.371385	0.084107	1.829528	0.070882
2500	1.959123	0.123098	2.131728	0.068371
3000	2.124783	0.144136	2.420268	0.091678
3500	2.155428	0.138708	2.42213	0.086495
4000	2.576686	0.148556	3.381164	0.244509
4500	2.212409	0.17172	4.127832	0.174517
5000	1.831046	0.166723	3.533525	0.256367
5500	1.942201	0.144307	3.101634	0.284038
6000				

Table 9. FFT Amplitude Statistics for Roller Designs 7, 8 and 9

point as a function of engine speed is presented in Figure 47. The seventh and eighth roller designs performed within +-0.00008 or +/-0.0042% of each other. These two designs increased the amplitude sum between 0.275161 at 2500 RPM to 1.288794 at 4500 RPM. The ninth design increased the amplitude sum between 0.414567 at 2000 RPM to 1.702466 at 4500 RPM. The seventh and eighth roller designs added less vibrational energy at every speed except 1500 RPM. The performance of these damper designs confirmed the predictions made in the theoretical analysis of the viscous roller designs.

For the comparison of the maximum FFT amplitude at the nineteenth mass point, Figure 48 is provided. Again, the seventh and eighth roller designs performed within +/-0.000001 or 0.0016% of each other. These two designs increased the maximum between 0.006484 at 2000 RPM and 0.025314 at 5500 RPM. The ninth roller design added between 0.002177 at 1500 RPM to 0.025315 at 5500 RPM. The ninth roller design out performed the other designs at lowering the maximum FFT amplitude everywhere except 3500 RPM.

In Figure 49, the sum of the FFT amplitude of the tenth mass point is plotted verses the engine speed. The seventh and eighth roller design differed by no more than +/-0.00001 or 0.00076%. These designs altered the sum of the tenth mass point by -0.054874 at 1500 RPM to 0.604951 at 5000 RPM. These designs reduced the vibrational energy at 1500 RPM, 2500 RPM, and 4000 RPM. The nineteenth roller design altered the vibrational energy of the tenth mass point by -0.149724 at 2000 RPM to 0.034912. The ninth roller design behaved close to the free end's vibrational characteristics.

Figure 50 presents the FFT amplitude maximum of the tenth mass point as a

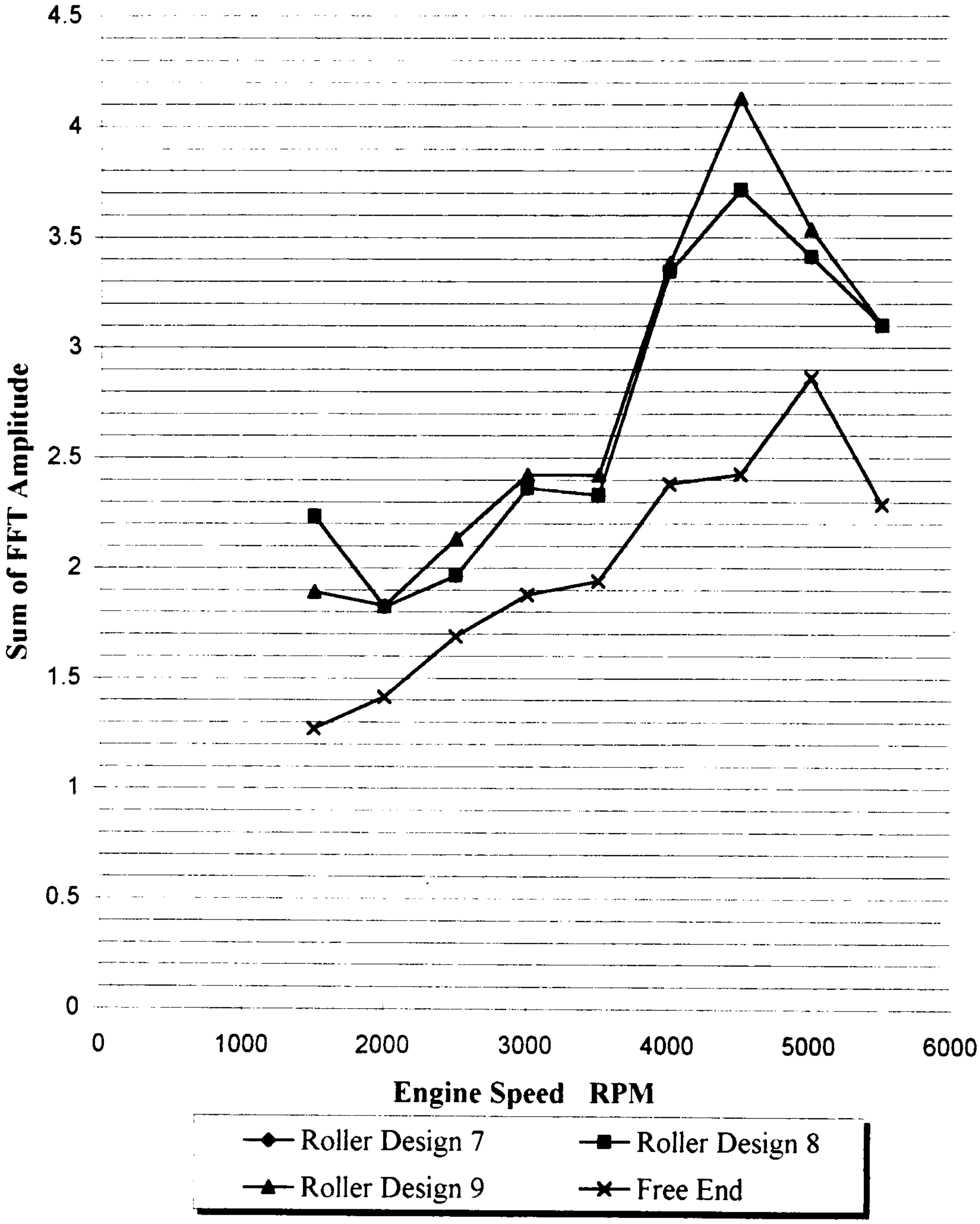

Figure 47. Roller Design 7, 8, and 9 FFT Amplitude Sum verses Engine Speed for Nineteenth Mass Point

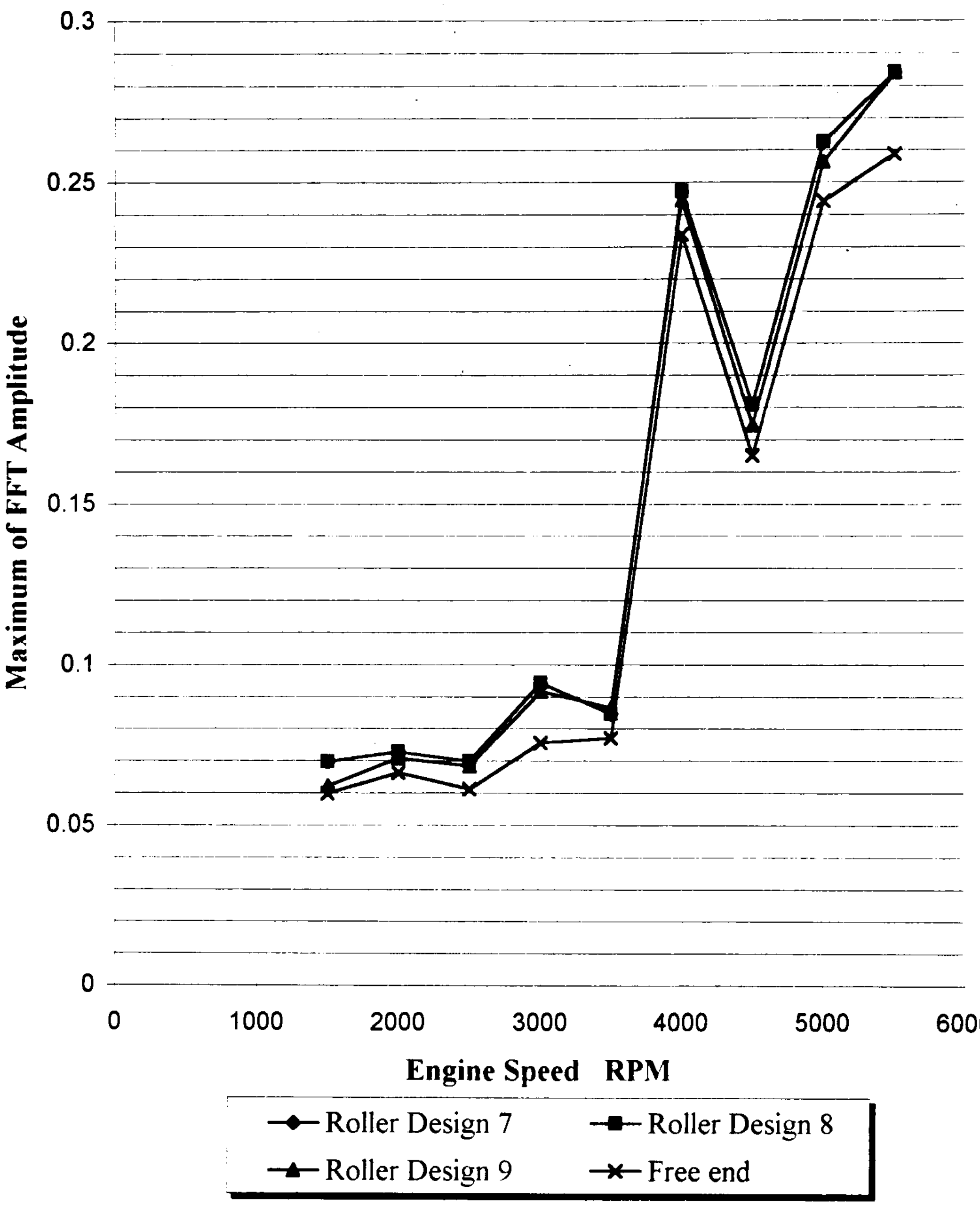

Figure 48. Roller Design 7, 8, and 9 FFT Amplitude Maximum verses Engine Speed for Nineteenth Mass Point

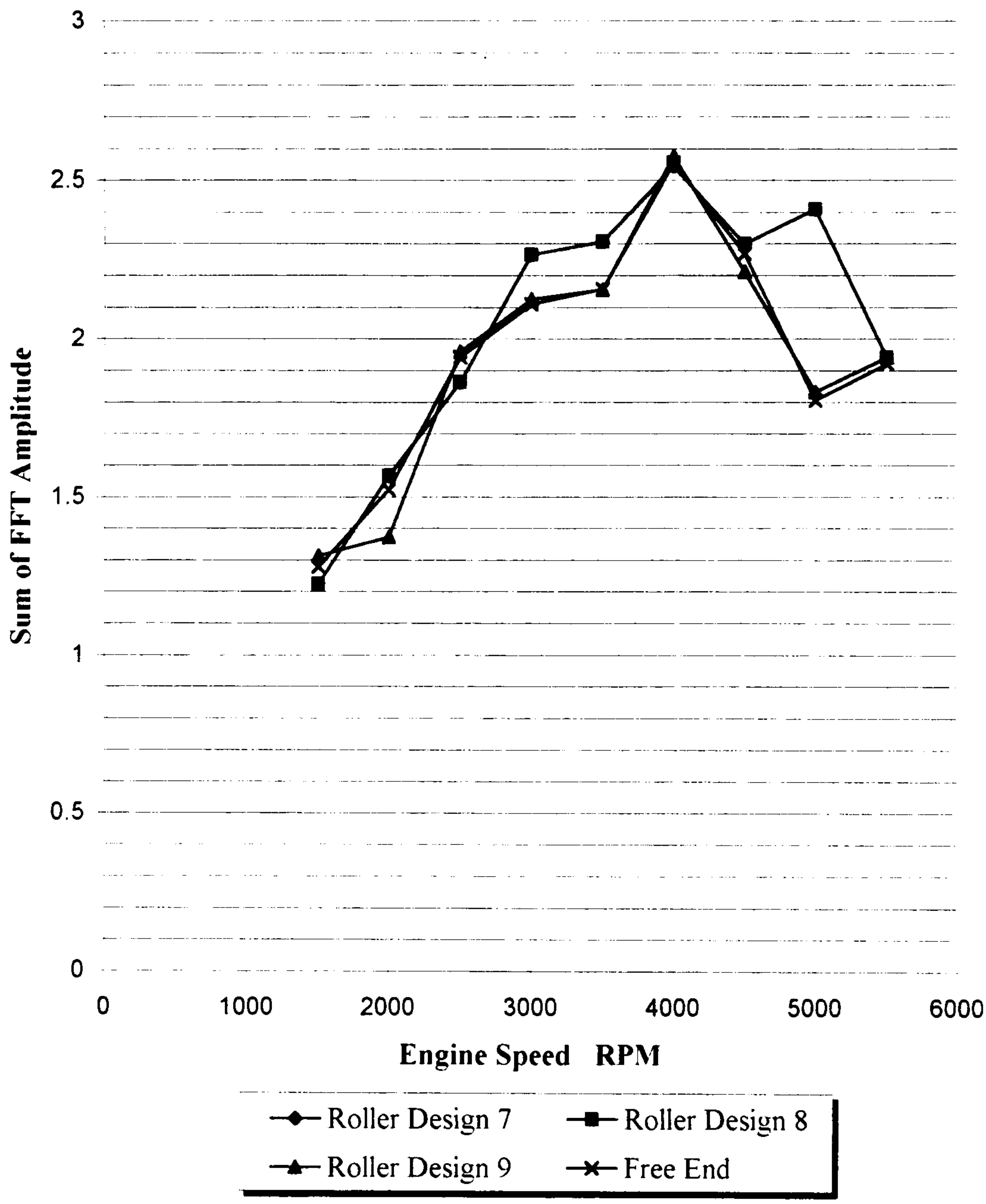

Figure 49. Roller Design 7, 8, and 9 FFT Amplitude Sum verses Engine Speed for the Tenth Mass Point

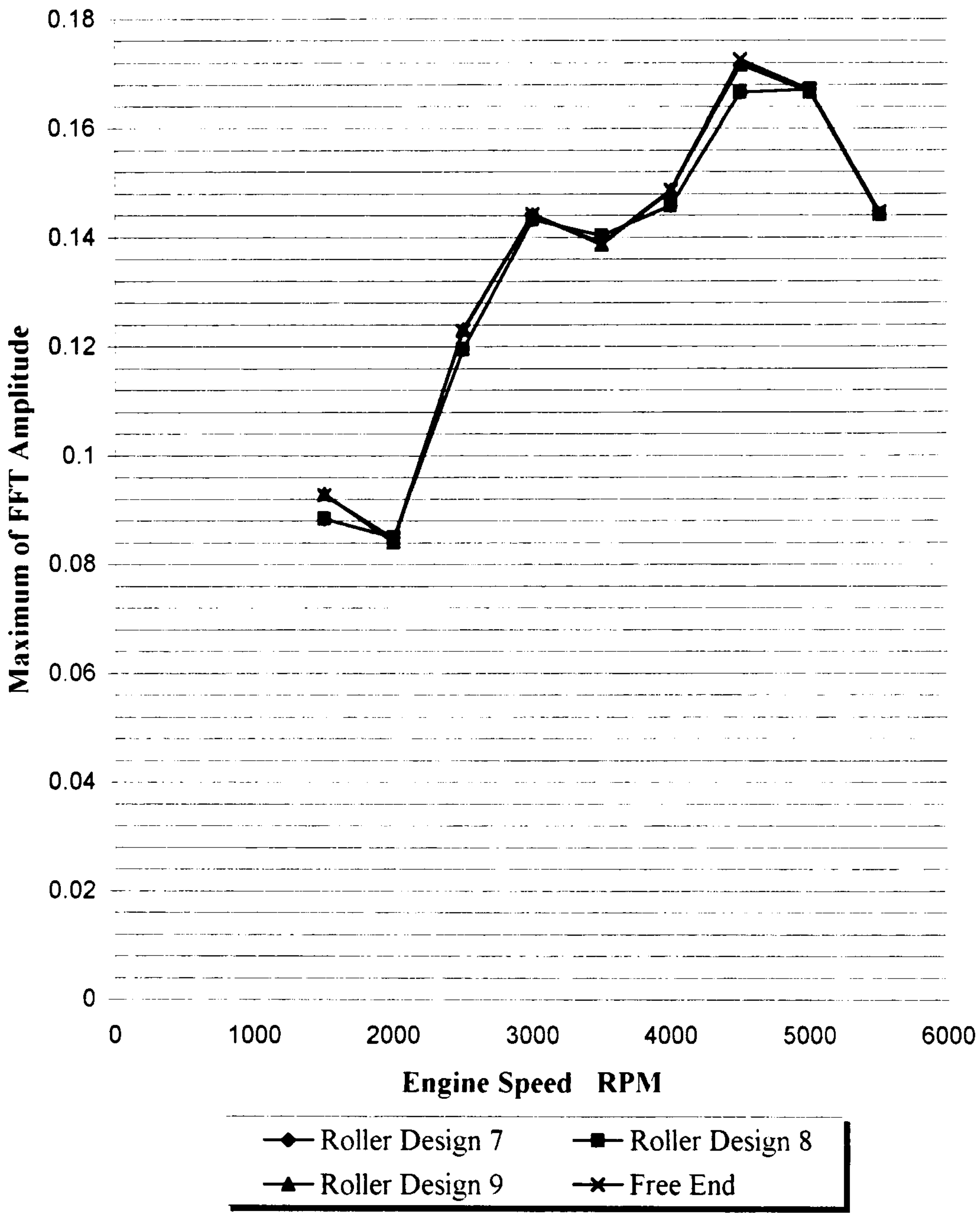

Figure 50. Roller Design 7, 8, and 9 FFT Amplitude Maximum verses Engine Speed for the Tenth Mass Point

function of engine speed. The seventh and eighth again were much the same. They differed by +/-0.000001. These designs altered the vibration by -0.005898 at 4500 RPM to 0.001415 at 3500 RPM. The designs lowered the maximum everywhere except at 2000 RPM, 3500 RPM, and 5000 RPM. The ninth roller design performed much the same as the free end situation. The ninth roller design altered the vibration by -0.000616 at 2000 RPM to 0.000181 at 2500 RPM.

The strong increase in the FFT sum of the nineteenth mass point at 4500 RPM was of great interest. This design had interesting characteristics at this speed. Roller design 9's FFT amplitude peaks for the tenth and nineteenth mass points are tabulated in Table 10. The differences between the free end and roller design 9 plots the peaks can be studied. Figure 51 is a plot of the information about the amplitude peaks. The tenth mass point's largest peak was at 250 Hz, and there were two smaller peaks at 322 Hz and 465 Hz. The nineteenth mass point contained one more peak frequency than the tenth mass point, 430 Hz. The nineteenth mass point's largest peak was at 178 Hz with smaller peaks at 465 Hz, 250 Hz, and 322 Hz. The maximum increase in FFT amplitude for roller design 9 at the nineteenth mass point occurred at 465 Hz. This was illustrated in Figure 52. Other increases occurred at 178 Hz and 357 Hz.

		Tenth			Nineteenth	
Peak Frequency(Hz)	Free End	Roller Design 9	Increase	Free End	Roller Design 9	Increase
178	0.083307	0.084165	0.000858	0.165125	0.174517	0.009392
215	0.039589	0.039710	0.000122	0.049072	0.052381	0.003309
250	0.172494	0.171720	-0.000774	0.089176	0.099145	0.009969
286	0.108277	0.107685	-0.000592	0.042191	0.050826	0.008635
322	0.123332	0.122830	-0.000502	0.064157	0.078249	0.014093
357	0.032766	0.033142	0.000376	0.042660	0.060335	0.017675
393	0.013673	0.013673	0.000000	0.028085	0.044323	0.016238
430				0.061071	0.098848	0.037777
465	0.039321	0.041247	0.001926	0.073684	0.138598	0.064914
501	0.020666	0.021796	0.001130	0.024740	0.051016	0.026276
536	0.012169	0.011786	-0.000383	0.007782	0.027105	0.019323

Table 10. Increase in FFT Amplitude for Roller Designs 9 at 4500 RPM

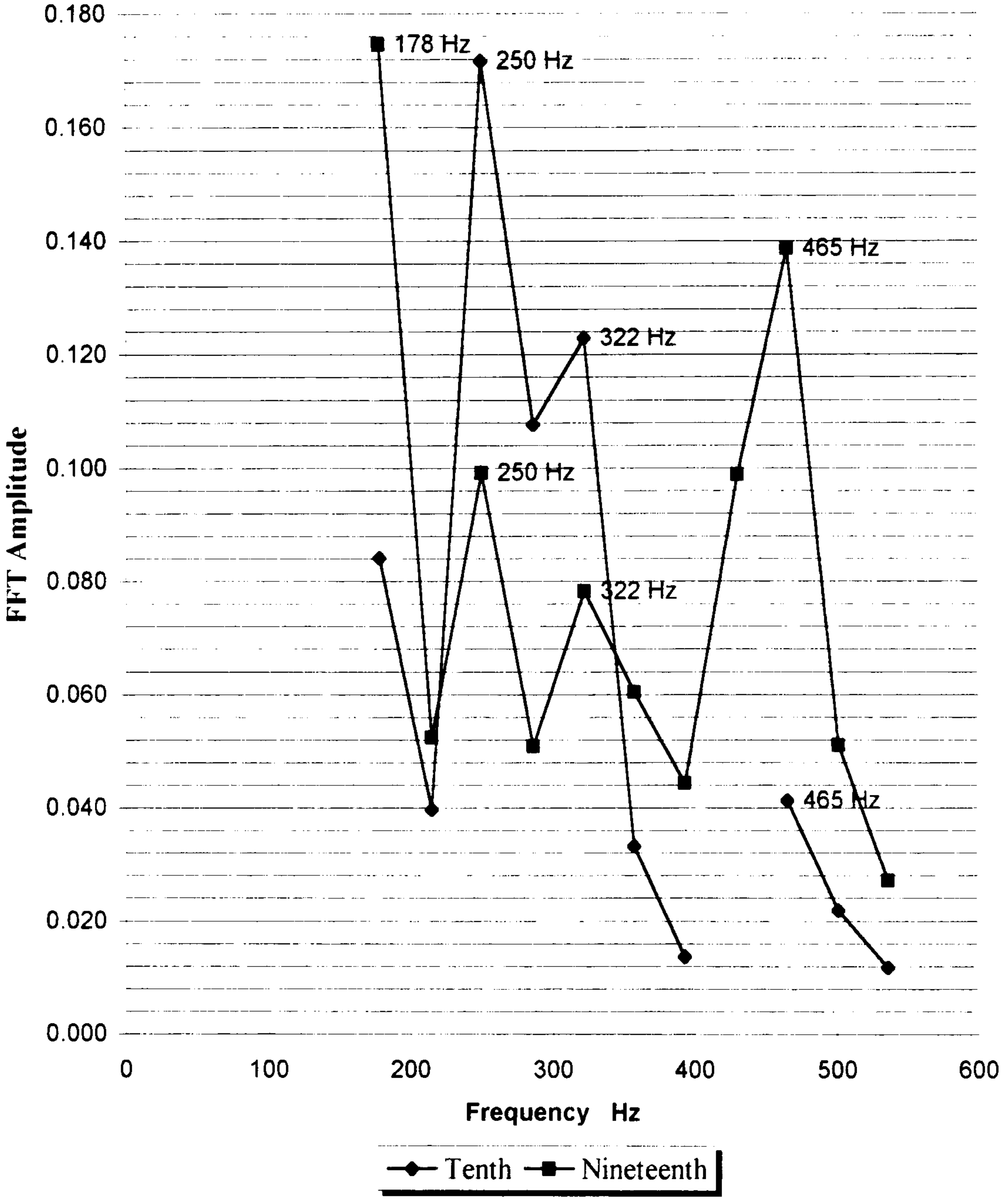

Figure 51. Roller Design 9's FFT Amplitude Peaks for Tenth and Nineteenth Mass Points at 4500 RPM

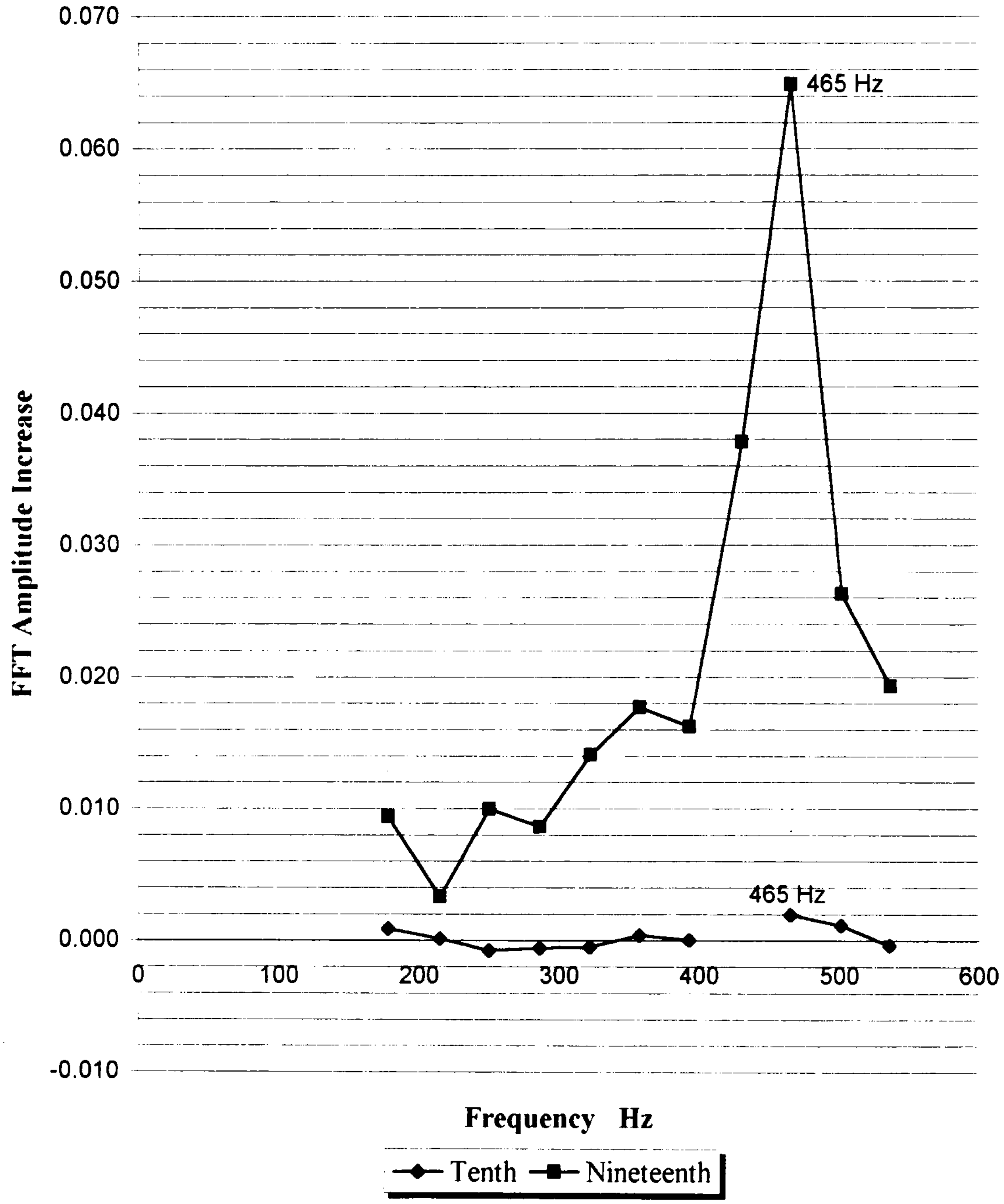

Figure 52. FFT Amplitude Increase for Both of Roller Design 9's Mass Points at 4500 RPM

Design Comparison

Each of the different damping schemes tested had a design that performed the best. These best performers were compared to choose the best design tested by the study. The theoretical damper of 100 performed the best of the ideal dampers tested. It acted against the nineteenth mass point's rotational motion. The second flywheel design performed better than any other flywheel tested. This flywheel was 7.50 inches in diameter and 1.25 inch thick. The second elastomer damper performed better than the first elastomer design. The second elastomer design had a 10 inch diameter, and its flywheel disk is 0.15 inch thick. The inertial ring had an inside diameter of 2.25 inches with a thickness of 1.25 inch. The elastomer ring was fashioned of Dupont Vitron A, and both disks were made of steel. The viscous roller damper had an 8 inch outside diameter and 1.25 inch thickness. The roller cavities were 0.75 inch in diameter and 4 inches long. Of the three fluids tested, water performed the best given the three test clearances, 0.001 inch, 0.005 inch, and 0.01 inch. Roller design 9, with the 0.01 inch clearance, performed the best of the roller dampers.

Table 11 tabulates all of these different damper designs and the free end. The first method of comparison was the FFT amplitude sum at the nineteenth mass point. The best preforming designs' sums are represented in Figure 53. The theoretical damper was the only design to reduce the amplitude sum in the problem frequency band. The flywheel design was the runner up, but it increased the FFT amplitude sum throughout the speed range. The elastomer design was the second runner up. While the roller design 9 performed better than the elastomer design until 4000 RPM, it had a sharp peak

Free End

Speed	sum 10th	max 10th	sum 19th	max 19th
1500	1.277817	0.092767	1.271844	0.059827
2000	1.521109	0.084723	1.414961	0.066156
2500	1.941089	0.122917	1.689947	0.061116
3000	2.10947	0.144313	1.877408	0.075605
3500	2.156297	0.138919	1.93978	0.077119
4000	2.555046	0.148634	2.380842	0.233832
4500	2.2676	0.172494	2.425366	0.165125
5000	1.804418	0.167083	2.862557	0.24424
5500	1.921216	0.144657	2.287038	0.258723
6000				

Ideal Damper=100

Speed	sum 10th	max 10th	sum 19th	max 19th
1500	1.480689	0.064776	1.028277	0.045978
2000	1.835307	0.074724	1.297358	0.063400
2500	1.861422	0.121698	1.551939	0.062994
3000	2.132605	0.144548	1.868890	0.076173
3500	2.179244	0.139693	1.670948	0.075180
4000	2.488485	0.144159	2.290877	0.236389
4500	1.915261	0.168085	2.228066	0.168382
5000	1.788843	0.167584	2.534853	0.248150
5500	2.184951	0.139074	2.562334	0.257238
6000	2.482940	0.127383	2.833324	0.245566

Flywheel Design 2

Speed	sum 10th	max 10th	sum 19th	max 19th
1500	1.495967	0.086586	1.341791	0.068546
2000	1.332803	0.08224	1.719899	0.069573
2500	2.190471	0.115391	2.195614	0.066431
3000	2.117266	0.144331	2.250579	0.078932
3500	2.215054	0.140162	2.10555	0.082847
4000	2.508272	0.145257	2.853501	0.245943
4500	1.901036	0.168666	3.128507	0.180479
5000	1.856941	0.167891	3.682286	0.259111
5500	2.225607	0.138477	3.151325	0.278465
6000	2.782844	0.131487	3.339649	0.259018

Elastomer Design 2

Speed	sum 10th	max 10th	sum 19th	max 19th
1500	1.500505	0.087908	1.493535	0.070167
2000	1.298363	0.081896	2.005867	0.070774
2500	2.286424	0.116586	2.146171	0.069204
3000	2.141946	0.145847	2.602622	0.111571
3500	2.225525	0.139455	2.604442	0.109498
4000	2.511199	0.142934	3.300135	0.253031
4500	1.888774	0.165737	3.041063	0.184531
5000	1.855325	0.165067	3.631237	0.260359
5500	2.186394	0.138446	3.794549	0.279065
6000	2.331851	0.127303	3.758491	0.263846

Roller Design 9

Speed	sum 10th	max 10th	sum 19th	max 19th
1500	1.312729	0.09301	1.890584	0.062004
2000	1.371385	0.084107	1.829528	0.070882
2500	1.959123	0.123098	2.131728	0.068371
3000	2.124783	0.144136	2.420268	0.091678
3500	2.155428	0.138708	2.42213	0.086495
4000	2.576686	0.148556	3.381164	0.244509
4500	2.212409	0.17172	4.127832	0.174517
5000	1.831046	0.166723	3.533525	0.256367
5500	1.942201	0.144307	3.101634	0.284038
6000				

Table 11. Damper Design Comparisons

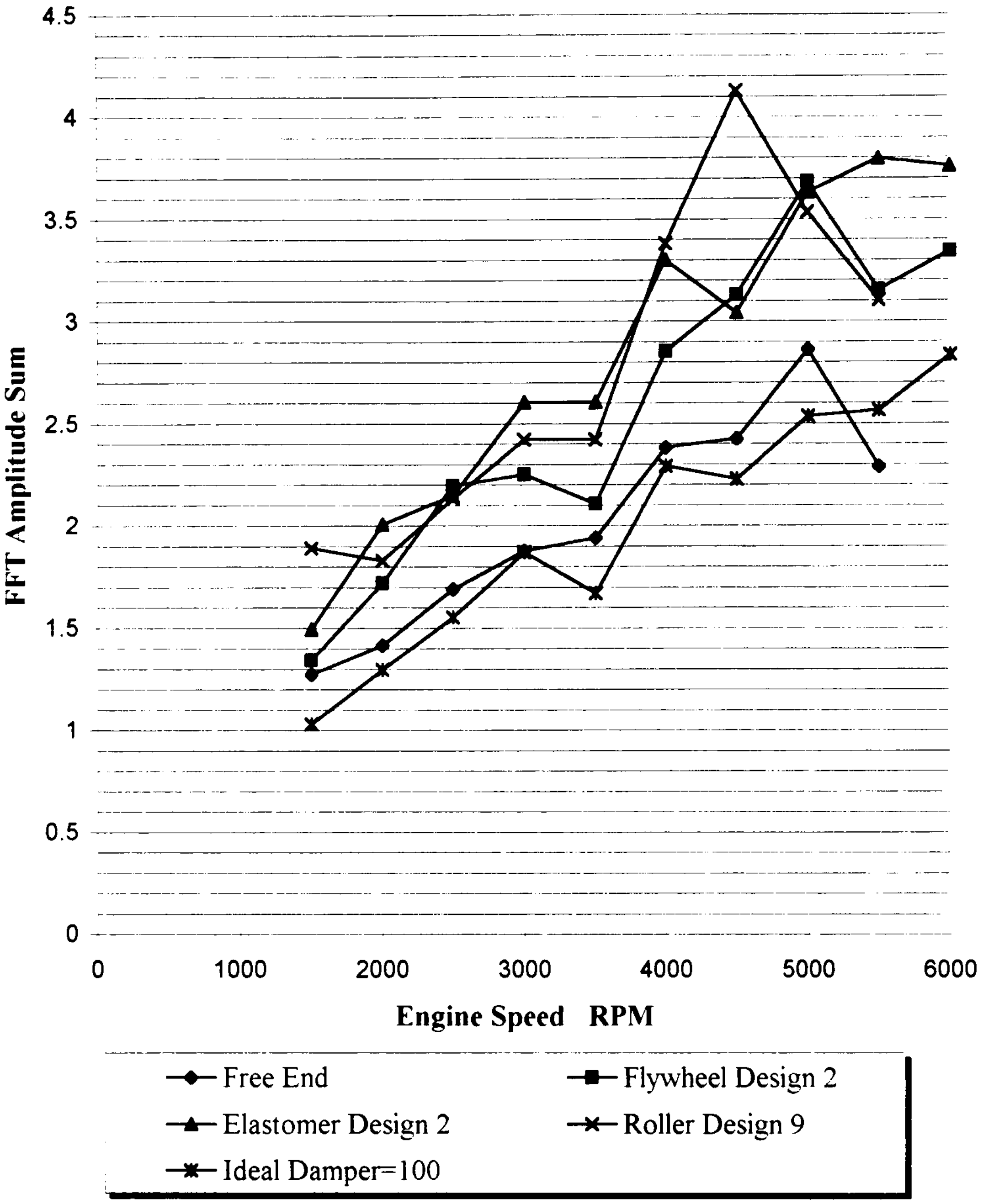

Figure 53. FFT Amplitude Sum verses Engine Speed for the Nineteenth Mass Point for the Comparison of Different Damper Designs

at 4500 RPM. This peak caused it to be in last place.

The next measure used was the FFT maximum at the nineteenth mass point. A graph of the FFT maximum verses engine speed for the different designs is provided as Figure 54. The theoretical damper was the only design to decrease the maximum. The decrease was only slight at 2000 RPM, 3500 RPM, and 5500 RPM. With the exception of one speed, 3000 RPM, the roller damper 9 design performed better than the other real designs. The flywheel design performed slightly worse than the roller damper design. The elastomer design performed the worst of the damper designs. A particular problem occurred in the 2500 RPM to 3500 RPM speed range with the elastomer damper. The largest differences in the different damper design occurred at 1500 RPM, 3000 RPM, and 5500 RPM.

The next method of comparison was the FFT amplitude sum at the tenth mass point. Figure 55 is a graph of the different damper design's FFT amplitude sum verses engine speed. No one design performed best throughout the entire speed range. The theoretical damper design increased the sum at speeds below 2000 RPM or above 5000 RPM. These increase were relatively severe at 2000 RPM and 5500 RPM. The flywheel design varied wildly at speeds below 3000 RPM. In this range the amplitude sum was either significantly raised or lowered from speed to speed. In the 3000 RPM to 5000 RPM range, the flywheel had only a slight effect on the free end sum except at 4500 RPM. Above 5000 RPM the flywheel sharply raised the sum. The elastomer design had much the same behavior as the flywheel design. The only differences were at 2000 RPM, 2500

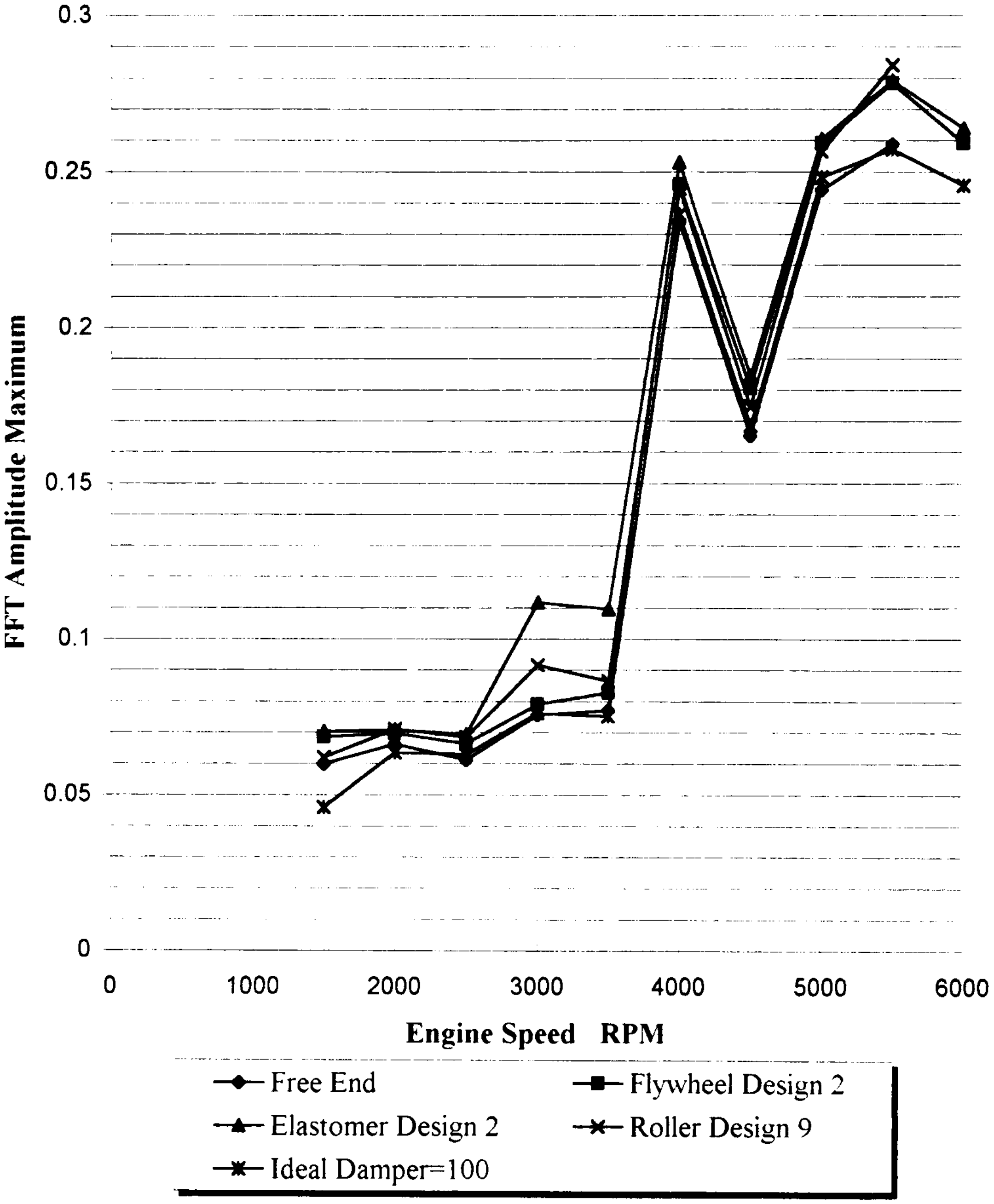

Figure 54. FFT Amplitude Maximum verses Engine Speed for the Nineteenth Mass Point for Comparison of Different Damper Designs

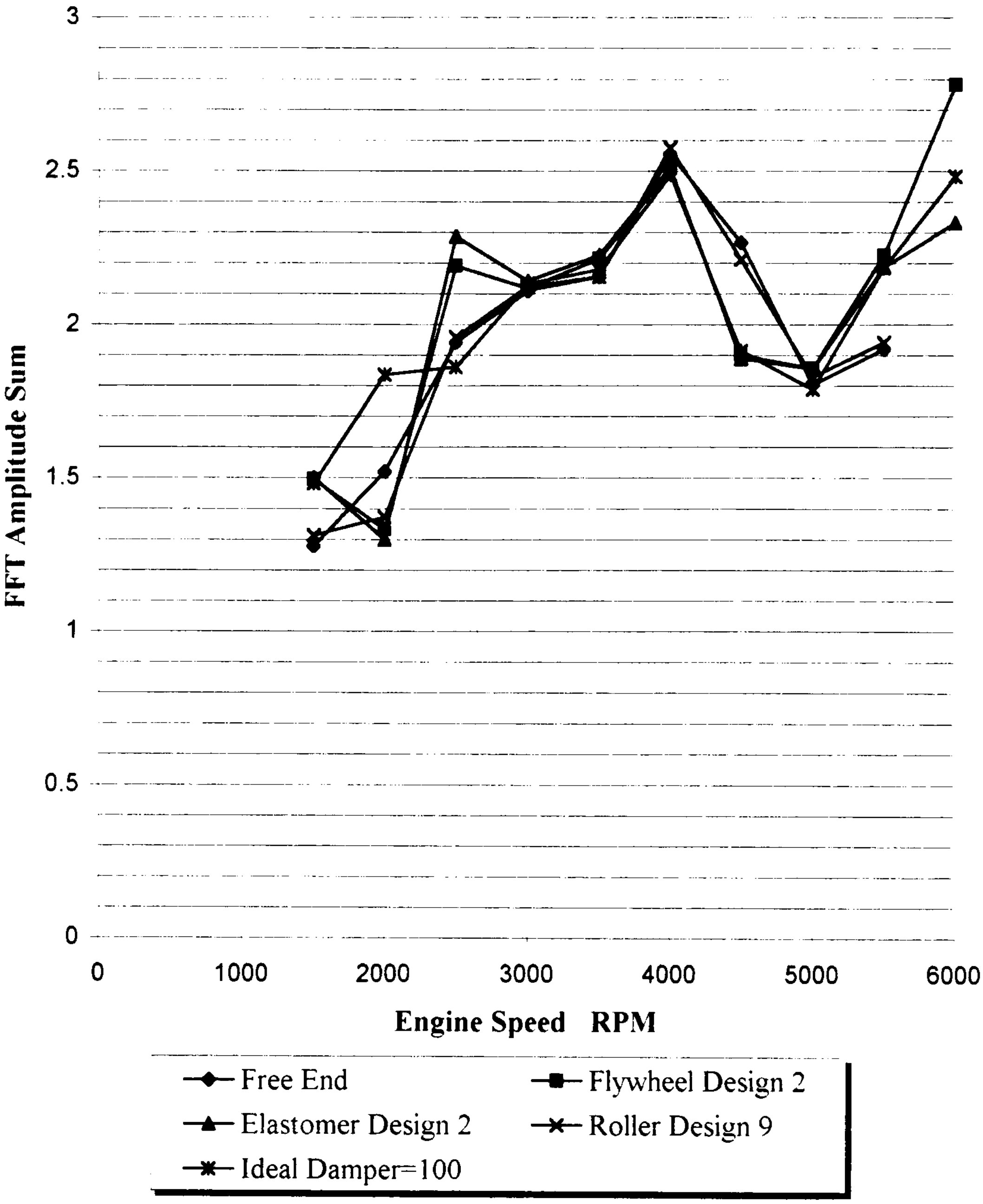

Figure 55. FFT Amplitude Sum verses Engine Speed for the Tenth Mass Point for Comparison of Different Damper Designs

RPM, and 6000 RPM. At these speeds the elastomer design exaggerated the difference between the free end and flywheel sums. The roller design had very little effect on the free end amplitude sum. The only discernible difference was at 2000 RPM where the sum was decreased. All of the designs, except the roller design, significantly decreased the FFT amplitude sum at the tenth mass point at 4500 RPM.

The roller design had little effect on the free end FFT amplitude maximum throughout the entire speed range. This is seen in Figure 56, a plot of the FFT amplitude maximum at the tenth mass point verses engine speed. The largest improvements were made at 1500 RPM and 5500 RPM where the theoretical damper, flywheel, and the elastomer damper decreased the maximum. The elastomer damper performed the better than the other dampers in the 3500 RPM to 5000 RPM speed range.

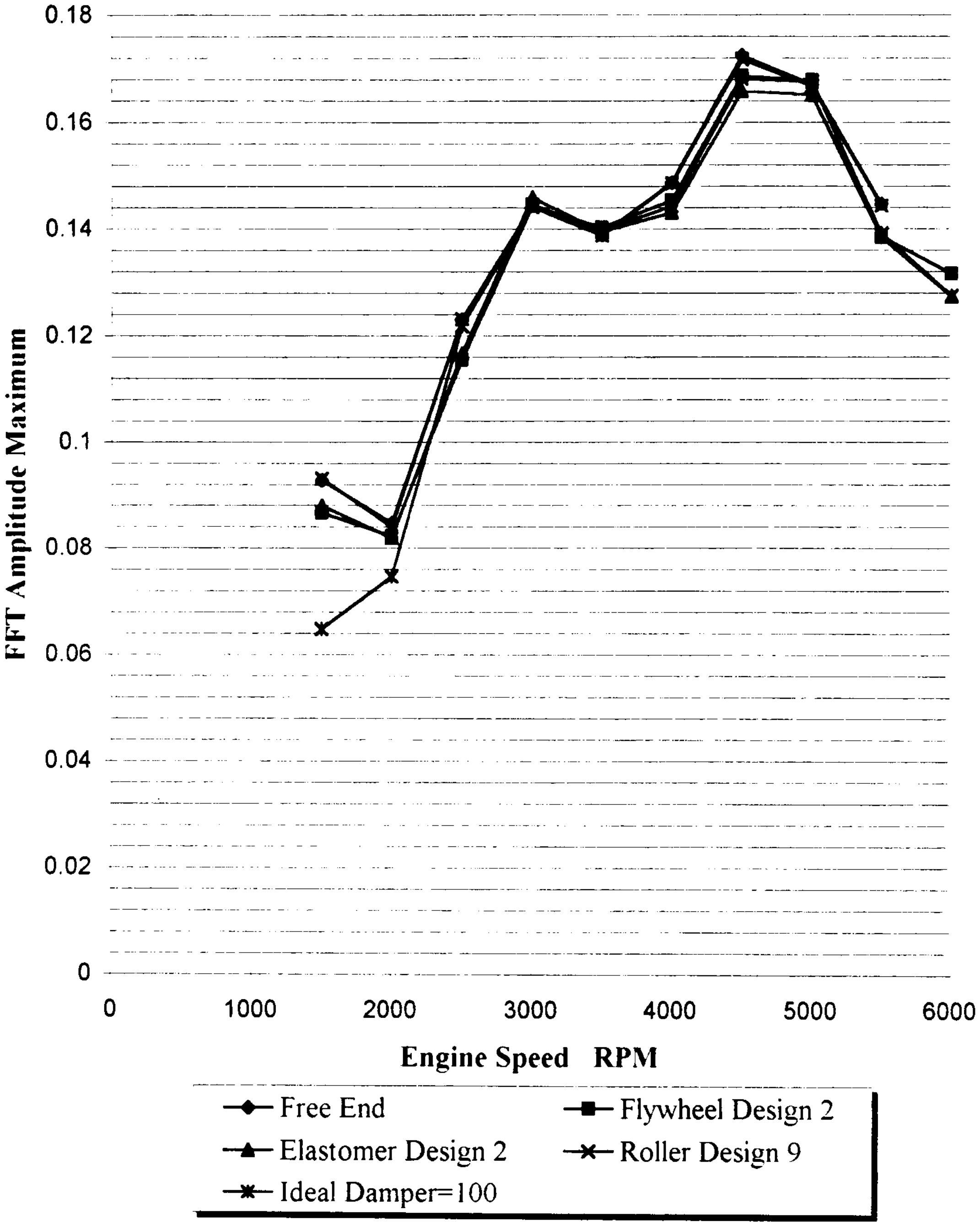

Figure 56. FFT Amplitude Maximum verses Engine Speed for the Tenth Mass Point for Comparison of Different Damper Designs

Chapter Five

Conclusions

A bending response code was written to model the bending vibrational response of an inline four cylinder crankshaft. The code solved the second order linear coupled differential equations using a Runge-Kutta solution technique. These equations described the transitional and rotational components of the discrete mass points that modeled the crankshaft. The code modeled the five bearing points using the hydrodynamic and structure elasticity of the bearings. The firing of the four pistons was modeled using a theoretical single cylinder torque curve and a common firing order. The code provided the transitional and rotational displacement and velocity for each mass point. For each design, the code was run at an engine speed range from 1500 RPM to 6000 RPM in 500 RPM increments. The results of the code were confirmed by other experimental and theoretical studies [1-8].

Several different damper and, or absorber designs were added to the system to combat the bending vibration. The first of these dampers was a theoretical damper acting in the rotational component's equation. This theoretical damper's results represented the maximum damping that can be added to the system. The second type of damper was the commonly used flywheel. This type of damper tuned the vibrational characteristics through the use of added inertial mass. The third type of damper was an elastomer damper. Vibrational energy was absorbed by the deformation of an elastomer between two inertial masses. The elastomer damper was added to the crankshaft system in place of the standard flywheel. The last damper type was an invention of Dr. Frank Speckhart and was the original focus of the study. The damper dissipated vibrational energy through the viscous interaction between a roller suspended in a fluid and a damper case. Through the course of the study sixteen variations of these damping designs were tested.

From studying the vibrational characteristics of the free end or no damper configuration, several facts were revealed. The 4000 RPM to 5000 RPM speed range was the critical speed range for the crankshaft's vibrational characteristics. Most of the vibrational energy was in the 250 Hz to 322 Hz band for the tenth mass point, and most of the vibrational energy for the nineteenth mass point was less than 178 Hz or greater than 393 Hz. The greatest increase occurs at 178 Hz as the engine speed was increased. The number of vibrational peaks decreased while their amplitudes increased for increasing engine speed.

Each of the different design variations had a champion of those tested. This champion performed better than the other variations of that design. The first of these champions was the theoretical damper of 100. The theoretical damper of 100 was the most damping that was tested in this study. The theoretical damper was the only tested damper design to reduce the vibrational energy at the nineteenth mass point. This conclusion was based upon the sum of the FFT amplitudes in the 150 Hz to 550 Hz frequency range. Because the end of the crankshaft was restricted, the vibration at the tenth mass point was affected. The vibration at the tenth mass point was decreased by the addition of the damper except at 3000 RPM, 3500 RPM, 5500 RPM, and 6000 RPM.

Of the remaining designs, the 7.50 inch diameter by 1.25 inch thick flywheel added the least amount of vibrational energy to the system at the nineteenth mass point. At the tenth mass point, the vibration, as measures by the FFT amplitude sum, was decreased at 2000 RPM, 4000 RPM, and 4500 RPM. The vibration was increased everywhere else. The vibration at the tenth mass point varied radically at speeds below 3000 RPM The decrease in the sum of the FFT amplitudes can be attributed to the tuning of the crankshaft system by the addition of the flywheel. Tuning happened in two ways. First, the resonant frequency of the system was changed by the addition of inertial mass to the system. Secondly, the modal shapes of the vibration changed with the addition at the end of the crankshaft system. The flywheel was a simple and inexpensive means of combating bending vibration.

The roller damper 9 design performed better than the second elastomer damper except at the 4500 RPM speed. The roller damper design experienced a sharp increase at this speed. The largest increase occurred at 465 Hz at 4500 RPM. It was because of this increase that the second elastomer design performs better than the viscous roller design 9 at the nineteenth mass point. At the tenth mass point, the roller damper design 9 performed much the same as the free end. It decreased the vibration only at 2000 RPM. The second elastomer damper design performed much the same as the flywheel except at 2000 RPM, 2500 RPM, and 6000 RPM. At these speeds the elastomer damper exaggerated the crankshaft vibration.

The vibration at the interior mass points caused powerplant vibration due to solid propagation through the bearings into the engine block. This vibration can be reduced by the addition of a damping device to the rear of the crankshaft. Results obtained through the investigation were encouraging. The viscous effects of the fluid utilized in the roller damper can make a dramatic difference in its vibrational response. Results of the elastomer damper were also encouraging. The damper's tuning, relative mass sizes and elastomer choice, made a dramatic effect on each damper's vibrational response.

References

References

1. Kamiyi, Tamotsu et al. "Toyota's New Type of Crankshaft Pulley to Improve the Compartment Tone Quality". SAE Paper No. 880078. Society of Automotive Engineers, 1988.

2. Kinoshita, Masaru et al. "An Experimental Study of a Torsional/Bending Damper Pulley for an engine Crankshaft." SAE Paper No. 891127. Society of Automotive Engineers, 1990.

3. Ide, Shoichiro et al. "Improvement of Engine Sound Quality Through a New Flywheel System Flexibly Mounted to the Crankshaft". SAE Paper No. 900391. Society of Automotive Engineers, 1990.

4. Hodgetts, D. "The Whirl Modes of Vibration of a Crankshaft". Institution of Mechanical Engineers Conference Publications. Mechanical Engineering Publications Limited, 1976.

5. Oakamura, M.A. et al. "Dynamic Stiffness Matrix Method for the Three-Dimensional Analysis of Crankshaft Vibrations". Proceedings of the Institution of Mechanical Engineers. Mechanical Engineering Publications Limited, 1988.

6. Schwibinger, Peter et al. "Reduction of Vibration and Noise in the Powertrain of Passenger Cars with Elastomer Dampers". SAE Paper No. 910616. Society of Automotive Engineers, 1991.

7. Uchida, Takanao et al. "Honda New In-line Five Cylinder Engine -- Noise and Vibration Reduction". SAE Paper No. 900389. Society of Automotive Engineers, 1990.

8. Priebsch, Hans H. et al. "Structure Borne Noise Prediction Techniques." SAE Paper No. 900019. Society of Automotive Engineers, 1990.

9. Priebsch, H.-H. et al. "Prediction Technique for Stress and Vibration of Nonlinear Supported, Rotating Crankshafts." Journal of Engineering for Gas Turbines and Power. Society of Engineering for Gas Turbines and Power, 1993. Vol. 115, 711-719.

10. Pestel, Edward C. Matrix Methods in ElastoMechanics. McGraw-Hill Book Company. 1963.

11. Shigley, et al. Mechanical Engineering Design. McGraw-Hill Book Company. 1989. p. 479-523.
12. Taylor, Charles F. The Internal-Combustion Engine in Theory and Practice Volume II: Combustion, Fuels, Materials, Design. The M.I.T Press, 1984. p. 240-692.

13. Radzimovsky, E.I. Lubrication of Bearings: Theoretical Principals and Design. Ronald Press Company, New York, 1956. p. 21, 41-45.

14. Harris, Cyril M. Shock and Vibration Handbook. McGraw-Hill Book Company, New York, 1993. p. 35.1-39.1.

15. Ferry, John D. Viscoelastic Properties of Polymers. John Wiley & Sons, INC. New York, 1978. p. 437-454.

16. Charrier, Jean-Michel. Polymeric Materials and Processing: Plastics, Elastomers, and Composites. Hanser Publishers, Munich, 1990. p. 294-555.

17. Dostal, Cyril A. et al. Engineered Materials Handbook Engineering Plastics. ASM International, Ohio, 1985. p.109-112.

18. Avallone, Eugene A. Mark's Standard Handbook for Mechanical Engineers. McGraw-Hill Book Company, New York, 1987. p.8.116-8.117.

19. Kutz, Myer. Mechanical Engineers' Handbook. John Wiley & Sons, INC. New York, 1986. p.464-469.

20. Boroski, V.J. et al. "Reducing Vibration of Reciprocating Engines with Crankshaft Pendulum Vibration Absorbers". SAE Paper No. 911876. Society of Automotive Engineers, 1991.

Appendix A

Appendix A contains the programs used in the study including:

1. Free end Crankshaft Bending Response Code,
2. Gas Force Calculation Code,
3. PSPlot Input Signal Code,
4. Flywheel added Crankshaft Bending Response Code,
5. Elastomer Damper added Crankshaft Bending Response Code,
6. Viscous Roller Damper added Crankshaft Bending Response Code,

Free End Crankshaft Bending Response Code

```
* This program calculates the response of a model crankshaft with a Free End
* Initialize the variables
        Integer Pts, N, J, JJ, I
        Real pi, ID, OD, Length, gr, E, ZETACS, Tmax, Speed, Rcr, Lcr, T9, T8, T7, T
        Real RO, GG, Ksp, damp, EI, L, II, Mass, Area, MASST, II, C, P, CD, Y
        Real Z, YD, CSangle, CSphangl, Fcr, Fcrwp, Bdamp
*       REAL ETIME,TM(2)
* open and dimension variables
        Dimension damp(30), Mass(25), YD(4, 148), Fcrwp(25), Ksp(25), Y(148),
            Z(148)
        Dimension VL(148), ML(148), L(148), II(148), AREA(148), EI(148), C(148),
            g(150)
        Dimension P(148), MR(148), R(148), S(148), CD(148)
        OPEN (unit=10,file='t1-1500.dat',status='unknown')
* ------------------> INPUTS <--------------------
* Mesh sizing
* Number of mass elements
        Pts = 19
* Number of equations
        N = Pts * 4

* Geometeric and material Specifications
        pi = 3.14159
        ID = 0
        OD = 2.25
        Length = 1.025
        gr = 386
        E = 3E+07
* Damping ratio of the crankshaft
        ZETACS = 0.003
* Engine Specifications
        Tmax = 2000
        Speed = 1500
        Rcr = 1.6
        Lcr = 3.55

* Calculation increments and times
        T9 = 150 / ((Speed) / 60)
        T8 = .0002
        D1 = .000001
        T7 = 9E9
        T = .000001
* Calculated values
```

```
      RO = .28 / gr
      GG = (11.5 / 5) * E
      T8 = T8 / D1
* Spring constants and Dampers
      Ksp(2) = 1000000
      damp(2) = 0.0500
      Ksp(6) = 1000000
      damp(6) = 0.0500
      Ksp(10) = 1000000
      damp(10) = 0.0500
      Ksp(14) = 1000000
      damp(14) = 0.0500
      Ksp(18) = 1000000
      damp(18) = 0.0500
      bdamp = 10
      WRITE (10,*) Speed, bdamp, damp(2), Ksp(2), T8

      MASST = 0
      do 100 j= 1, Pts,1
      AREA(J) = pi * (OD ** 2 - ID ** 2) / 4
      EI(J) = E * pi * (OD ** 4 - ID ** 4) / 64
      L(J) = Length
      Mass(J) = L(J) * AREA(J) * RO
  100 continue
* addition of counterweights and pistons
      Mass(3) = 0.009566
      Mass(17) = Mass(3)
      Mass(5) = 0.0045781
      Mass(7) = Mass(5)
      Mass(13) = Mass(5)
      Mass(15) = Mass(5)
      Mass(9) = 0.00735787
      Mass(11) = Mass(9)
      Mass(4) = Mass(4) +0.00239
      Mass(8) = Mass(8) + 0.00239
      Mass(12) = Mass(12) + 0.00239
      Mass(16) = Mass(16) + 0.00239

      do 105 J = 1, Pts, 1
      MASST = MASST + Mass(J)
      II(J) = Mass(J) * L(J) ** 2 / 12 + L(J) * .25 * pi * RO * ((OD / 2) ** 4 - (ID / 2)
     &    ** 4)
  105 continue
```

```
      II(3) = (Mass(3)/12)*(3**2 + .75**2) + Mass(3)*1.25**2
      II(17) = II(3)
      II(5) = (Mass(5)/12)*(2.25**2 + 1**2) + Mass(5)*0.8**2
      II(7) = II(5)
      II(13) = II(5)
      II(15) = II(5)
      II(9) = (Mass(9)/12)*(2.5**2 + .75**2) + Mass(9)*0.5**2
      II(11) = II(9)
      II(4) = II(4) + Mass(4)*1.6**2
      II(8) = II(8) + Mass(8)* 1.6**2
      II(12) = II(12) + Mass(12)* 1.6**2
      II(16) = II(16) + Mass(16) * 1.6**2

      do 107 j = 1, Pts,1
      C(J) = L(J) ** 3 / (3 * EI(J))
      g(J) = L(J) / EI(J)
      P(J) = L(J) ** 2 / (2 * EI(J))
 107  continue

* Damping of the Jth element
      do 110 J = 1, Pts - 1,1
      CD(J) = 2 * ZETACS * SQRT(3 * EI(J) * Mass(J + 1) / L(J) ** 3)
 110  continue
* Initial Conditions
      do 115 I = 1, N,1
      Y(I) = 0
 115  continue
      Y(1) = 0
      do 120 I = 1, N,1
      Z(I) = Y(I)
 120  continue

*
**************************Don't TOUCH*********************************
*--------------> CONTROL<--------------------
* Runge-Kutta solution method
 50   do 130 J = 1, 4, 1
            if (J.EQ.1) then
              goto 10
              endif
            if (J.EQ.2) then
              goto 20
              endif
            if (J.EQ.3) then
```

```
            goto 30
            endif
          if (J.EQ.4) then
            goto 40
            endif
**************** First pass through the equations
 20     T = T + D1 * .5
* Force recalculation for the time advance
        CSangle = T * Speed * 2 * pi / 60
        CSphangl = CSangle
        Call Force (CSphangl,Tmax,T,Rcr,Lcr,pi,Fcr)
        Fcrwp(4)=Fcr
        CSphangl = CSangle + pi/2
        Call Force (CSphangl,Tmax,T,Rcr,Lcr,pi,Fcr)
        Fcrwp(16)=Fcr
        CSphangl = CSangle + pi
        Call Force (CSphangl,Tmax,T,Rcr,Lcr,pi,Fcr)
        Fcrwp(8)=Fcr
        CSphangl = CSangle + 3 * pi/2
        Call Force(CSphangl,Tmax,T,Rcr,Lcr,pi,Fcr)
        Fcrwp(12)=Fcr
        do 135 I = 1, N, 1
        Y(I) = YD(1, I) * D1 * .5 + Z(I)
  135  continue
        GOTO 10
************** Second pass through the equations
 30    do 140 I = 1, N, 1
        Y(I) = YD(2, I) * D1 * .5 + Z(I)
  140  continue
        GOTO 10
************** Third pass through the equations
 40    T = T + D1 * .5
* Force recalculation for the time advance
        CSangle = T * Speed * 2 * pi / 60
        CSphangl = CSangle
        Call Force (CSphangl,Tmax,T,Rcr,Lcr,pi,Fcr)
        Fcrwp(4)=Fcr
        CSphangl = CSangle + pi/2
        Call Force (CSphangl,Tmax,T,Rcr,Lcr,pi,Fcr)
        Fcrwp(16)=Fcr
        CSphangl = CSangle + pi
        Call Force (CSphangl,Tmax,T,Rcr,Lcr,pi,Fcr)
        Fcrwp(8)=Fcr
        CSphangl = CSangle + 3 * pi/2
```

```
        Call Force(CSphangl,Tmax,T,Rcr,Lcr,pi,Fcr)
        Fcrwp(12)=Fcr

*
        do 145 I = 1, N, 1
        Y(I) = YD(3, I) * D1 + Z(I)
 145  continue
****** Enter the first order equations
* Force and moment calculations
 10  do 150 JJ = 1, Pts - 1, 1
        R(JJ) = Y(2 * JJ + 1) - Y(2 * JJ - 1) - L(JJ) * Y(2 * JJ + ((2 * Pts) - 1))
        S(JJ) = Y(2 * JJ + ((2 * Pts) + 1)) - Y(2 * JJ + ((2 * Pts) - 1))
        DEMM = g(JJ) * C(JJ) - P(JJ) ** 2
        ML(JJ + 1) = (-R(JJ) * P(JJ) + S(JJ) * C(JJ)) / DEMM
        VL(JJ + 1) = (P(JJ) * S(JJ) - g(JJ) * R(JJ)) / DEMM
        MR(JJ) = ML(JJ + 1) - L(JJ) * VL(JJ + 1)
 150  continue
* ----------------> DEFLECTIONS <---------------------
* F= ma for the first mass
        YD(J, 1) = Y(2)
        YD(J, 2) = (-VL(2) + (CD(1) * (Y(4) - Y(2)))) / Mass(1)
* F = ma for 2 through 10
        do 155 JJ = 2, Pts - 1, 1
        FD = CD(JJ - 1) * (Y(2 * JJ - 2) - Y(2 * JJ)) - CD(JJ) * (Y(2 * JJ) - Y(2 * JJ + 2))
        YD(J, 2 * JJ - 1) = Y(2 * JJ)
        YD(J, 2 * JJ) = (VL(JJ) - VL(JJ + 1) + FD - Ksp(JJ) * Y(2 * JJ - 1) - damp(JJ) *
Y(2 * JJ) - Fcrwp(JJ)) / Mass(JJ)
 155  continue
* F = ma for Pts
        YD(J, (2 * Pts) - 1) = Y(2 * Pts)
        YD(J, 2 * Pts) = (VL(Pts) + CD(Pts - 1) * (Y(2 * Pts - 2) - Y(2 * Pts)) - bdamp *
              Y(2 * Pts - 1)) / Mass(Pts)
* ----------------> ROTATIONS <-----------------
* T = I* alpha for 1
        YD(J, (2 * Pts) + 1) = Y((2 * Pts) + 2)
        YD(J, (2 * Pts) + 2) = (MR(1)) / II(1)
* For mass points 2 through Pts-1
        do 160 JJ = 2, Pts - 1, 1
        YD(J, 2 * JJ + (2 * Pts) - 1) = Y(2 * JJ + (2 * Pts))
        YD(J, 2 * JJ + 2 * Pts) = (MR(JJ) - ML(JJ)) / II(JJ)
 160  Continue
* For mass point Pts
        YD(J, N - 1) = Y(N)
        YD(J, N) = (-ML(Pts) - bdamp * Y(N)) / II(Pts)
```

```
 130   continue
* -------------> End control Group <-----------
* calculation of the new Y's for this time step
        do 165 I = 1, N, 1
        Z(I) = Z(I) + D1 * (YD(1, I) + YD(4, I) + 2 * (YD(3, I) + YD(2, I))) / 6
 165   continue
        do 170 I = 1, N, 1
        Y(I) = Z(I)
 170   continue
        T7 = T7 + 1
* Is it time to print?
                IF (T7.LE.T8 - 0.0002) THEN
                 goto 200
                 endif
        T7 = 0
* ---------------------> OUTPUTS <----------------
                If (T.le.0.7) THEN
                  goto 200
                  endif
        counter=counter+1
                If (counter.Ge.4097) THEN
                  goto 200
                  endif
        Write (10,*) T, Y(19), Y(37), Y(57), Y(75)

*
 200          IF (T.LE.T9) THEN
                 goto 50
                 endif
*       Write(10,*) ETIME(TM)
        END
```

Gas Force Calculation Code

```
* Gas Force calculations
* This subroutine calculates the forces at each cylinder in their proper phase
      Subroutine Force(CSphangl,Tmax,T,Rcr,Lcr,pi,Fcr)
      Real Tmax, CSphangl,theta,Fcr,Torquee,pi,Lcr
      Fsm = 40


            IF (CSphangl.ge.12.56637) THEN
             Cycles = AINT(CSphangl / (4 * pi))
             CSphangl = CSphangl - (Cycles * 4 * pi)
            endif
      theta = (Rcr / Lcr) * SIN(CSphangl)
            IF (CSphangl.le.3.14159) THEN
             goto 1
            endif
            IF (CSphangl.gt.3.14159.AND.CSphangl.le.3.31612) THEN
             goto 2
             endif
            If (CSphangl.gt.3.31612.AND.CSphangl.le.6.10865) THEN
             goto 3
            endif
            IF (CSphangl.gt.6.10865.AND.CSphangl.le.6.45772) THEN
             goto 4
            endif
            IF (CSphangl.gt.6.45772.AND.CSphangl.le.9.07571) THEN
             goto 3
            endif
            IF (CSphangl.gt.9.07571.AND.CSphangl.le.9.77384) THEN
             goto 5
            endif
            IF (CSphangl.gt.9.77384.AND.CSphangl.le.11.1701) THEN
             goto 3
            endif
            IF (CSphangl.gt.11.1701.AND.CSphangl.le.12.56637) THEN
             goto 6
            endif

* different Force Curves
  1  Torquee = Tmax * SIN(CSphangl)
      Fcr = Torquee / (Rcr * COS((pi / 2 - CSphangl - theta) + 0.00001))
      RETURN
  2  Fcr = Tmax * COS(5 * CSphangl + pi)
      RETURN
```

```
3  Torque = -.1 * Tmax
   Fcr = Torque / (Rcr * COS((pi / 2 - CSphangl - theta) + .00001))
   RETURN
4  Fcr = Tmax * SIN(CSphangl + pi)
   RETURN
5  Fcr = Fsm * SIN(CSphangl)
   RETURN
6  Torque = Tmax * .4 * SIN(CSphangl * 2)
   Fcr = Torque / (Rcr * COS((pi / 2 - CSphangl - theta) + .00001))
   RETURN
   End
```

PSPlot Input Signal Code

```
' The purpose of this program is to create a data file to check the PSPlot program
' This program creats a digital signal sampled at 5000 Hz composed of given components
' The data is written to an output file on the hard drive
OPEN "O", #1, "c:PSCHECK.DAT"
' Program Reset
T = 0
n = 0

10 n = n + 1
' Frequency Components
A = 10 * SIN(2 * 3.14159 * 20 * T)
B = 10 * SIN(2 * 3.14159 * 100 * T)
D = 10 * SIN(2 * 3.14159 * 60 * T)
E = 10 * SIN(2 * 3.14159 * 140 * T)
F = 10 * SIN(2 * 3.14159 * 180 * T)

' Elapsed Time Counter
T = T + .0002

' Superposition of Signal
c = A + B + D + E + F

' Screen Output
PRINT c

' File Output
WRITE #1, c

IF n = 4096 THEN 100
GOTO 10
100 CLOSE 1
END
```

Flywheel added Crankshaft Bending Response Code

```
* This program calculates the response of a model crankshaft with a Flywheel in Place
* Initialize the variables
      Integer Pts, N, J, JJ, I
      Real pi, ID, OD, Length, gr, E, ZETACS, Tmax, Speed, Rcr, Lcr, T9, T8, T7, T
      Real RO, GG, Ksp, damp, EI, L, II, Mass, Area, MASST, II, C, P, CD, Y
      Real Z, YD, CSangle, CSphangl, Fcr, Fcrwp, Bdamp
*     REAL ETIME,TM(2)
* open and dimension variables
      Dimension damp(30), Mass(25), YD(4, 148), Fcrwp(25), Ksp(25), Y(148),
           Z(148)
      Dimension VL(148), ML(148), L(148), II(148), AREA(148), EI(148), C(148),
           g(150)
      Dimension P(148), MR(148), R(148), S(148), CD(148)
      OPEN (unit=10,file='f360.dat',status='unknown')
* ------------------> INPUTS <--------------------
* Mesh sizing
* Number of mass elements
      Pts = 19
* Number of equations
      N = Pts * 4

* Geometeric and material Specifications
      pi = 3.14159
      ID = 0
      OD = 2.25
      Length = 1.025
      gr = 386
      E = 3E+07
* Damping ratio of the crankshaft
      ZETACS = 0.003
* Engine Specifications
      Tmax = 2000
      Speed = 6000
      Rcr = 1.6
      Lcr = 3.55

* Calculation increments and times
      T9 = 150 / ((Speed) / 60)
      T8 = .0002
      D1 = .000001
      T7 = 9E9
      T = .000001
      Nout =0
```

```
* Calculated values
      RO = .28 / gr
      GG = (11.5 / 5) * E
      T8 = T8 / D1
* Spring constants and Dampers
      Ksp(2) = 1000000
      damp(2) = 0.0500
      Ksp(6) = 1000000
      damp(6) = 0.0500
      Ksp(10) = 1000000
      damp(10) = 0.0500
      Ksp(14) = 1000000
      damp(14) = 0.0500
      Ksp(18) = 1000000
      damp(18) = 0.0500
      bdamp = 0

      WRITE (10,*) Speed, Tmax, damp(2), Ksp(2), bdamp, D1, T8

      MASST = 0
      do 100 j= 1, Pts,1
      AREA(J) = pi * (OD ** 2 - ID ** 2) / 4
      EI(J) = E * pi * (OD ** 4 - ID ** 4) / 64
      L(J) = Length
      Mass(J) = L(J) * AREA(J) * RO
 100  continue

* addition of counterweights and pistons
      Mass(3) = 0.009566
      Mass(17) = Mass(3)
      Mass(5) = 0.0045781
      Mass(7) = Mass(5)
      Mass(13) = Mass(5)
      Mass(15) = Mass(5)
      Mass(9) = 0.00735787
      Mass(11) = Mass(9)
      Mass(4) = Mass(4) +0.00239
      Mass(8) = Mass(8) + 0.00239
      Mass(12) = Mass(12) + 0.00239
      Mass(16) = Mass(16) + 0.00239
      do 105 J = 1, Pts, 1
      MASST = MASST + Mass(J)
      II(J) = Mass(J) * L(J) ** 2 / 12 + L(J) * .25 * pi * RO * ((OD / 2) ** 4 - (ID / 2)
           ** 4)
```

```
 105  continue

      II(3) = (Mass(3)/12)*(3**2 + .75**2) + Mass(3)*1.25**2
      II(17) = II(3)
      II(5) = (Mass(5)/12)*(2.25**2 + 1**2) + Mass(5)*0.8**2
      II(7) = II(5)
      II(13) = II(5)
      II(15) = II(5)
      II(9) = (Mass(9)/12)*(2.5**2 + 0.75**2) + Mass(9)*0.5**2
      II(11) = II(9)
      II(4) = II(4) + Mass(4)*1.6**2
      II(8) = II(8) + Mass(8)* 1.6**2
      II(12) = II(12) + Mass(12)* 1.6**2
      II(16) = II(16) + Mass(16) * 1.6**2

      do 107 j = 1, Pts,1
      C(J) = L(J) ** 3 / (3 * EI(J))
      g(J) = L(J) / EI(J)
      P(J) = L(J) ** 2 / (2 * EI(J))
 107  continue

* for the flywheel
      ODF=8
      IDF=4
      Lf=1
      AREA(19) = pi * (ODF ** 2 - IDF ** 2) / 4
      EI(19) = E * pi * (ODF ** 4 - IDF ** 4) / 64
      L(19) = Lf
      Mass(19) = L(19) * AREA(19) * RO
      II(19) = Mass(19) * L(19) ** 2 / 12 + L(19) * .25 * pi * RO * ((ODF / 2) ** 4 -
            (IDF / 2) ** 4)
      C(19) = L(19) ** 3 / (3 * EI(19))
      g(19) = L(19) / EI(19)
      P(19) = L(19) ** 2 / (2 * EI(19))
* Damping of the Jth element
      do 110 J = 1, Pts - 1,1
      CD(J) = 2 * ZETACS * SQRT(3 * EI(J) * Mass(J + 1) / L(J) ** 3)
 110  continue
* Initial Conditions
      do 115 I = 1, N,1
      Y(I) = 0
 115  continue
      Y(1) = 0
```

```
        do 120 I = 1, N,1
        Z(I) = Y(I)
 120   continue

*
**************************Don't TOUCH*********************************
*--------------> CONTROL<--------------------
* Runge-Kutta solution method
  50    do 130 J = 1, 4, 1
                if (J.EQ.1) then
                  goto 10
                  endif
                if (J.EQ.2) then
                  goto 20
                  endif
                if (J.EQ.3) then
                  goto 30
                  endif
                if (J.EQ.4) then
                  goto 40
                  endif
**************** First pass through the equations
 20     T = T + D1 * .5
* Force recalculation for the time advance
        CSangle = T * Speed * 2 * pi / 60
        CSphangl = CSangle
        Call Force (CSphangl,Tmax,T,Rcr,Lcr,pi,Fcr)
        Fcrwp(4)=Fcr
        CSphangl = CSangle + pi/2
        Call Force (CSphangl,Tmax,T,Rcr,Lcr,pi,Fcr)
        Fcrwp(16)=Fcr
        CSphangl = CSangle + pi
        Call Force (CSphangl,Tmax,T,Rcr,Lcr,pi,Fcr)
        Fcrwp(8)=Fcr
        CSphangl = CSangle + 3 * pi/2
        Call Force(CSphangl,Tmax,T,Rcr,Lcr,pi,Fcr)
        Fcrwp(12)=Fcr
        do 135 I = 1, N, 1
        Y(I) = YD(1, I) * D1 * .5 + Z(I)
 135   continue
        GOTO 10
************** Second pass through the equations
 30   do 140 I = 1, N, 1
        Y(I) = YD(2, I) * D1 * .5 + Z(I)
```

```
 140  continue
      GOTO 10
************** Third pass through the equations
 40   T = T + D1 * .5
* Force recalculation for the time advance
      CSangle = T * Speed * 2 * pi / 60
      CSphangl = CSangle
      Call Force (CSphangl,Tmax,T,Rcr,Lcr,pi,Fcr)
      Fcrwp(4)=Fcr
      CSphangl = CSangle + pi/2
      Call Force (CSphangl,Tmax,T,Rcr,Lcr,pi,Fcr)
      Fcrwp(16)=Fcr
      CSphangl = CSangle + pi
      Call Force (CSphangl,Tmax,T,Rcr,Lcr,pi,Fcr)
      Fcrwp(8)=Fcr
      CSphangl = CSangle + 3 * pi/2
      Call Force(CSphangl,Tmax,T,Rcr,Lcr,pi,Fcr)
      Fcrwp(12)=Fcr

*
      do 145 I = 1, N, 1
      Y(I) = YD(3, I) * D1 + Z(I)
 145  continue
****** Enter the first order equations
* Force and moment calculations
 10   do 150 JJ = 1, Pts - 1, 1
      R(JJ) = Y(2 * JJ + 1) - Y(2 * JJ - 1) - L(JJ) * Y(2 * JJ + ((2 * Pts) - 1))
      S(JJ) = Y(2 * JJ + ((2 * Pts) + 1)) - Y(2 * JJ + ((2 * Pts) - 1))
      DEMM = g(JJ) * C(JJ) - P(JJ) ** 2
      ML(JJ + 1) = (-R(JJ) * P(JJ) + S(JJ) * C(JJ)) / DEMM
      VL(JJ + 1) = (P(JJ) * S(JJ) - g(JJ) * R(JJ)) / DEMM
      MR(JJ) = ML(JJ + 1) - L(JJ) * VL(JJ + 1)
 150  continue
* ----------------> DEFLECTIONS <---------------------
* F= ma for the first mass
      YD(J, 1) = Y(2)
      YD(J, 2) = (-VL(2) + (CD(1) * (Y(4) - Y(2)))) / Mass(1)
* F = ma for 2 through 18
      do 155 JJ = 2, Pts - 1, 1
      FD = CD(JJ - 1) * (Y(2 * JJ - 2) - Y(2 * JJ)) - CD(JJ) * (Y(2 * JJ) - Y(2 * JJ + 2))
      YD(J, 2 * JJ - 1) = Y(2 * JJ)
      YD(J, 2 * JJ) = (VL(JJ) - VL(JJ + 1) + FD - Ksp(JJ) * Y(2 * JJ - 1) - damp(JJ) *
           Y(2 * JJ) - Fcrwp(JJ)) / Mass(JJ)
 155  continue
```

```
* F = ma for N
        YD(J, (2 * Pts) - 1) = Y(2 * Pts)
        YD(J, 2 * Pts) = (VL(Pts) + CD(Pts - 1) * (Y(2 * Pts - 2) - Y(2 * Pts))) /
                Mass(Pts)
* ----------------> ROTATIONS <-----------------
* T = I* alpha for 1
        YD(J, (2 * Pts) + 1) = Y((2 * Pts) + 2)
        YD(J, (2 * Pts) + 2) = (MR(1)) / II(1)
* For mass points 2 through Pts-1
        do 160 JJ = 2, Pts - 1, 1
        YD(J, 2 * JJ + (2 * Pts) - 1) = Y(2 * JJ + (2 * Pts))
        YD(J, 2 * JJ + 2 * Pts) = (MR(JJ) - ML(JJ)) / II(JJ)
 160   Continue
* For mass point Pts
        YD(J, N - 1) = Y(N)
        YD(J, N) = (-ML(Pts) - bdamp * Y(N)) / II(Pts)
 130   continue
* -------------> End control Group <-----------
* calculation of the new Y's for this time step
        do 165 I = 1, N, 1
        Z(I) = Z(I) + D1 * (YD(1, I) + YD(4, I) + 2 * (YD(3, I) + YD(2, I))) / 6
 165   continue
        do 170 I = 1, N, 1
        Y(I) = Z(I)
 170   continue
        T7 = T7 + 1
* Is it time to print?
                IF (T7.LE.T8 - 0.0002) THEN
                 goto 200
                 endif
        T7 = 0
* ---------------------> OUTPUTS <----------------
                If (T.le.0.7) THEN
                  goto 200
                  endif
        Nout = Nout + 1
                If (Nout.ge.4097) THEN
                   goto 200
                   endif
        Write (10,*) T,Y(19),Y(37),Y(57),Y(75)

*
 200        IF (T.LE.T9) THEN
                goto 50
```

```
          endif
*       Write(10,*) ETIME(TM)
        END
```

Elastomer Damper added Crankshaft Bending Response Code

```
* This program calculates the response of a model crankshaft with an elastomer damper
* Initialize the variables
        Integer Pts, N, J, JJ, I
        Real pi, ID, OD, Length, gr, E, ZETACS, Tmax, Speed, Rcr, Lcr, T9, T8, T7, T
        Real RO, GG, Ksp, damp, EI, L, II, Mass, Area, MASST, II, C, P, CD, Y
        Real Z, YD, CSangle, CSphangl, Fcr, Fcrwp, Bdamp
        Real ODD,DL,ODIR,IDIR,LIR,Darea,Gp,Gpp,mu,arm,thick
*       REAL ETIME,TM(2)
* open and dimension variables
        Dimension damp(30), Mass(25), YD(4, 148), Fcrwp(25), Ksp(25), Y(148),
            Z(148)
        Dimension VL(148), ML(148), L(148), II(148), AREA(148), EI(148), C(148),
            g(150)
        Dimension P(148), MR(148), R(148), S(148), CD(148)
        OPEN (unit=10,file='el260.dat',status='unknown')
* ------------------> INPUTS <---------------------
* Mesh sizing
* Number of mass elements
        Pts = 20
* Number of equations
        N = Pts * 4

* Geometeric and material Specifications
        pi = 3.14159
        ID = 0
        OD = 2.25
        Length = 1.025
        gr = 386
        E = 3E+07
* Damping ratio of the crankshaft
        ZETACS = 0.003
* Engine Specifications
        Tmax = 2000
        Speed = 6000
        omega = Speed*2*pi/60
        Rcr = 1.6
        Lcr = 3.55
************** Flywheel properties *******************************
* Disk
        ODD = 10
        DL = 0.75
* inertial ring
        ODIR = 10
```

```
      IDIR = 2.25
      LIR = 1.25
      Darea = pi*(ODIR**2-IDIR**2)/4
* elastomer material data
      Gp = 2.00
      Gpp = 1.60
      mu = Gpp / 2*pi*100
      arm = (ODIR-IDIR)/2 + IDIR
      thick= 0.05

* Calculation increments and times
      T9 = 150 / ((Speed) / 60)
      T8 = .0002
      D1 = .000001
      T7 = 9E9
      T = .000001
* Calculated values
      RO = .28 / gr
      GG = (11.5 / 5) * E
      T8 = T8 / D1
* Spring constants and Dampers
      Ksp(2) = 1000000
      damp(2) = 0.0500
      Ksp(6) = 1000000
      damp(6) = 0.0500
      Ksp(10) = 1000000
      damp(10) = 0.0500
      Ksp(14) = 1000000
      damp(14) = 0.0500
      Ksp(18) = 1000000
      damp(18) = 0.0500
      bdamp = 0

      WRITE (10,*) Speed, Tmax, damp(2), Ksp(2), bdamp, D1, T8

      MASST = 0
      do 100 j= 1, Pts,1
      AREA(J) = pi * (OD ** 2 - ID ** 2) / 4
      EI(J) = E * pi * (OD ** 4 - ID ** 4) / 64
      L(J) = Length
      Mass(J) = L(J) * AREA(J) * RO
  100 continue

* addition of counterweights and pistons
```

```
      Mass(3) = 0.009566
      Mass(17) = Mass(3)
      Mass(5) = 0.0045781
      Mass(7) = Mass(5)
      Mass(13) = Mass(5)
      Mass(15) = Mass(5)
      Mass(9) = 0.00735787
      Mass(11) = Mass(9)
      Mass(4) = Mass(4) +0.00239
      Mass(8) = Mass(8) + 0.00239
      Mass(12) = Mass(12) + 0.00239
      Mass(16) = Mass(16) + 0.00239
      do 105 J = 1, Pts, 1
      MASST = MASST + Mass(J)
      II(J) = Mass(J) * L(J) ** 2 / 12 + L(J) * .25 * pi * RO * ((OD / 2) ** 4 - (ID / 2)
            ** 4)
 105  continue


      II(3) = (Mass(3)/12)*(3**2 + .75**2) + Mass(3)*1.25**2
      II(17) = II(3)
      II(5) = (Mass(5)/12)*(2.25**2 + 1**2) + Mass(5)*.8**2
      II(7) = II(5)
      II(13) = II(5)
      II(15) = II(5)
      II(9) = (Mass(9)/12)*(2.25**2 + 0.75**2) + Mass(9)*0.5**2
      II(11) = II(9)
      II(4) = II(4) + Mass(4)*1.6**2
      II(8) = II(8) + Mass(8)* 1.6**2
      II(12) = II(12) + Mass(12)* 1.6**2
      II(16) = II(16) + Mass(16) * 1.6**2

      do 107 j = 1, Pts,1
      C(J) = L(J) ** 3 / (3 * EI(J))
      g(J) = L(J) / EI(J)
      P(J) = L(J) ** 2 / (2 * EI(J))
 107  continue

* For the elastomer damper
* the first disk
      AREA(19) = pi * (ODD ** 2 ) / 4
      EI(19) = E * pi * (ODD ** 4 ) / 64
      L(19) = DL
      Mass(19) = L(19) * AREA(19) * RO
```

```
        II(19) = Mass(19) * L(19) ** 2 / 12 + L(19) * .25 * pi * RO * ((ODD / 2) ** 4 )
        C(19) = L(19) ** 3 / (3 * EI(19))
        g(19) = L(19) / EI(19)
        P(19) = L(19) ** 2 / (2 * EI(19))
* the inertial ring
        AREA(20) = pi * (ODIR ** 2 -IDIR ** 2) / 4
        EI(20) = E * pi * (ODIR ** 4 - IDIR ** 4) / 64
        L(20) = DL
        Mass(20) = L(20) * AREA(20) * RO
        II(20) = Mass(20) * L(20) ** 2 / 12 + L(20) * .25 * pi * RO * ((ODD / 2) ** 4 -
(IDIR /2)**4)
        C(20) = L(20) ** 3 / (3 * EI(20))
        g(20) = L(20) / EI(20)
        P(20) = L(20) ** 2 / (2 * EI(20))
* Damping of the Jth element
        do 110 J = 1, Pts - 1,1
        CD(J) = 2 * ZETACS * SQRT(3 * EI(J) * Mass(J + 1) / L(J) ** 3)
  110   continue
* Initial Conditions
        do 115 I = 1, N,1
        Y(I) = 0
  115   continue
        Y(1) = 0
        do 120 I = 1, N,1
        Z(I) = Y(I)
  120   continue

*
**************************Don't TOUCH*******************************
*--------------> CONTROL<--------------------
* Runge-Kutta solution method
  50    do 130 J = 1, 4, 1
                if (J.EQ.1) then
                  goto 10
                  endif
                if (J.EQ.2) then
                  goto 20
                  endif
                if (J.EQ.3) then
                  goto 30
                  endif
                if (J.EQ.4) then
                  goto 40
                  endif
```

```
**************** First pass through the equations
 20     T = T + D1 * .5
* Force recalculation for the time advance
        CSangle = T * Speed * 2 * pi / 60
        CSphangl = CSangle
        Call Force (CSphangl,Tmax,T,Rcr,Lcr,pi,Fcr)
        Fcrwp(4)=Fcr
        CSphangl = CSangle + pi/2
        Call Force (CSphangl,Tmax,T,Rcr,Lcr,pi,Fcr)
        Fcrwp(16)=Fcr
        CSphangl = CSangle + pi
        Call Force (CSphangl,Tmax,T,Rcr,Lcr,pi,Fcr)
        Fcrwp(8)=Fcr
        CSphangl = CSangle + 3 * pi/2
        Call Force(CSphangl,Tmax,T,Rcr,Lcr,pi,Fcr)
        Fcrwp(12)=Fcr
        do 135 I = 1, N, 1
        Y(I) = YD(1, I) * D1 * .5 + Z(I)
 135    continue
        GOTO 10
************** Second pass through the equations
 30     do 140 I = 1, N, 1
        Y(I) = YD(2, I) * D1 * .5 + Z(I)
 140    continue
        GOTO 10
************** Third pass through the equations
 40     T = T + D1 * .5
* Force recalculation for the time advance
        CSangle = T * Speed * 2 * pi / 60
        CSphangl = CSangle
        Call Force (CSphangl,Tmax,T,Rcr,Lcr,pi,Fcr)
        Fcrwp(4)=Fcr
        CSphangl = CSangle + pi/2
        Call Force (CSphangl,Tmax,T,Rcr,Lcr,pi,Fcr)
        Fcrwp(16)=Fcr
        CSphangl = CSangle + pi
        Call Force (CSphangl,Tmax,T,Rcr,Lcr,pi,Fcr)
        Fcrwp(8)=Fcr
        CSphangl = CSangle + 3 * pi/2
        Call Force(CSphangl,Tmax,T,Rcr,Lcr,pi,Fcr)
        Fcrwp(12)=Fcr

*
        do 145 I = 1, N, 1
```

```
        Y(I) = YD(3, I) * D1 + Z(I)
  145  continue
****** Enter the first order equations
* Force and moment calculations
  10  do 150 JJ = 1, Pts - 1, 1
        R(JJ) = Y(2 * JJ + 1) - Y(2 * JJ - 1) - L(JJ) * Y(2 * JJ + ((2 * Pts) - 1))
        S(JJ) = Y(2 * JJ + ((2 * Pts) + 1)) - Y(2 * JJ + ((2 * Pts) - 1))
        DEMM = g(JJ) * C(JJ) - P(JJ) ** 2
        ML(JJ + 1) = (-R(JJ) * P(JJ) + S(JJ) * C(JJ)) / DEMM
        VL(JJ + 1) = (P(JJ) * S(JJ) - g(JJ) * R(JJ)) / DEMM
        MR(JJ) = ML(JJ + 1) - L(JJ) * VL(JJ + 1)
  150  continue
* ----------------> DEFLECTIONS <--------------------
* F= ma for the first mass
        YD(J, 1) = Y(2)
        YD(J, 2) = (-VL(2) + (CD(1) * (Y(4) - Y(2)))) / Mass(1)
* F = ma for 2 through 18
        do 155 JJ = 2, Pts - 2, 1
        FD = CD(JJ - 1) * (Y(2 * JJ - 2) - Y(2 * JJ)) - CD(JJ) * (Y(2 * JJ) - Y(2 * JJ + 2))
        YD(J, 2 * JJ - 1) = Y(2 * JJ)
        YD(J, 2 * JJ) = (VL(JJ) - VL(JJ + 1) + FD - Ksp(JJ) * Y(2 * JJ - 1) - damp(JJ) *
Y(2 * JJ) - Fcrwp(JJ)) / Mass(JJ)
  155  continue
* F = ma for the damper disk
        FD = CD(18) * (Y(36) - Y(38)) - CD(19) * (Y(38) - Y(40))
        YD(J, 37) = Y(38)
        YD(J, 38) = (VL(19) - VL(20) + FD) / Mass(19)
* F = ma for ther inertial ring
        YD(J, 39) = Y(40)
        YD(J, 40) = (VL(20) + CD(19) * (Y(18) - Y(20))) / Mass(20)
* ----------------> ROTATIONS <-----------------
* T = I* alpha for 1
        YD(J, (2 * Pts) + 1) = Y((2 * Pts) + 2)
        YD(J, (2 * Pts) + 2) = (MR(1)) / II(1)
* For mass points 2 through Pts-1
        do 160 JJ = 2, Pts - 2, 1
        YD(J, 2 * JJ + (2 * Pts) - 1) = Y(2 * JJ + (2 * Pts))
        YD(J, 2 * JJ + 2 * Pts) = (MR(JJ) - ML(JJ)) / II(JJ)
  160  Continue
* For the damper disk
        strain = arm/thick * (sin(Y(77))-sin(Y(79)))
        YD(J, 2 * 19 + (2 * Pts) - 1) = Y(2 * 19 + (2 * Pts))
        YD(J, 2 * 19 + 2 * Pts) = (ML(19) - 0.25*Darea*arm * (Gp*strain + mu*
arm/thick * (Y(78)-Y(80))) ) / II(19)
```

```
* For inertial ring
        YD(J, N - 1) = Y(N)
        YD(J, N) = (-arm*sin(Y(79))*mass(20)*omega**2 + 0.25*Darea*arm *
(Gp*strain + mu* arm/thick * (Y(80)-Y(78)))) / II(Pts)
  130   continue
* -------------> End control Group <-----------
* calculation of the new Y's for this time step
        do 165 I = 1, N, 1
        Z(I) = Z(I) + D1 * (YD(1, I) + YD(4, I) + 2 * (YD(3, I) + YD(2, I))) / 6
  165   continue
        do 170 I = 1, N, 1
        Y(I) = Z(I)
  170   continue
        T7 = T7 + 1
* Is it time to print?
              IF (T7.LE.T8 - 0.0002) THEN
               goto 200
               endif
        T7 = 0
* ---------------------> OUTPUTS <----------------
              If (T.le.0.7) THEN
               goto 200
               endif
        counter=counter+1
              If (counter.Ge.4097) THEN
               goto 200
               endif

        Write (10,*) T,Y(19), Y(37), Y(57), Y(75)

*
 200         IF (T.LE.T9) THEN
               goto 50
               endif
*       Write(10,*) ETIME(TM)
        END
```

Viscous Roller Damper added Crankshaft Bending Response Code

```
* This program calculates the response of a model crankshaft with a viscous roller damper
in place
* Initialize the variables
      Integer Pts, N, J, JJ, I
      Real pi, ID, OD, Length, gr, E, ZETACS, Tmax, Speed, Rcr, Lcr, T9, T8, T7, T
      Real RO, GG, Ksp, damp, EI, L, II, Mass, Area, MASST, II, C, P, CD, Y
      Real Z, YD, CSangle, CSphangl, Fcr, Fcrwp, Bdamp
      Real ODF, Lf, d, ODC, ODR, IDR, excent, clearen, viscous, arm, Lr
      Real Massfly, Mcavity, masscyl2, masshaf2, omega
*     REAL ETIME,TM(2)
* open and dimension variables
      Dimension damp(30), Mass(25), YD(4, 148), Fcrwp(25), Ksp(25), Y(148),
           Z(148)
      Dimension VL(148), ML(148), L(148), II(148), AREA(148), EI(148), C(148),
           g(150)
      Dimension P(148), MR(148), R(148), S(148), CD(148)
      OPEN (unit=10,file='r615.dat',status='unknown')
* ------------------> INPUTS <--------------------
* Mesh sizing
* Number of mass elements
      Pts = 19
* Number of equations
      N = Pts * 4 + 2

* Geometeric and material Specifications
      pi = 3.14159
      ID = 0
      OD = 2.25
      Length = 1.025
      gr = 386
      E = 3E+07
* Damping ratio of the crankshaft
      ZETACS = 0.003
* Engine Specifications
      Tmax = 2000
      Speed = 1500
      omega = Speed*2*pi/60
      Rcr = 1.6
      Lcr = 3.55

* Calculation increments and times
      T9 = 150 / ((Speed) / 60)
      T8 = .0002
```

```
      D1 = .000001
      T7 = 9E9
      T = .000001
      Nout =0
* Calculated value
      RO = .28 / gr
      GG = (11.5 / 5) * E
      T8 = T8 / D1
* Spring constants and Dampers
      Ksp(2) = 1000000
      damp(2) = 0.0500
      Ksp(6) = 1000000
      damp(6) = 0.0500
      Ksp(10) = 1000000
      damp(10) = 0.0500
      Ksp(14) = 1000000
      damp(14) = 0.0500
      Ksp(18) = 1000000
      damp(18) = 0.0500
      bdamp = 0

*     WRITE (10,*) Speed, Tmax, damp(2), Ksp(2), bdamp

      MASST = 0
      do 100 j= 1, Pts,1
      AREA(J) = pi * (OD ** 2 - ID ** 2) / 4
      EI(J) = E * pi * (OD ** 4 - ID ** 4) / 64
      L(J) = Length
      Mass(J) = L(J) * AREA(J) * RO
 100  continue

* addition of counterweights and pistons
      Mass(3) = 0.009566
      Mass(17) = Mass(3)
      Mass(5) = 0.0045781
      Mass(7) = Mass(5)
      Mass(13) = Mass(5)
      Mass(15) = Mass(5)
      Mass(9) = 0.00735787
      Mass(11) = Mass(9)
      Mass(4) = Mass(4) +0.00239
      Mass(8) = Mass(8) + 0.00239
      Mass(12) = Mass(12) + 0.00239
      Mass(16) = Mass(16) + 0.00239
```

```
      do 105 J = 1, Pts, 1
      MASST = MASST + Mass(J)
      II(J) = Mass(J) * L(J) ** 2 / 12 + L(J) * .25 * pi * RO * ((OD / 2) ** 4 - (ID / 2)
     &     ** 4)
105   continue


      II(3) = (Mass(3)/12)*(3**2 + .75**2) + Mass(3)*1.25**2
      II(17) = II(3)
      II(5) = (Mass(5)/12)*(2.25**2 + 1**2) + Mass(5)*0.8**2
      II(7) = II(5)
      II(13) = II(5)
      II(15) = II(5)
      II(9) = (Mass(9)/12)*(2.5**2 + 0.75**2) + Mass(9)*0.5**2
      II(11) = II(9)
      II(4) = II(4) + Mass(4)*1.6**2
      II(8) = II(8) + Mass(8)* 1.6**2
      II(12) = II(12) + Mass(12)* 1.6**2
      II(16) = II(16) + Mass(16) * 1.6**2

      do 107 j = 1, Pts,1
      C(J) = L(J) ** 3 / (3 * EI(J))
      g(J) = L(J) / EI(J)
      P(J) = L(J) ** 2 / (2 * EI(J))
107   continue
* For the Damper
* Flywheel Data
      ODF = 8
      Lf= 1.25
      d = 7
      ODC = 0.75
      ODR = 0.748
      IDR = ODR - 0.0625
      Lr = 4
      excent = (4*IDR)/(3*pi)
      clearen = ODC/2 - ODR/2
      arm = d + ODR/2 - clearen
      viscous = 0.0000035
* Computed Flywheel values
      AREA(19) = pi * (ODF ** 2) / 4
      EI(19) = E * pi * (ODF ** 4) / 64
      L(19) = Lf
      Massfly = L(19) * AREA(19) * RO
      Mcavity = (pi/4) * (0.75**2) * 4 * 4 * RO
```

```
        Mass(19) = Massfly - Mcavity
        II(19) = (Mass(19)/48) * (3*ODF**2 +4*Lf**2) - 2*(((Mcavity/4)/8)*ODC**2 +
                  ((Mcavity/4)*d**2))
        C(19) = L(19) ** 3 / (3 * EI(19))
        g(19) = L(19) / EI(19)
        P(19) = L(19) ** 2 / (2 * EI(19))
* Computed Roller values
        masscyl2 = (pi*(ODR**2 - IDR**2)/4) * Lr * RO
        masshaf2 = RO * Lr * .5 *(pi*IDR**2)/4
        AREA(20)= pi * (ODR**2 - IDR**2)/4 + .5 * (pi/4 * IDR**2)
        Mass(20)= Lr*AREA(20)*RO
        EI(20) = E*pi*(ODR**4 - IDR**4)/64
        L(20) = Lr
        II(20) = masscyl2/8 * (ODR**2 - IDR**2) + .5* masshaf2 * ((IDR/2)**2) +
             masshaf2 * excent**2
*       pause
* Damping of the Jth element
        do 110 J = 1, Pts - 1,1
        CD(J) = 2 * ZETACS * SQRT(3 * EI(J) * Mass(J + 1) / L(J) ** 3)
 110    continue
* Initial Conditions
        do 115 I = 1, N,1
        Y(I) = 0
 115    continue
        Y(1) = 0
        do 120 I = 1, N,1
        Z(I) = Y(I)
 120    continue

*
**************************Don't TOUCH*********************************
*-------------> CONTROL<-------------------
* Runge-Kutta solution method
 50     do 130 J = 1, 4, 1
                if (J.EQ.1) then
                  goto 10
                  endif
                if (J.EQ.2) then
                  goto 20
                  endif
                if (J.EQ.3) then
                  goto 30
                  endif
                if (J.EQ.4) then
```

```
              goto 40
              endif
**************** First pass through the equations
 20     T = T + D1 * .5
* Force recalculation for the time advance
        CSangle = T * Speed * 2 * pi / 60
        CSphangl = CSangle
        Call Force (CSphangl,Tmax,T,Rcr,Lcr,pi,Fcr)
        Fcrwp(4)=Fcr
        CSphangl = CSangle + pi/2
        Call Force (CSphangl,Tmax,T,Rcr,Lcr,pi,Fcr)
        Fcrwp(16)=Fcr
        CSphangl = CSangle + pi
        Call Force (CSphangl,Tmax,T,Rcr,Lcr,pi,Fcr)
        Fcrwp(8)=Fcr
        CSphangl = CSangle + 3 * pi/2
        Call Force(CSphangl,Tmax,T,Rcr,Lcr,pi,Fcr)
        Fcrwp(12)=Fcr
        do 135 I = 1, N, 1
        Y(I) = YD(1, I) * D1 * .5 + Z(I)
 135   continue
        GOTO 10
************** Second pass through the equations
 30    do 140 I = 1, N, 1
        Y(I) = YD(2, I) * D1 * .5 + Z(I)
 140   continue
        GOTO 10
************** Third pass through the equations
 40    T = T + D1 * .5
* Force recalculation for the time advance
        CSangle = T * Speed * 2 * pi / 60
        CSphangl = CSangle
        Call Force (CSphangl,Tmax,T,Rcr,Lcr,pi,Fcr)
        Fcrwp(4)=Fcr
        CSphangl = CSangle + pi/2
        Call Force (CSphangl,Tmax,T,Rcr,Lcr,pi,Fcr)
        Fcrwp(16)=Fcr
        CSphangl = CSangle + pi
        Call Force (CSphangl,Tmax,T,Rcr,Lcr,pi,Fcr)
        Fcrwp(8)=Fcr
        CSphangl = CSangle + 3 * pi/2
        Call Force(CSphangl,Tmax,T,Rcr,Lcr,pi,Fcr)
        Fcrwp(12)=Fcr
```

```
*
        do 145 I = 1, N, 1
        Y(I) = YD(3, I) * D1 + Z(I)
 145  continue
****** Enter the first order equations
* Force and moment calculations
 10  do 150 JJ = 1, Pts - 1, 1
        R(JJ) = Y(2 * JJ + 1) - Y(2 * JJ - 1) - L(JJ) * Y(2 * JJ + ((2 * Pts) - 1))
        S(JJ) = Y(2 * JJ + ((2 * Pts) + 1)) - Y(2 * JJ + ((2 * Pts) - 1))
        DEMM = g(JJ) * C(JJ) - P(JJ) ** 2
        ML(JJ + 1) = (-R(JJ) * P(JJ) + S(JJ) * C(JJ)) / DEMM
        VL(JJ + 1) = (P(JJ) * S(JJ) - g(JJ) * R(JJ)) / DEMM
        MR(JJ) = ML(JJ + 1) - L(JJ) * VL(JJ + 1)
 150  continue
* ----------------> DEFLECTIONS <---------------------
* F= ma for the first mass
        YD(J, 1) = Y(2)
        YD(J, 2) = (-VL(2) + (CD(1) * (Y(4) - Y(2)))) / Mass(1)
* F = ma for 2 through 18
        do 155 JJ = 2, Pts - 1, 1
        FD = CD(JJ - 1) * (Y(2 * JJ - 2) - Y(2 * JJ)) - CD(JJ) * (Y(2 * JJ) - Y(2 * JJ + 2))
        YD(J, 2 * JJ - 1) = Y(2 * JJ)
        YD(J, 2 * JJ) = (VL(JJ) - VL(JJ + 1) + FD - Ksp(JJ) * Y(2 * JJ - 1) - damp(JJ) *
                Y(2 * JJ) - Fcrwp(JJ)) / Mass(JJ)
 155  continue
* F = ma for 19
        YD(J, 37) = Y(38)
        YD(J, 38) = (VL(19) + CD(18) * (Y(36) - Y(38))) / Mass(19)
* F = ma for 20
*       YD(J, 39) = Y(40)
*       YD(J, 40) = (VL(20))/Mass(20)
* ----------------> ROTATIONS <-----------------
* T = I* alpha for 1
        YD(J, (2 * Pts) + 1) = Y((2 * Pts) + 2)
        YD(J, (2 * Pts) + 2) = (MR(1)) / II(1)
* For mass points 2 through Pts-1
        do 160 JJ = 2, Pts - 1, 1
        YD(J, 2 * JJ + (2 * Pts) - 1) = Y(2 * JJ + (2 * Pts))
        YD(J, 2 * JJ + 2 * Pts) = (MR(JJ) - ML(JJ)) / II(JJ)
 160  Continue
* For mass point 19

        YD(J, 75) = Y(76)
```

```
        YD(J, 76) = (-ML(19)-(viscous/clearen)*2*pi*Lr*ODR**3*(Y(76)-
              Y(78)))/II(19)
* For mass point 20

        YD(J, N - 1) = Y(N)
        YD(J, N) = ( (viscous/clearen)*2*pi*Lr*ODR**3*(Y(76)-Y(78))-
              2*excent*arm*Mass(20)*sin(Y(77))*omega**2)/II(20)
 130   continue

* -------------> End control Group <-----------
* calculation of the new Y's for this time step
        do 165 I = 1, N, 1
        Z(I) = Z(I) + D1 * (YD(1, I) + YD(4, I) + 2 * (YD(3, I) + YD(2, I))) / 6
 165   continue
        do 170 I = 1, N, 1
        Y(I) = Z(I)
 170   continue

        T7 = T7 + 1
* Is it time to print?
              IF (T7.LE.T8 - 0.0002) THEN
               goto 200
               endif
        T7 = 0
* ---------------------> OUTPUTS <----------------
*       do 2600 f= 1, N, 1
*       print*, Y(f)
* 2600  continue
*       print*, AREA(19),EI(19),L(19),Mass(19),II(19),AREA(20)
              If (T.le.0.7) THEN
                goto 200
                endif
        Nout = Nout + 1
              If (Nout.ge.4097) THEN
                goto 200
                endif
        Write (10,*) T,Y(19),Y(37),Y(59),Y(77)
*
 200        IF (T.LE.T9) THEN
              goto 50
              endif
*       Write(10,*) ETIME(TM)
        END
```

Appendix B

Appendix B contains:

1. Record of Invention

RECORD OF INVENTION

Engine Vibration Damper

This invention pertains to the design of a device to control and/or reduce bending vibrations in the crankshaft in internal combustion engines. Its intended use is for all internal engines including diesel and any number of cylinders, 2 or 4 cycle. It is a vibration damper (VD). By reducing the bending vibration of a crankshaft, the life of the crankshaft will increase and the noise will decrease.

Figure 1 shows a view of a schematic of the VD. The device can be attached to the front or rear portion of the crankshaft. The larger the physical size, the more effective is the VD.

The device would consist of a main body having holes spaced around the circumference, cylinder fitting inside the holes, a viscous liquid such as oil in the holes, and end caps to restrain the rollers inside the holes and to seal the liquid. The holes are perpendicular to the axis of the crankshaft. The cylinders are weighted such that the center of mass is not located at the geometric center. Figure 1 shows the rollers in the expected position for steady rotation of the main body. The holes are usually equally spaced but need not to be equally spaced around the circumference. Since the VA rotates with the speed of the crankshaft, the holes and cylinders need to be spaced for proper static and dynamic balance.

The proper hole size and roller diameter may depend upon the number of cylinders, 2 or 4 cycle engine, and the radius of the holes from the center of rotation.

When the engine is running, it receives torque power pulses from the pistons at a frequency proportional to the speed of the engine. These torque pulses applied from the pistons to the crankshaft will cause the crankshaft to bend. The VA will be attached to the end of the crankshaft and will move with the crankshaft. Since the crankshaft is both rotating and bending, the VA attached to the crankshaft will "wobble." Because the cylinders which are located inside the main body are not symmetrical in weight, the centrifugal force due to the rotation of the VA will tend to keep the heavy portion of the cylinders to the outside as shown in Figure 1. Consequently there is relative motion between the main body and the cylinders. This is illustrated by the exaggerated motion shown by views 1 and 2 of Figure 1. This relative motion is made in the presence of a viscous liquid. This relative rotational motion between the cylinders and main body will dissipate energy and consequently damp the bending vibrations of the crankshaft. The rotational mass moment of inertia about the longitudinal axis of the cylinder will also tend to keep the cylinder from rotating and add to the effectiveness of the VA.

Inventor:.....[signature]..........................Date: 8/23/1995...
Frank H. Speckhart

Understood on this date by [signature] Date: 8-24-1995

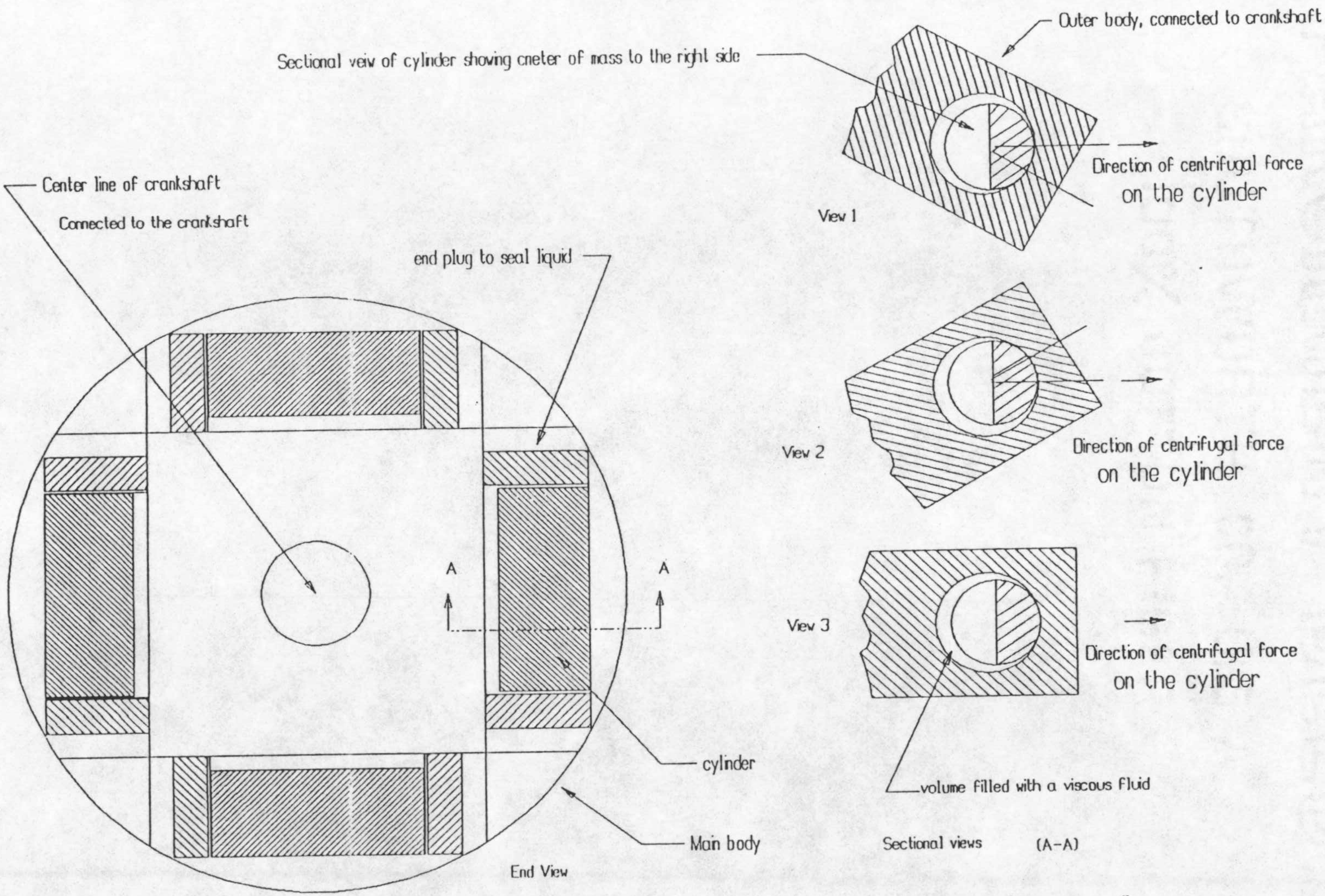

Figure 1

Schematic view of bending vibration damper
Frank H. Specthart August 22, 1995 (tvabend)

Vita

Walter Scott Pope was born in Corvallis, Oregon on May 12, 1971. He graduated from the Warren High School in Warren, Arkansas in May, 1989. He entered the University of Arkansas in August, 1989. There he studied Mechanical Engineering until he was awarded a Bachelor of Science in Mechanical Engineering in December, 1993. Upon graduation he donated his time to the Church of the Modern Day Trout Stream until he entered the University of Tennessee in June, 1993. He studied Mechanical Engineering until he was awarded a Masters of Science in Mechanical Engineering in May, 1997.

He is presently working for Sanders, a Lockheed Martin Company. He works on defensive countermeasures for military systems. He has also entered the church's seminary school.